Tree-ring blue intensity based temperature reconstructions for temperate North America

A Dissertation

Presented in Partial Fulfillment of the Requirements for the

Degree of Doctor of Philosophy

with a

Major in Geography

in the

College of Science

University of Idaho

by

Karen J. Heeter

Major Professor: Grant L. Harley, Ph.D.

Committee Members: John Abatzoglou, Ph.D.; Justin Maxwell, Ph.D.; Erika Rader, Ph.D.

Department Administrator: Alistair Smith, Ph.D.

May 2022

Abstract

Tree-ring records are invaluable sources of seasonally-to-annually-resolved paleoclimate information that allow for the multi-centennial to multi-millennial length contextualization of modern instrumental observations and trends. Within the Northern Hemisphere, substantial temporal and spatial limitations exist regarding the understanding of past temperature variability from within the tree-ring record. In this body of work, I detail the refinement and application of the novel dendrochronological technique, blue intensity (BI), in order to develop a new network of tree-ring-based temperature proxy records across the mid-latitudes of North America. This dissertation, which heavily relies on the fundamental tree-ring principle of limiting factor, utilizes high-elevation tree-ring collections derived from *Picea rubens* and *Picea engelmannii* populations across the Appalachian, United States Rocky, and Sangre de Cristo Mountain ranges to examine the relationships between numerous tree-ring metrics (total ring-width, BI, and maximum latewood density) and climatic variables in temperature-limited montane environments. This body of work illustrates the first broad-scale application of BI methods as well as the first BI-based temperature reconstructions in North America below 45°latitude. In Chapter 1, I examine and demonstrate a strong, positive, and temporally stable relationship between late-growing season maximum air temperatures and the delta BI parameter using a *P. rubens* chronology from the southern Appalachian mountains of the eastern United States. In Chapter 2, I examine the application of using BI methods to develop a late-summer maximum temperature reconstruction for the southern Rocky Mountains—a mid-latitude (*i.e.* 36 °N), arid region in North America, spanning 1735−2015 CE using a composite latewood BI (LWB) *Picea engelmannii* chronology from multiple sites across the Sangre de Cristo Mountains in northern New Mexico. The reconstruction demonstrates fluctuating warm and cool periods during the latter portion of the Little Ice Age (*ca.* 1730–1850) and also documents substantial warming over the last decade, the trend of which appears to be anomalous within the context of the past *ca.* 280 years. In Chapter 3, I demonstrate the use of LWB to reconstruct current-year growing (warm) season maximum temperatures in the low-to-mid latitudes (30°-50°N) of western North America. I detail the development of a new tree-ring network comprised of 26 LWB chronologies developed from living, high-elevation *Picea engelmannii* sampled across the western United States. From this network, I develop 4 individual temperature reconstructions, which characterize regional temperature histories across western North America from northern Mexico to southern British Columbia over the past 4 centuries. Further, I compare these 4 temperature reconstructions to highlight the spatial patterns of regional temperature trends throughout time. This body of work and the subsequent reconstructions provide important updates and increased data point density to the tree ring temperature proxy network of the Northern Hemisphere.

Additionally, I highlight the use of blue intensity methods at both low- and mid-latitude upper tree line locations to increase the presence of strongly temperature-sensitive records at increasingly lower latitudes of the Northern Hemisphere. I conclude this dissertation with a brief synthesis detailing the current state of the global BI network and the anticipated future trajectory of BI methods within the paleoclimate community.

Acknowledgements

I would first like to thank all field and laboratory assistants who contributed their time and efforts to this research. I would also like to acknowledge the instructors, participants, and staff of the North American Dendroecological Fieldweeks 2017-present.

Dedication

This work is dedicated to Danny, Mom, Dad, Charlotte, and Ken.

Table of Contents

List of Tables

List of Figures

Statement of Contribution

Chapter 1: Published

Heeter KJ[1]: conceived and designed project, generated data, analyzed data, wrote manuscript, edited manuscript, corresponding author

Harley GL[2]: conceived and designed project, edited manuscript

Van De Gevel SL[3]: collected samples, edited manuscript

White PB[4]: collected samples, edited manuscript

Chapter 2: Published

Heeter KJ[1]: conceived and designed project, generated data, analyzed data, wrote manuscript, edited manuscript, corresponding author

Harley GL[2]: conceived and designed project, edited manuscript

Maxwell JT[3]: collected samples, edited manuscript

McGee JH[4]: collected samples

Matheus TJ[5]: collected samples

Chapter 3: Published

Heeter KJ[1]: collected samples, conceived and designed project, generated data, data analysis, wrote manuscript, edited manuscript, corresponding author

Harley GL[2]: collected samples, conceived and designed project, edited manuscript

Maxwell JT[3]: project conceptualization, collected samples, edited manuscript

Wilson RJ[4]: project conceptualization, collected samples, edited manuscript

Abatzoglou JT[5]: project conceptualization, edited manuscript

Rayback SA[6]: edited manuscript

Rochner ML[7]: collected samples

Kitchens KA[8]: collected samples, generated data

Chapter 1: Blue intensity as a temperature proxy in the eastern United States: A pilot study from a southern disjunct population of Picea rubens (Sarg.)

Published: Heeter KJ, Harley GL, Van De Gevel SL, White PB (2019) Blue intensity as a temperature proxy in the eastern United States: A pilot study from a southern disjunct population of Picea rubens (Sarg.). Dendrochronologia 55:105-109

1.1 Abstract

Annual surface air temperatures across the eastern United States (US) have increased by more than 1°C within the last century, with the recent decades marked by an unprecedented warming trend. Tree-rings have long been used as a proxy for climate reconstruction, but few truly temperature-sensitive trees have been documented for the eastern US, much less the Appalachian Mountains in the Southeast. Here, we measure blue intensity (BI) and ring width (RWI) in red spruce growing at the southernmost latitudinal range margin of the species on the North Carolina-Tennessee border to test the efficacy of using either metric as a temperature proxy in the eastern US. The BI and RWI chronologies spanned 1883-2008 and had an interseries correlations of 0.42 and 0.54, respectively, but time series were trimmed to the period 1950-2008 due to low sample depth. We discovered strong, positive, and stable correlations between both current-year early fall (September-October) T_{max} (r=0.62; p< 0.001) and T_{mean} (r=0.51; p < 0.001) and delta BI (ΔBI) during the period 1950-2008, but found no significant relationships between temperature and RWI. We show BI metrics measured in red spruce to be a promising temperature proxy for the southern Appalachian Mountain region. Future research should focus on testing [1] the efficacy of using BI on red spruce collected from across the species range, and [2] the potential for using BI as a temperature proxy in other conifers distributed in the eastern US.

1.2 Introduction

Anthropogenic activities are the foremost contributors to the increasing severity of global climate variability. Notably, annual surface air temperatures across the eastern United States (US) have increased by more than 1°C within the last century (Pachauri et al., 2014). This warming trend is expected to

continue, increasing surface air temperatures across the southern Appalachian Mountains and Southeast US by at least 2.5°C within the next century (Kunkel et al., 2013; Horton, 2014). Tree-rings have long been used as a proxy dataset for climate reconstruction. However, there are few reported tree-ring proxies of temperature in the eastern US (*e.g.* Cook and Johnson 1989; Pearl et al. 2017), and none for the Southeast. Red spruce (*Picea rubens* Sarg.) is a common conifer species in the eastern US, with a core distribution in the northeastern US and Canada, and small, disjunct populations extending down to the highest-elevations of the southern Appalachian Mountains on the North Carolina-Tennessee border. These low-latitude, disjunct populations of climate refugia species left over after the last glacial period–such as red spruce–could be critically important for providing a historical context for past temperatures.

In recent years, Blue Intensity (BI) metrics have been refined and increasingly integrated into the field of dendroclimatology (McCarroll et al., 2002; Björklund et al., 2014; Rydval et al., 2014; Wilson et al., 2014; Dolgova, 2016). However, most BI studies are focused on high-latitude species. In the northeastern US, maximum latewood density (MXD) was used successfully to reconstruct summer monthly temperatures (Conkey, 1986; Briffa et al., 1992). Delta BI (ΔBI; the difference of latewood BI and earlywood BI, which has comparable temperature correlations to MXD (*e.g.* Björklund et al. 2015), offers an efficient and cost-effective alternative for reconstructing temperature. To date, no BI-derived temperature proxies have been explored for the eastern US. In this paper, we demonstrate successful use of ΔBI as a temperature proxy using red spruce growing at the southern range limit for the species. Given the extensive distribution of red spruce from North Carolina/Tennessee into Canada, we highlight the potential of using BI techniques to produce temperature reconstructions across the eastern US (Figure 1.1).

1.3 Methods

1.3 Study area

Tree-ring samples for this study were collected from Roan Mountain, North Carolina/Tennessee, US (36.10°N, 82.13°W; Figure 1.1). The Roan Mountain area covers approximately 19 km^2 of the southern Appalachian Mountains and is located in the Blue Ridge physiographic province. Roan Mountain elevation ranges between 786 and 1916m, and the area is classified as Cfb (marine temperate climate) under the Köppen climate classification system (White et al., 2012). Soils are well-drained Inceptisol loams that form on steep, rocky slopes and ridge tops. Overstory species composition is heavily dominated by red spruce and Fraser fir (*Abies fraseri* (Pursh) Poir.), with notable presence of associate species such as yellow birch (*Betula alleghaniensis* Britt.), mountain maple (*Acer spicatum* Lam.), and American beech (*Fagus grandifolia* Ehrh.) (White et al., 2012).

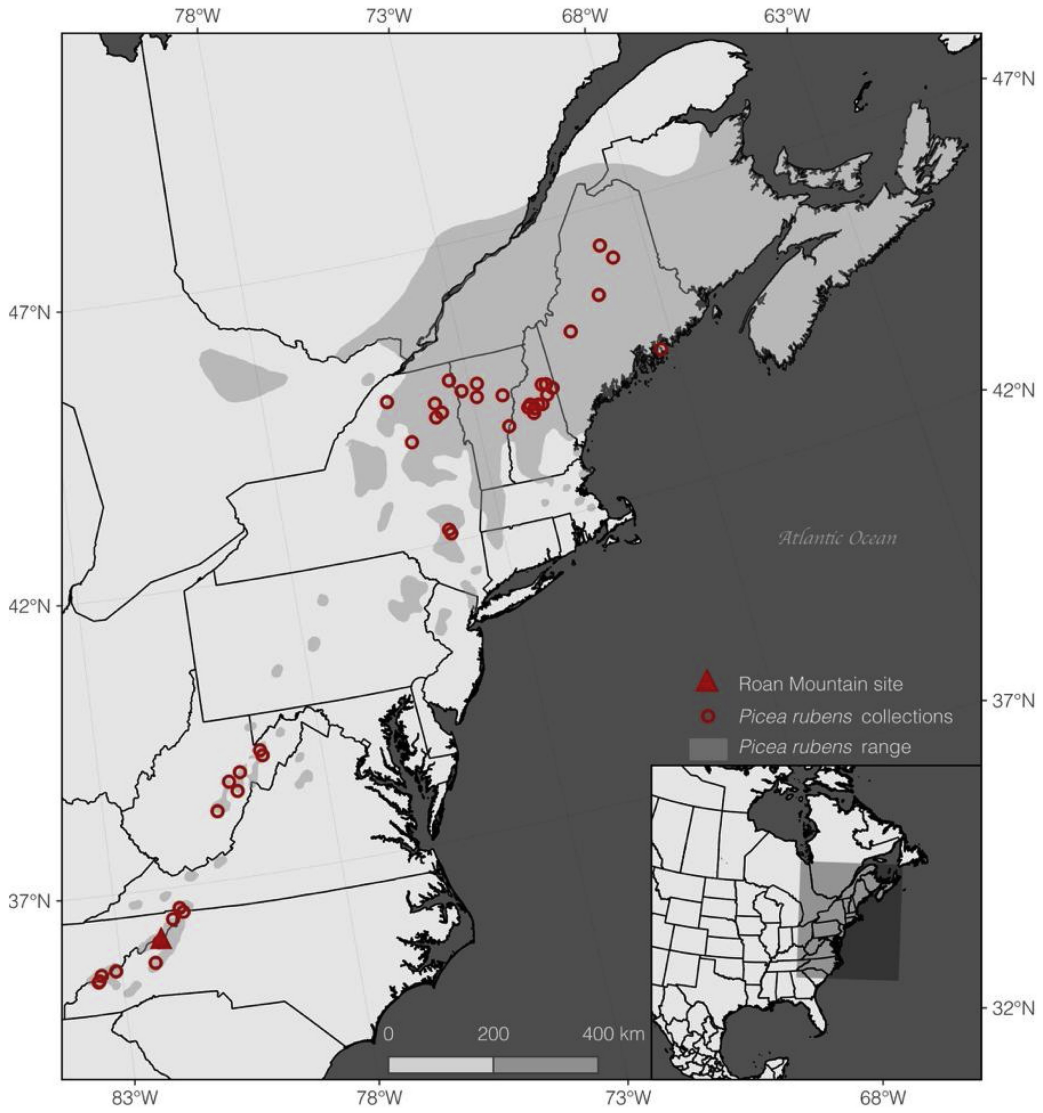

Figure 1.1: Historical range (gray polygon; Little and Viereck 1971) of red spruce (*Picea rubens* Sarg.) in North America shown with the location of the Roan Mountain, North Carolina/Tennessee, USA study site (this study; triangle) and previously-documented locations of red spruce tree-ring collections (circles) in the literature and/or on the International Tree Ring Data Bank.

1.3 Sample selection

In 2008, increment cores were collected from red spruce within six high elevation (>1800m) circular 0.05ha fixed-radius (12.66m) plots (separated by at least 100m) as part of a study detailed in White et al. (2012). All plots were downslope from the ridgeline and predominately on the south-eastern aspect. Samples were collected as close to the root-shoot interface to obtain the maximum amount of growth rings for each individual (Fritts, 1976). For the purposes of this study, we selected increment cores from

White et al. (2012) that [1] derived from canopy dominant trees, [2] contained the greatest number of growth rings, and [3] exhibited minimal disturbance trends in ring-width patterns.

1.3 Chronology development

Red spruce cores were first mounted, then progressively sanded to 1000 grit (Speer, 2010). We scanned all samples at 2400 dpi on an Epson Expression XL 12,000 scanner using an IT8.7/2 calibration card coupled with 89 Silverfast software to ensure reproducibility. After calibration, we delineated rings and obtained ring-width (RWI) and ΔBI data using CooRecorder (Larsson, 2014). Although we investigated multiple BI metrics (i.e. earlywood maximum reflectance, latewood minimum reflectance (LWBI)), we used the ΔBI metric because it greatly reduces the inherent bias of BI data resultant from potential inter-ring discoloration (Björklund et al., 2013).

All samples were crossdated visually, then checked using the software COFECHA (Holmes, 1983). After examining the effects of both the age-dependent and 2/3 spline interactive detrending approaches, we ultimately detrended both the red spruce RWI and ΔBI series using the Signal-Free (SF) detrending approach (Melvin and Briffa, 2008) with a 2/3 spline to produce chronologies with less bias in the mid-lower frequencies. Because the increment cores selected for analysis were of similar age, the 2/3 spline proved a better fit compared to the age-dependent spline. Further, initial climate-growth correlation tests with both the 2/3 and age-dependent spline chronologies revealed similar but stronger agreement between temperature data and the 2/3 spline chronology. We used the expressed population statistic (EPS) to assess the signal strength of all detrended series.

1.3 Climate analysis

We tested Pearson correlation coefficients between the RWI and ΔBI and temperature datasets temporally using the TreeClim package in R (Team et al., 2013; Zang and Biondi, 2015) and spatially using the KNMI Climate Explorer (Trouet and Van Oldenborgh, 2013). We performed our statistical tests using mean (T_{mean}) and maximum (T_{max}) monthly temperatures from the Parameter-elevation Relationships on Independent Slopes Model (PRISM) (Daly et al., 1994) surface temperature dataset at 4k resolution and taken from the Roan Mountain region (36.21-35.17°N, 82.09-81.05°W). Correlations were calculated over the 1950â2008 period based on the low sample depth and EPS prior to 1950. We used TreeClim to test for signal stability using forward moving interval correlation analysis (c.f. Saladyga and Maxwell 2015).

1.4 Results

We selected 52 red spruce increment cores out of the 286 total cores collected by White et al. (2012) based on the radial growth parameters provided in the Methods section. The ΔBI chronology spanned the period 1883-2008 and had an interseries correlation of 0.42. However, sample depth and thus EPS dropped below 0.85 at the year 1949, so the final ΔBI time series used for analyses spanned 1950-2008 (Figure 1.2A). The RWI chronology spanned 1883-2008 with an intersersies correlation was 0.54 and had an EPS value of > 0.85 during the period 1904-2008. For comparison purposes, we used the common period of both chronologies, 1950-2008, for subsequent analyses.

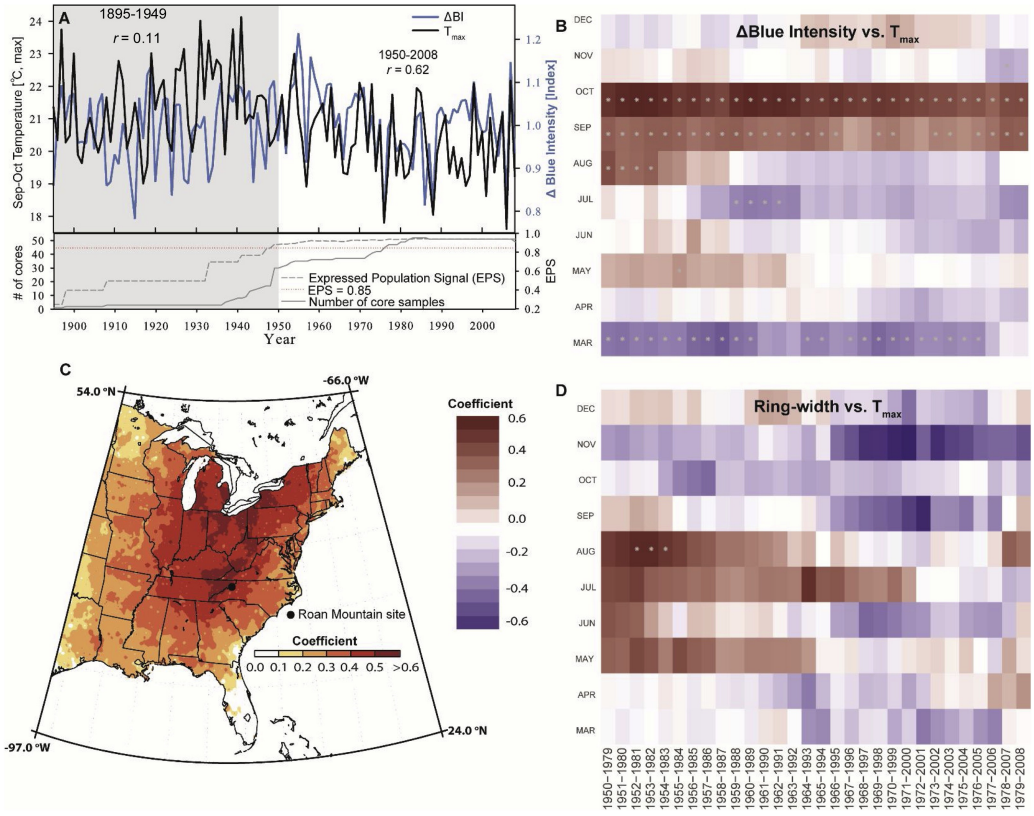

Figure 1.2: (A) Relationship between the red spruce (*Picea rubens* Sarg.) delta blue intensity (ΔBI) chronology (blue) from Roan Mountain, North Carolina/Tennessee (n=52) and 4k PRISM Sep-Oct maximum temperature (T_{max}; °C; black) values taken from the region: 36.21-35.17°N, 82.09-81.05°W during the period 1950-2008. (B) Forward moving monthly correlations during the 1950-2008 period between the ΔBI chronology and Sep-Oct T_{max}. (C) Spatial correlations between gridded 4k PRISM Sep-Oct T_{max} during the period 1950-2008 and ΔBI. (D) Forward moving monthly correlations during the period 1950-2008 between RWI and Sep-Oct T_{max}.

We tested a number of BI metrics and discovered the strongest correlations between the temperature data and ΔBI. We found current-year early fall (September-October) T_{max} ($r = 0.62$; $p < 0.001$) and T_{mean} ($r = 0.51$; $p < 0.001$) were positively correlated with ΔBI during the period 1950-2008 (Figure 1.2A; results for T_{mean} not shown). We also found strong agreement between LWBI and Sep-Oct T_{max} ($r = 0.51$; $p < 0.001$) and T_{mean} ($r = 0.54$; $p < 0.001$). Agreement between ΔBI and both T_{max} ($r = 0.11$; $p > 0.10$) and T_{mean} ($r = 0.10$; $p > 0.10$) dropped significantly prior to 1950 due to a decrease in the number of samples. Temporally, the stability of the ΔBI-T_{max} and ΔBI-T_{mean} relationships were strong for the months of September and October from 1950 to 2008 (only T_{max} shown Figure 1.2B). Spatially, Sep-Oct T_{max} showed the highest seasonal correlation values ($r > 0.60$), as we found Roan Mountain red spruce to be spatially representative of maximum temperature centralized along the southern Ridge and Valley and Blue Ridge provinces and extending north through the Piedmont and Appalachian Plateau to the Adirondack Mountains (Figure 1.2C). Our analysis showed no significant correlations between RWI and T_{max} ($r = 0.11$; $p > 0.10$) or T_{mean} ($r = 0.02$; $p > 0.10$) (for comparison, RWI-T_{max} shown in Figure 1.2D).

1.5 Discussion

In the context of impending temperature increase during the next few decades, tree-ring based reconstructions- which provide valuable information about regional to hemispheric climate history- allow for a better understanding of climate variability over time and enable us to place the current warming trend into historical context. Our study shows BI analysis performed on red spruce growing on Roan Mountain, North Carolina/Tennessee to be a viable method for assessing temperature variability for the southern Appalachian Mountain region. As a result of the logging legacy visible through much of the Appalachian region (*e.g.* White and Cogbill 1992), our sample population was young, even-aged, and overall limited by a lack of older individuals (*e.g.* > 60 years). This demonstrated that generally, more BI samples are needed to carry the overall population signal compared to RWI (c.f. Rydval et al. 2014; Wilson et al. 2014). Hence, over-sampling and targeting older individuals is a practice that should be noted as application of BI extends throughout the eastern US.

To our knowledge, this study is the first to formally document the efficacy of using ΔBI as a temperature proxy in the eastern US. Our results suggest that ΔBI has a strong relationship with instrumental temperature data compared to RWI, and thus should be investigated elsewhere in viable conifers across the eastern US. Previous studies correlating RWI and temperature in the eastern US (*e.g.* McLaughlin et al. 1987; Johnson et al. 1988; Webster et al. 2004) have related unstable climate-growth relationships to the dendroecology and decline of red spruce throughout its range, and Roan Mountain red spruce

shows similar results. Yet, Pearl et al. (2017) provide a robust and skillful temperature reconstruction for the northeast US using RWI of Atlantic white cedar (*Chamaecyparis thyoides* L.), which like red spruce, exhibits a unique distribution characterized by range disjunctions and climate refugia.

For red spruce, RWI is likely more heavily influenced by residual signal noise from ecological disturbances (*e.g.* White et al. 2012, 2014), and therefore, requires more vigorous detrending methods (*e.g.* Cook and Jacoby 1977; Conkey 1979; Pederson et al. 2004) than ΔBI data. White et al. (2014) observed a general decline in red spruce RWI from the Roan Mountain site starting in the 1960s and continuing until *ca.* 1990. They attributed the decline in RWI to the possible effects of acid deposition, which has been shown to be a potential contributor to overall red spruce decline throughout the region (*e.g.* Johnson and Siccama 1983; Adams and Eagar 1992; Soulé 2011). We did not observe this apparent decreasing trend in ΔBI as reported for RWI by White et al. (2014).

Because we performed our study on individuals located at the southern range limit for red spruce, similar if not stronger results should be found within higher-latitude portions of the range. Further, future investigations should focus on testing the efficacy of using other conifer species distributed across the eastern US for a temperature signal via BI. Yet, discoloration (*e.g.* resin pocket, blue stain: *Grosmannia clavigera*) is one of the greatest sources of bias and error in BI analysis (Rydval et al., 2014). We observed a lack of visual pigment variation between the heartwood and sapwood in red spruce collected from the Roan Mountain site. Additionally, we observed an overall absence of discoloring resins in cores. This combination of favorable wood characteristics ultimately allowed us to analyze our cores without the need of any color-removing sample preparation such as ethanol or acetone treatments (Rydval et al., 2014), but this might not be the case with other conifers tested in the eastern US.

Although our overall ΔBI chronology was short and did not extend beyond the observed period (*ca.* 1895), we demonstrate the potential to extend the BI network throughout other portions of the species range (Figure 1.1) using extant collections. Numerous red spruce chronologies on the International Tree Ring Data Bank, many of which extend back to the 16$^{\text{th}}$ century, may prove valuable for reconstruction models. Future research should focus on filling the spatial gaps in temperature proxies throughout the eastern US by testing [1] the efficacy of using ΔBI on red spruce collected from throughout the species range, and [2] the potential for using ΔBI, or other BI metrics (*e.g.* LWBI, earlywood maximum reflectance), as a temperature proxy in other conifers, such as Fraser fir, eastern hemlock (*Tsuga canadensis*), Carolina hemlock (*Tsuga caroliniana*), Atlantic white cedar (*e.g.* Pearl et al. 2014), black spruce (*Picea mariana*), and balsam fir (*Abies balsamea*).

1.6 Acknowledgements

We thank initial conversations with Dr. Rob Wilson for the inspiration to investigate blue intensity in the eastern US, and conversations with Dr. Justin Maxwell and Dr. Stockton Maxwell regarding this paper. This study was funded by the University of Idaho and further supported by the Department of Geography and Planning at Appalachian State University. We thank Dr. Pete Soulé for assistance with red spruce data collection. We thank two reviewers for offering suggestions that improved earlier drafts of this manuscript.

Chapter 2: Late summer temperature variability for the Southern Rocky Mountains (USA) since 1735 CE: Applying blue light intensity to low-latitude *Picea engelmannii* Parry ex Engelm.

Published: Heeter KJ, Harley GL, Maxwell JT, McGee JH, Matheus TJ (2020) Late summer temperature variability for the Southern Rocky Mountains (USA) since 1735 CE: applying blue light intensity to low-latitude Picea engelmannii Parry ex Engelm. Climatic Change pp 1-24

2.1 Abstract

Our study examines the application of using blue intensity (BI) methods to develop a late-summer maximum temperature (T_{max}) reconstruction for the Southern Rocky Mountains—a mid-latitude (*i.e.* 36 °N), arid region in North America. We reconstruct Aug−Sep (AS) T_{max} for the period 1735−2015 CE using a composite latewood BI (LWB) Engelmann spruce (*Picea engelmannii* Parry ex Engelm.) chronology from multiple sites across the Sangre de Cristo Mountains in northern New Mexico, USA. This study presents the first BI-derived temperature reconstruction for the lower mid-latitudes (30–45°N) of North America. We compare the climate response of multiple tree-ring parameters: latewood BI (LWB), earlywood BI (EWB), ΔBI (earlywood BI minus latewood BI), ring width (RW), and maximum latewood density (MXD). Of all parameters, the site-composite LWB and ΔBI chronologies show the strongest correlations with AS T_{max}. Reconstructed AS T_{max} demonstrates fluctuating warm and cool periods during the latter portion of the Little Ice Age (*ca.* 1730–1850) and pronounced warming through the early to mid 20^{th} century (*ca.* 1920–1950s). The reconstruction also documents substantial warming over the last decade, the trend of which appears to be anomalous within the context of the past *ca.* 280 years. We highlight the potential for BI methods to be successfully used at high elevation, mid-latitude locations where temperature proxy datasets are scarce or non-existent. As many places across the mid-latitudes lack contiguous, temporally-resolved, decadal-scale paleo-temperature proxies, we suggest here that BI methods can be effective at improving the spatial gaps in the Northern Hemisphere temperature proxy network.

2.2 Introduction

Climate change is one of the foremost drivers of ecosystem modification (Mooney et al., 2009) and imposes increasing vulnerabilities on both human and natural communities (Thornton et al., 2014). As much of our understanding of climate change relies heavily on the assessment of instrumental data limited to the modern era, proxy datasets are useful tools for better understanding the effects of human influence on climate variability over longer temporal scales. Warming surface air temperatures over the last century are one of the most widely documented effects of climate change globally (Jones et al., 1999). In North America, increasing annual surface air temperatures are particularly pronounced in the American Southwest and Southern Rocky Mountains region of the United States (US), where in some areas, average surface air temperatures have increased upwards of 0.6 °C over the last decade (Blunden and Arndt, 2016). As this warming trend is expected to continue, mean surface air temperatures are projected to increase across the region by at least 2.5 °C within the next 30 years (Garfin et al., 2014). In 2019, instrumental records documented anomalously warm summer (June–August) mean temperatures across the southwest US. In August 2019, Utah, Colorado, and New Mexico all experienced the warmest monthly mean temperatures on record (NOAA 2019). The implications of the current warming trend are particularly challenging in the southwest US, one of the driest regions of the country, where the sustainability of both human and natural systems rely on water resource availability. The southwest US has one of the fastest growing regional populations that is projected to increase 68%, reaching to 94 million by 2050 (Jardine et al., 2013). In a region that is expected to only get hotter and drier, projections suggest that increased heat, coupled with changes to warm- (*e.g.* rainfall) and cool-season (*e.g.* snowpack) precipitation, will drastically affect the lives and economies of over 56 million people.

Recent advances in dendrochronology have allowed for the development of temperature reconstructions of varying spatial scales, ranging from local to hemispheric. Tree-ring based temperature reconstructions were historically accomplished using instrumental data in combination with chronologies developed from tree-ring parameters such as tree-ring width (RW) or maximum latewood density (MXD). In North America, the majority of tree-ring derived temperature reconstructions originate from high latitudes (>50°N), where temperature is expected to be the greatest limiting factor on tree growth (Jacoby and D'Arrigo, 1989; Briffa et al., 1992, 2001; Davi et al., 2003; Anchukaitis et al., 2013; Wiles et al., 2014; Wilson et al., 2016). However, the development of MXD and RW networks in the mid-latitudes of the continental US throughout the late 1980s and 1990s (*e.g.* Briffa et al., 1988, 1992; Schweingruber et al., 1993; Schweingruber and Briffa, 1996) increased the density of chronologies which allowed for reconstruction of summer temperatures across portions of the previously under-represented areas of North America. Networks of

tree-ring derived climate proxies, which often also allow for longer-term reconstructions of precipitation and temperature, are necessary to better understand regional spatial patterns of ecosystem response to climate change. As chronology networks are important for examining current and past climate over large spatial extents, they must be updated regularly to account for the most recent decades and added to in places where the spatial representation of local climate variables by tree ring parameters is weak or non-existent (Schneider et al., 2015; Stoffel et al., 2015; Wilson et al., 2016). Despite the fact that MXD is a robust parameter for reconstructing past summer temperatures, only a few MXD-derived paleoclimate endeavors have been accomplished within the continental US compared to within Europe, Canada, and the Alaskan US. Compared to ring-width, substantially fewer millennial length MXD records exists for North America (*e.g.* Luckman and Wilson, 2005), especially in in the low to mid-latitudes. The high cost associated with producing tree-ring densitometry data is often prohibitive to research institutions. This, in combination with time-consuming laboratory sample preparation requirements, are likely deterrents to conducting rigorous, widespread updates to existing MXD chronologies so that they account for warming trend since *ca.* 1990.

In attempts to remedy the issues relating to the time and cost-intensive nature of generating MXD data, the application and skill of alternative tree-ring parameters for temperature reconstructions are increasingly being evaluated. In recent years, refinement of blue intensity (BI) methods have allowed for the development of a temperature-responsive, alternative tree-ring parameter to MXD (McCarroll et al., 2002; Campbell et al., 2007; Björklund et al., 2014; Rydval et al., 2014; Wilson et al., 2014; Linderholm et al., 2015). Early development of BI methods emphasized the use of imaging analysis techniques to examine wood density properties, with the hypothesis that a strongly-coupled relationship between reflected visible light in the blue wavelengths and wood density allowed the former to act as a surrogate parameter for the latter (McCarroll et al., 2002). Sheppard et al. (1996) first demonstrated the successful use of reflected light brightness values across earlywood and latewood to reconstruct temperature. As late summer temperatures were found to be influential on the lignification of the secondary cell wall (Gindl et al., 2000), and shorter radiation wavelengths are more readily absorbed by lignin, the strongest association was identified between MXD and brightness resulting from the blue spectrum (McCarroll et al., 2002). Refinement in the analysis of blue spectrum reflected light and standardization of laboratory methods have resulted in the latewood blue intensity (LWB) parameter producing consistently comparable correlations to temperature as MXD (*e.g.* Björklund et al. 2015). Further, LWB offers a more time-efficient and cost-effective alternative to MXD for reconstructing temperature (Björklund et al., 2019). Despite these advantages over MXD, most BI studies to date are primarily geographically restricted to the high-latitudes. Given that BI methods are relatively new and still in an experimental phase, more

studies are needed to evaluate the applicability of BI methods across different regions, especially at high elevation, low latitude locations, where certain tree species still produce consistent annual growth rings (*e.g.* Brookhouse and Graham 2016; Buckley et al. 2018; Heeter et al. 2019). To date, no published BI data exist within the non-Alaskan continental US, and temperature-proxy data is especially spatially and temporally limited at high elevations in the mid-latitudes (30–50°N). Further, only a few attempts have been made to reconstruct temperature using tree-ring parameters in the arid southwest US (Briffa et al., 1992; Schweingruber and Briffa, 1996; Salzer and Kipfmueller, 2005). If BI methods can be successfully used to reconstruct summer temperatures in places where MXD records are either absent or temporally limited, this technique may improve the incomplete spatial and temporal coverage of paleoclimate records across North America and elsewhere.

We identified the Southern Rocky Mountains region of the US (southern Colorado, northern New Mexico) as a prime area to evaluate novel methods of developing tree-ring based climate reconstruction for a variety of logistical and environmental reasons. The Southern Rocky Mountains has adequate spatial and continuous temporal coverage of instrumental station data capable of documenting temperature trends since the turn of the 20$^{\text{th}}$ century. Additionally, the complex relief of the southwest US allows for local dominance and persistence of many long-lived, temperature-limited tree species growing at high elevation (>3000 m). Similar to how they perform at high latitudes, temperature proxies have historically been most successful at high altitudes, where inter annual climate variability strongly influences tree growth as the limiting factor (Fritts, 1976). Because of its persistence at high elevations and latitudes, Engelmann spruce (*Picea engelmannii* Parry ex Engelm.) has been shown to be an exceptional species for developing climate reconstructions from tree ring data (Parker and Henoch, 1971; Wilson and Luckman, 2003). This long-lived (>600 yrs), shade-tolerant, canopy-dominant species occupies a range extending from British Columbia in the north, through the western US, and becomes disjunct at the southern range extent in south-central New Mexico (NM). At its southern range periphery, Engelmann spruce becomes less dominant, as its distribution becomes more scarce and is limited to near tree line (Alexander and Sheppard, 1984). Engelmann spruce habitat is typically characterized as humid with long, cold winters and short, cool summers, with heavy snowfall and extreme temperature ranges. This habitat is considered one of the highest-elevation and coldest forest environments in the non-Alaskan continental US.

In this study, we assess the efficacy of using BI methods within the mid-latitudes of the Southern Rocky Mountains using three Engelmann spruce sites distributed across northern NM. Our successful demonstration of the ability of the LWB metric to track late-summer maximum temperature (T_{max}) enabled us to develop a temperature reconstruction for the northern Sangre de Cristo range of north-central NM. We reconstructed late-summer (August−September) T_{max} using a composite Engelmann

spruce LWB chronology spanning the period 1735−2015. Further, we enhanced our assessment of the application of BI methods with the examination of pre-existing RW and MXD data available within our immediate study area. Our study highlights the potential of using BI methods to produce larger-area temperature reconstructions for the mid-latitudes encompassing the American Southwest and elsewhere across the western US.

2.3 Methods

2.3 Study area

Our study area comprises three Engelmann spruce sites located at the southern geographical range limit of the species within the Sangre de Cristo Mountains, northern NM: Wheeler Peak (WHE) (36.57 °N, -105.42 °W), Serpent Lake (near Jicarita Peak; JIS) (36.06 °N, -105.56 °W), and San Leonardo Lakes (SLE) (36.00 °N, -105.65 °W) (Little and Viereck 1971; Figure 2.1). The sampling elevation at the WHE and JIS sites was between 3400 and 3600 m, which was at or near treeline at these sites (Figure 2.1; Table 2.1). At SLE, however, steep (>40°), unstable talus slopes restricted us to sampling at 3450 m, despite treeline being located at *ca.* 3750 m. Instrumental data obtained nearest to our sample locations indicate the local climate is characterized by minimum monthly average temperatures ranging from -11.8 in January to 11.1 in July, and maximum monthly average temperatures ranging from 4.2 in January to 29.2 in July. Annual precipitation ranges from 13.9 mm in February to 52.3 mm in August (averaged 1895−2018; US Climate Data 2019). For our study region, July and August are characterized as having the highest average maximum temperatures (29.2 and 27.7 , respectively) as well as receiving the greatest amount of monthly precipitation (36 mm and 48 mm, respectively) (US Climate Data 2019).

2.3 Sample collection

At each site, we collected increment cores from the largest-diameter and oldest-looking Engelmann spruce individuals between 3500 to 4000 m elevation. All cores were extracted at breast height (1.3 m above ground surface) using a 5.0 mm diameter increment borer. We sampled two cores from each tree parallel to the contour of the slope to reduce abnormalities in ring growth (Stokes and Smiley, 1968). We targeted trees that showed minimal outward evidence of landslide, insect, or wind damage. We collected a total of 32 increment cores from 16 trees at WHE, 54 cores from 27 trees at JIS, and 44 cores from 22 trees at SLE.

2.3 MXD data compilation

We gathered the MXD raw measurement dataset for WHE from the International Tree-Ring Data Bank (ITRDB) (Briffa et al., 1992). The MXD dataset from WHE spans the period 1830-1983 and increment cores were collected from trees at 3120 m.

2.3 Chronology development

While the development of BI methods is still in relative infancy compared to MXD, and due to the fact that BI-derived data produced by different laboratories are likely to be combined across regions, the importance of ensuring methods are standardized within the context of accuracy and precision is paramount (Björklund et al., 2019). Engelmann spruce cores were dried and mounted, then sanded at 220, 400, 600, 1000 American National Standards Institute (ANSI) grit increments. Cores were finished by hand sanding with a 9 μm film (Speer, 2010). Because the Engelmann spruce wood collected at these sites is characterized by a light color and generally does not exhibit any discoloration due to heartwood/sapwood differences or resins, no chemical pigment extraction, often necessary for BI methodology, was required for our samples. Before scanning, all samples were first crossdated visually using a 40x microscope.

We first calibrated our scanner to ensure accuracy of generated BI values, then scanned all samples at 2400 dpi on an Epson Expression XL 12000 scanner using an IT8.7/2 calibration card coupled with the 89 Silverfast software to ensure replication. We scanned a total of 52 series. We conservatively excluded cores from scanning if they possessed excessive amounts of traumatic resin ducts that formed

Table 2.1: Site location and chronology (ring-width(RW), blue intensity (BI), maximum latewood density (MXD)) information for the Wheeler Peak (WHE), Serpent Lake (JIS), and San Leonardo Lakes (SLE) study sites within the Sangre de Cristo Mountains, northern NM. Maximum Latewood Density (MXD) information from Briffa et al. 1992.

	WHE	**JIS**	**SLE**
Latitude(°N)	36.65	36.06	36.00
Longitude(°W)	105.42	105.56	105.65
Sampling elevation(m)	3600	3600	3450
RW: #cores (trees)	26 (16)	27 (20)	18 (13)
RW: Full period	1667−2015	1637−2014	1653−2015
BI: #cores (trees)	26 (16)	27 (20)	18 (13)
BI: Full period	1667−2015	1637−2014	1653−2015
MXD: Elevation	3120	−	−
MXD: #cores(trees)	20(10)	−	−
MXD: Full period	1830−1983	−	−
MXD: Elevation	3120	−	−

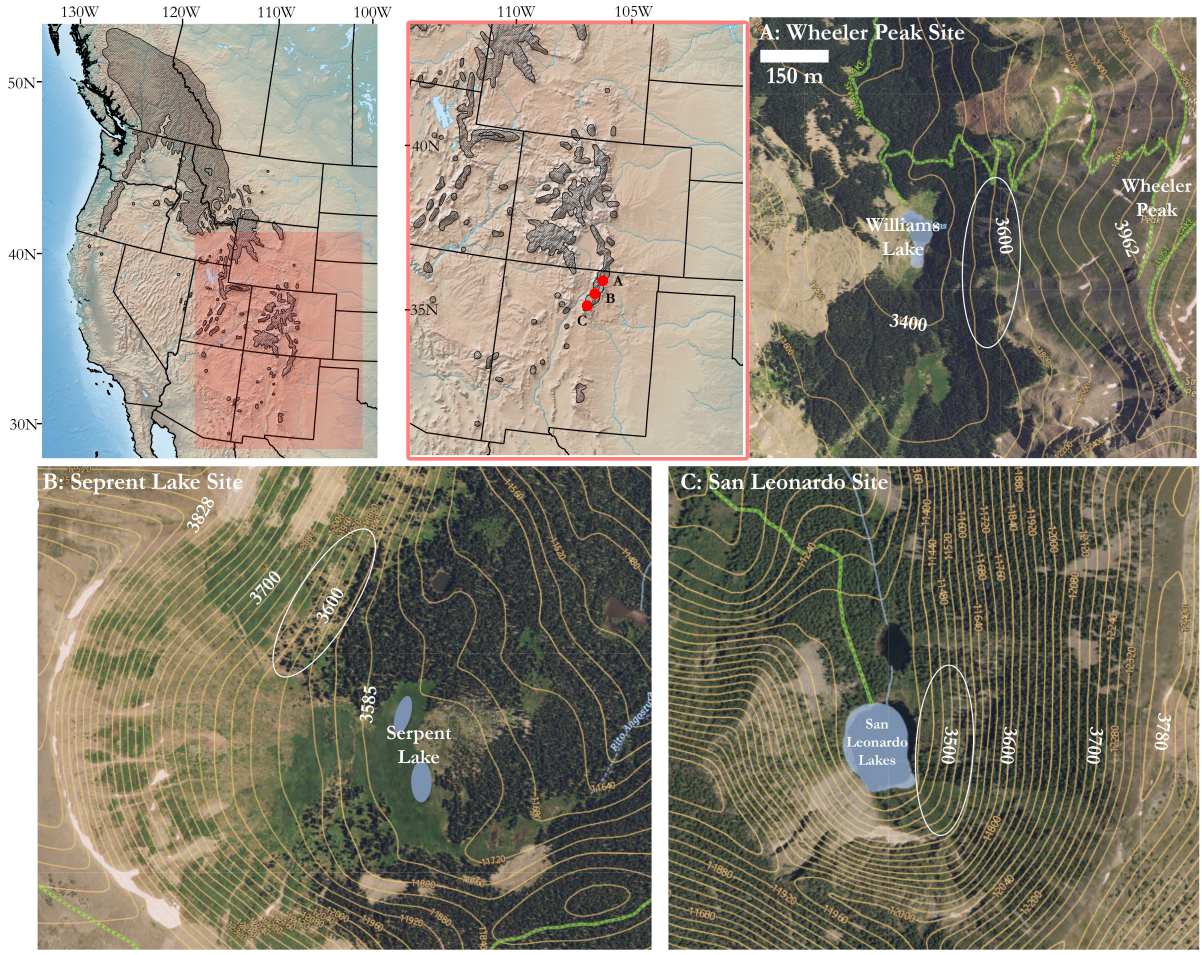

Figure 2.1: Map showing the locations and topographic settings (contours) of the three Engelmann spruce sites sampled for blue intensity, including (A) Wheeler Peak (WHE), (B) Serpent Lake (JIS), and (C) San Leonardo Lakes (SLE) site within the Sangre de Cristo Mountains, NM located at the southern range limit for the species (grey polygon; Little and Viereck 1971). Approximate tree sampling locations and elevations at each site are circled. Green lines in panels A-C represent hiking trails.

across the entire radial width of an annual ring, because a failure to avoid these cellular abnormalities results in inaccurate blue reflectance values. We also excluded cores that had continuous blue fungal stain. Although initial field sample collection was specifically designed to target the oldest trees with no outward obvious signs of insect, landslide, or wind damage, all agents which increase the likelihood of these types of wood abnormalities, we still removed between two and four cores from each site dataset for this reason. After cores were scanned, we delineated growth ring boundaries using automated detection in the program CooRecorder (Larsson, 2014) to generate RW values to the nearest 0.001 mm precision.

After obtaining RW measurements, we checked our dating accuracy using the software COFECHA (Holmes, 1983). Once we were confident that all samples were accurately dated, we collected BI values

using the CooRecorder software program. We modified BI collector settings in CooRecorder to collect raw latewood BI (LWB) and ΔBI data. Although Engelmann spruce collected from our sites did not show any sapwood/heartwood color changes, we decided to collect and examine the ΔBI metric to further explore the climate response and relationship between ΔBI and LWB. Because samples exhibited moderate age-related trends, we detrended the Englemann spruce RW, MXD, LWB, and ΔBI series. Since raw LWB is negatively correlated with MXD, we inverted the raw LWB data to allow for detrending of the data by methods similar to those used for MXD data (Rydval et al., 2014). We initially used interactive detrending to examine the effects of various conservative smoothing splines within the Signal-Free detrending (SFD) (Melvin and Briffa, 2008) framework (Figure S.1). All series were standardized using the power transformed residuals. We detrended the ΔBI data similarly to the LWB data, because the calculation of this metric inherently results in a positive correlation between inverted LWB and ΔBI (Wilson et al., 2017a). We ultimately detrended the RW, BI, and MXD data using the age-dependent spline (ADS) (Melvin et al., 2007) within the SFD framework, because the AD-spline produced the best curve fit to the data. This combination also best reduced the medium-frequency distortion (*e.g.* over-exaggeration) at the beginning and end segments of our chronologies (*e.g.* the 21st century climate warming trend) resulting from the curve-fitting process. Similar to this study, Wilson et al. (2019) also apply this detrending approach to both RW and LWB for the purpose of examining relationships between growth/density and summer temperatures. We used the expressed population signal (EPS; Wigley et al., 1984) with an arbitrary threshold of 0.80 to help evaluate the quality of our chronologies and to determine the period over which we had sample replication adequate for developing a reconstruction.

2.3 Climate Response

We used Pearson correlation analysis to test temporal relationships between temperature data and RW, MXD, EWB, LWB, and ΔBI data using the TreeClim package in R (Zang and Biondi, 2015). Further, we used the KNMI Climate Explorer (Trouet and Van Oldenborgh, 2013) to assess spatial correlations between temperature data and RWI, MXD, EWB, LWB, and ΔBI data. We performed these tests using monthly maximum and mean (T_{max}; T_{mean}) temperatures from the Parameter-elevation Relationships on Independent Slopes Model (PRISM) (Daly et al., 1994) surface temperature dataset at 4k resolution and averaged over the Southern Rocky Mountains (37.25–35.90 °N, 104.15–106.05 °W). Prior examination of all tree-ring metrics (RW, MXD, and BI metrics) with minimum temperature indicated either no or very weak significant relationships, thus, we excluded minimum temperature as a variable in any subsequent analysis for this study. We chose to use PRISM data because this gridded data product adequately provides high spatial resolution monthly temperature data that performs well in regions characterized by

complex terrain, such as in the heavily-dissected landscapes of the Southern Rocky Mountains. While PRISM pulled temperature data from multiple stations in the region (Table S.1), the primary source of temperature data pulled into the PRISM model for the area encompassing our sample area is the Red River station (36.17 °N, 105.40 °W). This rural station, situated in the cool conifer mountain terrain at 2644 m, provides temporally reliable and consistent temperature data from 1906 to 2015. Correlations were calculated over the period 1895-2015. We tested for signal stability by performing forward moving interval correlation analysis using TreeClim (Zang and Biondi, 2015). We assessed the spatial homogeneity between the three site chronology signals using principal component analysis (PCA) across all series over the well-replicated common period (1735–2015). Further, we examined the spatial loadings of the individual chronologies based upon the most prominent principal component (*e.g.* Wilson et al., 2007b).

2.3 Climate Reconstruction

We chose a principal components regression (PCR) technique to reconstruct late summer maximum temperatures (AS T_{max}) for the Southern Rocky Mountains. We initially pre-whitened the BI data and temperature data to provide a conservative estimate of BI-climate relationships that did not exhibit inflation due to auto-correlation. We used three correlation tests—Pearson, Robust Pearson, and Spearman—to examine the BI-climate relationships and retained chronologies that were significantly (p <0.01) related to AS T_{max} over the common period (1907-2015). For BI series which were significant, their original, non-pre-whitened chronologies were included in the PCR. Following the Kaiser-Guttman rule (Guttman, 1954; Kaiser, 1960), we retained the first n eigenvectors with eigenvalues >1.0 for the multiple regression. We determined the final subset of PCs by using the minimum Akaike information criterion (AIC), which includes a penalty term for increasing the number of predictors in the model (Akaike, 1974).

We split the instrumental period (1907-2015) into two equal periods termed the early period (1907-1961) and late period (1962-2015) to validate and cross-validate the AS T_{max} reconstruction model (Table S.5). To ensure stability over time, model validation was performed by calculating calibration statistics for the early period (1907-1961) and verification statistics for the late period (1962-2015), and vice-versa. We used two goodness-of-fit tests to validate the models: the reduction of error (RE) and coefficient of efficiency (CE) statistics (Fritts, 1976); (Cook et al., 1999). When RE values (ranges from -∞ to +1) are positive, the calibration model is a more skillful predictor of the target data than the mean of the instrumental data during the calibration period. Although CE has the same range and calculation, a positive CE value is more difficult to obtain because it relies on the verification period mean for a baseline

of predictive skill. The validation statistics produced were calibration and verification period coefficient of determination (CR^2 and VR^2), validation period reduction of error (VRE) and coefficient of efficiency (VCE), and root-mean-square error (RMSE). After successful determination that the model is time-stable, we used linear regression to estimate AS T_{max} calibrated over the full PRISM 4k instrumental period (1907-2015) with the composite LWB chronology and evaluated the model residuals for linear trends and first order auto-correlation (Durbin-Watson statistic) (Durbin and Watson, 1971).

To assess model uncertainty, we used the maximum entropy bootstrapping method (MEBoot) (Vinod et al., 2009) to produce 1,000 reconstruction replicates. We used MEBoot because it produces an empirical probability distribution for each reconstructed estimate (*e.g.* each year) on which the estimation of uncertainty is based (Cook and Kairiukstis, 2013). Additionally, MEBoot does not assume stationarity, preserves the auto-correlation structure of the time series, and calculations of uncertainty estimates for the calibration and verification statistics are semi-parametric (Cook et al., 2013b).

2.4 Results and Discussion

2.4 Signal strength and homogeneity

Individually, WHE contains 26 series, spanning the period 1667-2015 for RW, EWB, LWB, and ΔBI data (Table 2.1). MXD data for WHE contains 20 series and spans the period 1830−1983. JIS is comprised of 27 series and spans the period 1637−2014. SLE contains 18 series and spans the period 1653−2015. For each individual site, both RBAR and EPS values indicate that RW maintains the strongest common signal over the period where the EPS is >0.80 in comparison to BI and MXD (Table 2.2). The mean RBAR for RW across the three sample sites is 0.57 (ranging 0.54−0.59). For EWB, the mean RBAR is 0.27 (ranging 0.26−0.27). For LWB the mean RBAR is 0.28 (ranging 0.25−0.31), which is comparable to the EWB RBAR and the ΔBI mean RBAR of 0.31 (ranging 0.29−0.35). The mean RBAR for MXD, comprised of only one site (WHE), is 0.49.

The mean number of series from across the three sites required to meet an arbitrary EPS value of 0.80 is 3 for RW, 10 for EWB, 11 for LWB, 9 for ΔBI, and 5 for MXD. At each site, BI requires at least three times the amount of measured series than RW to meet the EPS threshold. This is consistent with other BI studies conducted in North America and Europe, which suggests that one of the caveats of BI is that it requires substantially more trees to reach the point of theoretical infinite replication and maintain a signal adequate for developing a reconstruction (Wilson et al., 2017a, 2019). The development of local networks comprised of data obtained across multiple nearby sites, such as in the case we present here, can be an effective way to overcome this problem of low sample depth. The LWB signal in the Southern Rocky

Mountains is surprisingly strong for the relatively few trees needed to reach the EPS threshold (Table 2.2). This may be attributed to increased commonality in growth response among individuals across these three study sites, or potentially be a result of increased densiometric (here, referring to the process of latewood lignification) synchrony of Engelmann spruce compared to other species (*e.g. Picea glauca*, white spruce). Similarly, the RBAR values for RW at each site are almost twice as high as those for BI. However, MXD displays superior signal commonality to BI, second to RW. Comparatively, MXD, like RW, requires fewer samples to achieve a strong common signal. The RBAR is also more comparable to RW than to any BI metric. Both EWB and the LWB have comparable signal commonality to ΔBI. This similarity can be expected due to the nature of the calculation of ΔBI, as ΔBI quantifies the difference between BI measurements collected from the earlywood and latewood zones of the annual ring.

Overall, tree-ring metrics across each site correlate strongly with one another (Table S.2). Strong, positive correlations ($p<0.01$) between metrics across different sites suggests strong spatial correspondence between overall growth and physiological response of same-species individuals at closely situated sample sites. The high level of agreement between tree-ring metrics at these three sites was the motivation to develop a composite chronology. As LWB, like MXD, acts as a representation of latewood density (Björklund et al., 2019), we should expect similar trends of cross-metric correlations between BI and RW as between MXD and RW. Under this assumption, we should expect that MXD is more highly correlated with LWB than with RW. As raw LWB data displays an inverse relationship with MXD, high correlations found between MXD and the inverted LWB is consistent with the literature. Surprisingly, the MXD taken from WHE correlates higher with JIS ΔBI ($r=0.57$) than WHE LWB or WHE ΔBI ($r=0.48$ and 0.34, respectively). This is likely a result of differences in sampling locations of WHE MXD and WHE BI/RW, as WHE MXD was collected at a significantly lower elevation (Table 2.1) and from different trees than those for WHE RW/BI. Across the three sites, SLE and JIS have the weakest positive correlation for the LWB variable. For each individual site, EWB has the weakest coupling with RW of all BI metrics, followed by LWB and ΔBI (Table S.2).

While the BI chronologies display strong signal commonality for the the most recent 200 years, they are not adequately replicated enough to meet an EPS value of 0.80 prior to 1786. The separate PCAs for RW, EWB, LWB, and ΔBI over the period $1735-2015$ revealed similar loadings for each of the four variables. The explained variance on the first eigenvector is 40.9% for RW, 30.7% for EWB, 35.3% for LWB, and 30.8% for ΔBI (Table S.3). In comparison to series originating from WHE and SLE, series from JIS load weakly to PC_1. This difference in loading is likely partially influenced by varying micro-topographical variables and JIS being the only site located on an east aspect rather than a west aspect. Based on PCA results, series from individual sites were pooled into one regional composite chronology

for RW, EWB, LWB, and ΔBI to maximize signal commonality over a longer time period. Our resulting composite chronologies for each parameter are better replicated over longer periods of time compared to individual site chronologies. Additionally, these composite chronologies allow for direct comparisons of multiple tree-ring parameters and for the better examination of various detrending techniques. While the composite chronologies extend from 1635 to 2015, chronology variants for RW, EWB, LWB, ΔBI, and MXD (Figure S.1) indicate that these composite chronologies have adequate signal commonality and sample representation (EPS>0.80) back to 1735. The composite RW chronology displays the highest amount of common signal variability (RBAR=0.33) and maintains an EPS>0.80 to 1713 (Table S.4). The LWB composite chronology shows the second highest common signal (RBAR=0.29) and maintains an EPS>0.80 to 1738.

The examination of using various detrending methods resulted in relatively similar resultant chronologies, especially in most recent 100 years, for all tree-ring metrics except for the EWB parameter. The LWB chronology shows the least sensitivity to various modes of detrending compared to all other tree-ring metrics examined in this study (Figure S.1). The $\frac{2}{3}$ and NEGEXP smoothing splines over and under-exaggerate, respectively, the end effects of the EWB chronology post-1950. All modes of detrending show the greatest amount of variability prior to 1800, where the sample depth is comparatively lower. For RW, EWB, LWB, and ΔBI, the chronology versions using the $\frac{2}{3}$ spline track the ADS variants the most similarly. From 1653 to present, the NEGEXP variants for composite RW, LWB, and ΔBI chronologies display lower mean z-scores over this period, and thus, show higher variance from 1653 to 1800 (period where EPS<0.80) than the $\frac{2}{3}$ spline and ADS variants. This exaggerated decrease in early period mean chronology values exemplifies the "end effect" artifact from applying a stiff, linear curve fit model to the data. We ultimately used a constrained ADS to minimize the loss in climate signal in the most recent period (Wilson et al., 2019). Compared to the composite RW chronology, the composite chronologies for all BI metrics show less variability over the entire period. This is consistent with other similar studies, which compare variants of RW and LWB (*e.g.* Wilson et al., 2019). The lower frequency (*e.g.* multi-decadal to centennial) signals are greatly affected by both the mode and practice of detrending (Figure S.1), as well as by innate proxy characteristics (*e.g.* changes in series length and sample depth). This notion is the impetus for further examination into the effects of combinations of such variables for continual refinement of novel methods in developing paleoclimate proxy records from natural sources (*e.g.* BI from tree rings). The EPS value intermittently waivers around 0.80 for LWB and ΔBI between 1725 and 1760 before consistently dropping below the 0.80 threshold. From here, we limit further analysis of our composite tree ring chronologies to the period 1735−2015, where we have adequate sample replication across all tree ring metrics.

Table 2.2: RBAR and the number of series needed to attain an EPS of 0.80 for all individual sample sites: Wheeler Peak (WHE), Serpent Lake (JIS), and San Leonardo Lakes (SLE). For RBAR values, all data were detrended using the Age-Dependent Spline in the Signal Free framework (AD-sf).

	WHE	**JIS**	**SLE**	**Mean**
RW RBAR	0.590	0.586	0.540	0.572
No.series EPS	3	3	4	3
Year EPS 0.80	1699	1709	1707	1705
EWB RBAR	0.259	0.262	0.274	0.265
No. series EPS	9	10	12	10
Year EPS 0.80	1800	1759	1778	1779
LWB RBAR	0.309	0.286	0.252	0.282
No. series EPS 0.80	9	11	12	11
Year EPS 0.8	1797	1768	1802	1789
ΔBI RBAR	0.294	0.350	0.295	0.313
No. series EPS 0.8	10	8	10	9
Year EPS 0.80	1804	1737	1818	1786
MXD RBAR	0.493	-	-	-
No. series EPS 0.80	5	-	-	-
Year EPS 0.80	1833	-	-	-

2.4 Climate response and regional expression

Our climate response analysis of RW, EWB, LWB, and ΔBI is conducted over the period 1907−2015, where there is continuous data from at least two individual stations within the sample region. Within the Sangre de Cristo mountain range of the Southern Rocky Mountains (37.25−35.90°N, 104.15−106.05°W), all parameters are more strongly correlated with T_{max} than T_{mean} (Table S.4. At each individual site, August and September T_{max} (AS T_{max}) consistently show the strongest relationships with both BI metrics (Figure 2.2A). The pooling of series from all sites into one regional chronology improves the climate response of all three BI metrics to AS T_{max} (Figure 2.2A). Individually, RW shows a minor positive response to AS T_{max} at JIS and SLE, but does not exhibit any significant response when pooled into the composite chronology. The lack of temperature signal of RW found here differs from signals found from RW in spruce-dominated boreal forests of higher latitude studies (*e.g.* Wilson et al. 2019; Luckman and Wilson 2005). We suggest that RW shows less of a temperature response because even though these high elevation spruce-dominated forests of northern NM are more humid than most other areas of the southwest US, the comparatively arid climate still heavily influences patterns of radial growth. We examined this further by running correlation tests for all composite chronologies against PRISM 4k precipitation data from the same spatial and temporal extents used to examine PRISM temperature data (Table S.5). Although RW is the only metric that shows a weak, positive correlation with precipitation (current and previous $year_{(-1)}$ data) over the entire 1907−2015 period, this metric does show strong,

positive correlations with $\text{May}_{(-1)}$ precipitation over the period 1980−2015 (r=0.54, p<0.01). This increasing response of RW to precipitation is coupled with decreased sensitivity to temperature in the most recent period (Figure S.4) and suggests the possibility of precipitation becoming an increasingly limiting factor on radial growth at high elevations within this region. EWB, LWB, and ΔBI show significant negative correlations with current year August precipitation. Similar to the trend seen with RW, these relationships strengthen after 1980. Here, the data suggest that changes in precipitation are increasingly influenced by changes in temperature (*e.g.* 21$^{\text{st}}$ century warming). This modern trend is well documented across other parts of the southwest US (Weiss et al., 2009; Cayan et al., 2010).

The strongest relationship with temperature exists between LWB and seasonal T_{max} (r=0.64). The regional LWB chronology is also a strong predictor of T_{mean} (r=0.54). The temperature signal of the EWB composite chronology is weaker and more spatially limited than the signals found in the LWB and ΔBI composite chronologies. Examination of EWB from these sites indicates that while the composite chronology shows significant positive relationships with both AS T_{mean} and AS T_{max} over the entire tested observational period (r=0.21 and 0.37, respectively), the temperature signal strength is spatially limited beyond the extent of the immediate study area (Figure S.3). Additionally, the EWB metric shows significant positive correlations with March T_{max} in the more recent decades (1960-present) (Figure S.4). This trend warrants further examination, as it may have important implications regarding the recent phenomenon of earlier onset of spring warming in the region, especially within the context of examining differences in the the anatomical basis for density between earlywood and latewood (*e.g.* Björklund et al., 2017). Changes to the seasonal timing and pace of spring snowmelt driven by rapidly warming spring temperatures in the latter 20$^{\text{th}}$ century is well documented across the western US (Cayan et al., 2001; Westerling et al., 2006; Cayan et al., 2010; Harley et al., 2020b). As the applicability of EWB as a dendroclimatic parameter has not yet been widely examined (*e.g.* Björklund et al., 2014, 2017; Buckley et al., 2018), future studies examining the temperature sensitivity of the EWB parameter warrant additional consideration.

To compare climate response of the WHE MXD data to the other metrics, we conducted additional analysis over a shortened period (Table S.4), which only includes the years during which MXD is represented (1907−1983). Compared to LWB, the climate response of MXD to AS T_{mean} and T_{max} is relatively low. This is consistent with results using these same MXD chronology data by Briffa et al. (2002). Strictly comparing LWB and MXD at WHE, there is a slight seasonal response difference between these two metrics. The decoupling of late-growing season temperature response between MXD and LWB is somewhat inconsistent with findings from other studies comparing climate response of MXD versus BI at higher latitudes (*e.g.* Björklund et al. 2014; Wilson et al. 2014; Björklund et al. 2015; Fuentes

et al. 2018; Kaczka et al. 2018). Instead, at WHE, MXD appears to have improved temperature response throughout the majority of the growing season (May−Aug) (Figure S.4). The difference in monthly climate response between LWB and MXD may be influenced by the ways in which each individual proxy represents lignification, as this process occurs after all radial cell growth has ceased at the end of the growing season (Gindl et al., 2000). While slight seasonal differences between the temperature response of MXD and LWB at WHE are likely due to the innate proxy characteristics themselves, we also consider the influence of differing sample locations for each proxy (*e.g.* differences in individual trees sampled, topographic position of sampled trees). For example, while both MXD and BI data originate from samples collected at WHE, MXD samples were taken from trees located at a lower elevation and different aspect. We suggest that future studies aiming to develop paleo-temperature proxies from BI methods in the southwest US should consider sampling at as high elevation as possible in order to capture the most robust temperature response from samples. Moreso, additional exploration is needed to better understand the influence of microtopography on temperature-limited trees in the the mid-latitudes of North America (*e.g.* Büntgen et al., 2008b).

We assess the temporal stability of positive relationships between PRISM 4k AS T_{max} data from the study region and RW, EWB, LWB, and ΔBI over the period 1907−2015, as well as the stability for MXD over the period 1907−1983 (Figure 2.2B, Figure S.4). Both the forward and backward moving correlation analyses indicate that the relationships between AS T_{max} and LWB and ΔBI are strong over the entire instrumental period. However, LWB shows less weakening in the relationship with temperature than ΔBI. We suspect the weakening in the ΔBI signal is likely attributed to the influence of the EWB data used for the calculation of the ΔBI data. MXD shows temporal stability similar to that of ΔBI, but only for the month of August. RW generally shows a weak and temporally-unstable relationship to T_{max} over the test period. However, RW does show a significant ($p<0.01$) negative relationship with March T_{max} in the most recent decades. RW also shows weak but significant positive correlations with August T_{max} in the early instrumental period (1910−1960) but exhibits a high degree of divergence from instrumental temperature data after 1960. We suspect that the weak and unstable RW-temperature signal is partially due to the presence of the strong previous spring precipitation signal in the composite RW chronology (Table S.5). These data suggest that warmer-than-average spring temperatures could have an increasingly negative affect on overall radial growth of Engelmann spruce at high elevations in this region, and that ring-width is not an adequate parameter for capturing and preserving a temperature signal. Further, the data support that within this region of the Southern Rocky Mountains, precipitation is becoming more of a limiting factor on radial tree growth than in previous decades.

The time stability of the composite LWB chronology over the full instrumental period is notable for this region. Unlike many of the extant RW-based chronologies encompassing the western US—including the composite RW chronology presented in this study—the composite LWB chronology does not exhibit a high degree of divergence (Wilson et al., 2007a; D'Arrigo et al., 2008) from regional temperature data in the most recent decades. As this is the first known publication of a LWB chronology published for this region, this study demonstrates the potential for this tree-ring parameter to improve the spatial resolution of temperature proxy records that adequately capture climatic trends of the most recent decades over broader regions (*e.g.* gridded network reconstructions). For example, hemispheric-scale temperature reconstructions, such as the temperature reconstruction for the Northern Hemisphere presented by Wilson et al. (2007a), used two chronologies from the mid-latitude continental US (Biondi et al., 1999; Salzer and Kipfmueller, 2005) due to the limited number of adequately temperature-responsive tree-ring chronologies in this area. While using a small number of tree-ring chronologies to accomplish a broad-scale, gridded network of temperature reconstructions may not be overly problematic due to the highly auto-correlated nature of instrumental temperature data, increasing the density of robust tree-ring based temperature proxy data sets will likely lead to sub-regional improvements in predictive skill for such reconstruction efforts. As the development and integration of BI methods at lower-latitude, temperature-limited locations continues to enhance the field of dendroclimatology, we suspect that the modern period can be adequately captured with the use of BI methods, in conjunction with MXD, to improve understandings of the temporal and spatial variability of past temperatures.

Compared to other tree ring metrics explored in this study, LWB shows the strongest and most spatially-resolved temperature signal over the entire instrumental period (Figures S.2; S.3). As expected due to the nature of the calculation, the strength and spatial distribution of correlations between ΔBI and AS T_{max} most resemble those produced by the LWB chronology. However, because we see no necessity to use the ΔBI metric due to heartwood/sapwood color homogeneity in our composite chronology series, we limit further examination of BI methods for late summer temperature reconstruction to the LWB metric. The spatial distribution of correlations produced by both the non-transformed and first-differenced versions of the composite AD-sf LWB chronology and PRISM 4k T_{max} closely resemble one another (Figure S.2). Both non-transformed and first-differenced versions of the LWB chronology demonstrate strong (r>0.50), significant (p<0.01) relationships the study area surface air temperatures, as well as with temperatures over the greater geographic area extending north-south along the Southern Rocky Mountain region (39.0−37.0 °N, 106.0−105.0 °W) of New Mexico and Colorado. While the non-transformed version of the LWB chronology shows the strongest (r>0.60) relationship with maximum temperature within the immediate study area, with the centroid of the strongest spatial correlation located along the Sangre de

Cristo range, the first-differenced chronology indicates a northward shift of the highest spatial correlations centered around the Rio Grande National Forest in southern Colorado. Additionally, the first-differenced chronology shows greater spatial smoothing and more concentric diffusion of the regional expression. Overall similarity of the non-transformed and first-differenced versions of the chronology suggests that the composite LWB record [1] is a robust and skilful representation of the regional climate, especially for AS T_{max}, and [2] maintains the regional temperature signal over the entire instrumental period, and is therefore a promising candidate to develop a reconstruction.

2.4 Climate Reconstruction

We provide a late summer maximum temperature (AS T_{max}) reconstruction for the Southern Rocky Mountains that spans the period 1735-2015 (Figure 2.3). The predictor time series in the reconstruction model is the AD-sf detrended composite LWB chronology, which is strongly and positively calibrated with the predictand data, AS T_{max}, during the instrumental period (1907−2015). The LWB chronology explains 42% of the instrumental AS T_{max} variance (R^2=0.42) from 1907 to 2015 (Figure 2.3A,B). Model performance is consistent and time-stable, with both early/late period (and vice-versa) statistics passing validation tests (Table S.6). The strongest model verification occurred by calibrating the model during the late period (1962-2015) and validating over the early period (1907-1961), which is a common finding likely due to the improved accuracy of instrumental data over time (*e.g.* Maxwell et al., 2017; Harley et al., 2017; Harley and Maxwell, 2018).

The AS T_{max} reconstruction for the Southern Rocky Mountains indicates multiple decadal-scale warming and cooling events over the past *ca.* 120 years (Figure 2.3). Comparison of our LWB-based reconstruction with other regional tree-ring based summer temperature reconstructions indicates overall general commonality of multi-decadal patterns for across many parts of Northern America (Figure 2.4). Four of the five warmest single-year anomalies occur from 1924 to 1939, and the 1930s, 1940s, and 1950s all rank as the 2nd, 1st, and 3rd warmest decades, respectively (Figure 2.4, Table S.7). The warmest decadal anomalies from our reconstruction show agreement with other regional summer temperature reconstructions. The two warmest decadal anomalies (1930s and 1940s) are also within the top five warmest decadal anomalies of reconstructions by Briffa et al. (1992); Trouet et al. (2013); Wilson et al. (2014, 2019) (Figure 2.4). The coldest decadal anomalies from our reconstruction also closely align with those from the (Wilson et al., 2019) LWB-based reconstruction, placing the 1760s, 1810s, and 1830s as the three coldest decades. In particular, the MXD-based reconstruction presented by Briffa et al. (1992) shows the most similarity of multi-decadal trends (r=0.53, p<0.01) over the common reconstructed period. This should

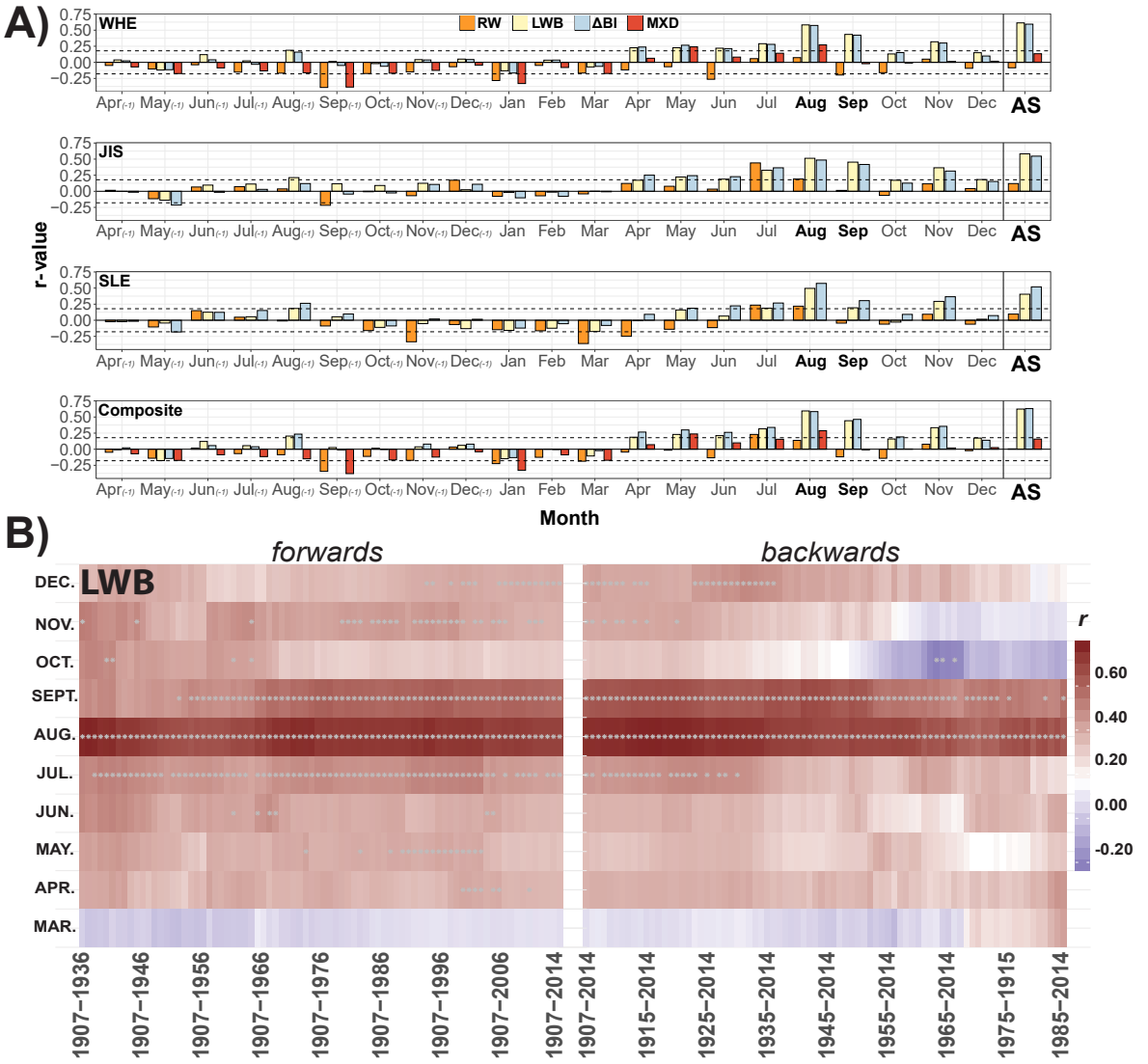

Figure 2.2: A) Monthly climate response of tree ring metrics: RW, LWB, ΔBI, and MXD to regional PRISM 4k T_{max} data for both the individual sites (WHE, JIS, SLE) and for the AD-sf detrended composite chronologies from previous year April ($Apr_{(-1)}$) through current year December. Climate response is calculated from previous year April ($Apr_{(-1)}$) to current year December over the period (1907−1983), and dashed line represents α=0.05; B) Forward and backward (evolutionary) moving correlation (gray dots represent α=0.05) of composite LWB chronology and regional PRISM 4k AS T_{max} over the period 1907−2015.

be expected due to the regional overlap between our reconstruction and the one presented by Briffa et al. (1992).

Late summer temperature conditions during the 20th and 21st centuries are most notable in the reconstruction from the Southern Rocky Mountain Region (Figure 2.4). The 20th century is characterized

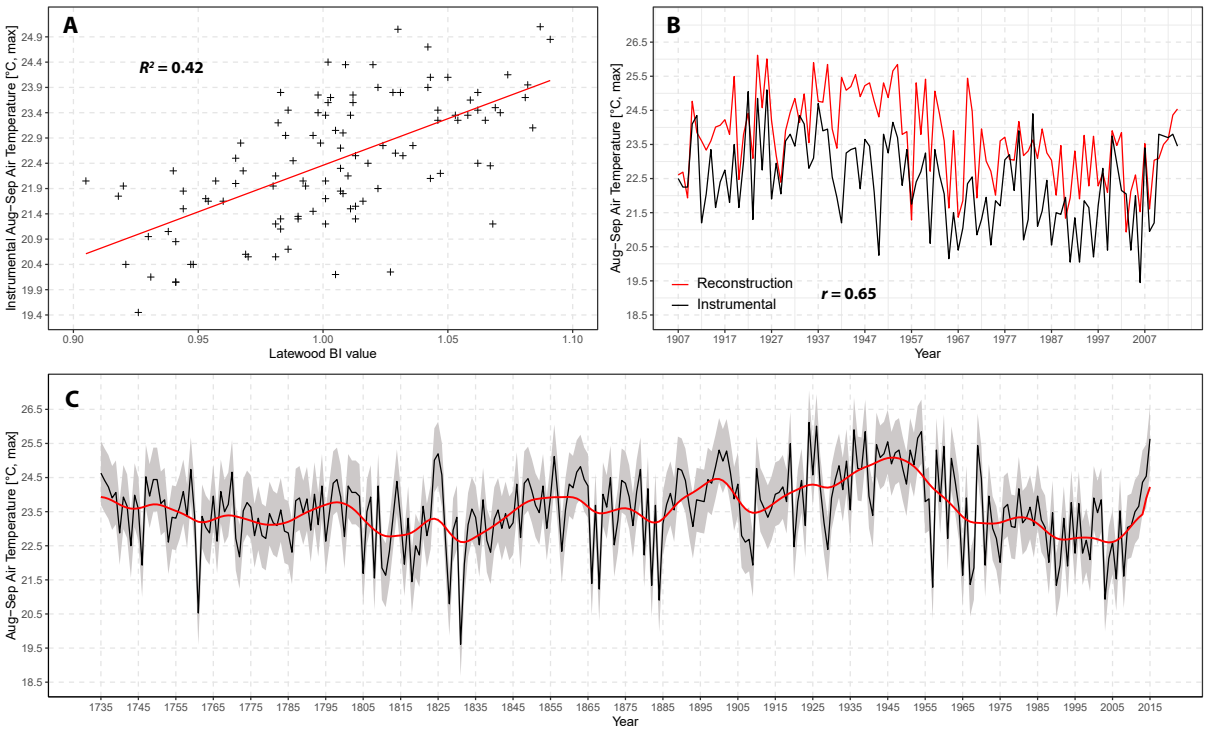

Figure 2.3: Late-summer maximum temperature (AS T_{max}) reconstruction for the Southern Rocky Mountains, United States. (A) Comparison of regional PRISM 4k AS T_{max} instrumental data (black) and reconstructed AS T_{max} values (red), (B) scatter plot of the AS T_{max} reconstructed versus instrumental values plotted with linear function (red) and standard error (blue), and (C) reconstruction of Aug−Sep T_{max} using the LWB AD-sf composite chronology extending from 1735 to 2015.

by steady warming until *ca.* 1955, with a marked imprint of the 1930s Dust Bowl—a series of anomalously dry and warm events experienced throughout portions of the southern plains of the US into northeast NM (Cook et al., 2014). Our reconstruction, which documents an average decadal anomaly of +0.88 during this time (Table S.7), agrees with the temperature anomalies presented by Cook et al. (2014), who document summer temperature anomalies for the Southern Rocky Mountains (ranging from +1 to +2) that are linked to the Dust Bowl of 1934. The period of prolonged warming in the 1930s through the 1950s is consistent with other reconstructions in other areas of North America (Briffa et al., 1992; Trouet et al., 2013; Wiles et al., 2019). This warming is most comparable with the warming period from 1930−1950 presented in the Briffa et al. (1992) MXD-based reconstruction as well as the reconstruction from Trouet et al. (2013). Primary causes of the Dust Bowl are linked to La Niña conditions in the Pacific Ocean, warm sea surface temperatures (SSTs) in the north Atlantic Ocean, and human-induced land degradation (Seager et al., 2008). A combination of dust storms and the vegetation reduction via the replacement of drought-resistant prairie grass with drought-sensitive wheat during the 1920s are shown

to be amplifiers of the anomalously high temperatures (Cook et al., 2009). Most maps detailing the spatial imprint of Dust Bowl temperature anomalies (*e.g.* Cook et al., 2008) include the easternmost NM counties. Here, we suggest that even at the highest elevations of the Sangre de Cristo Mountains of north-central NM, the Dust Bowl era includes the most pronounced warming event in the context of the past *ca.* 280 years.

After 1955, a cooling trend occurs for the next *ca.* 50 years until 2000. The most recent decade is marked by a rapid, extreme warming trend, a rate of change that appears unprecedented since at least 1735. The warming trend of the early 20$^{\text{th}}$ century, followed by a 50 year cooler-than-average period, followed by rapid warming in the last 15 years somewhat differs from many of the more general warming trends documented across the majority of the southwest US, which suggest continual warming from 1900 until present. Despite this difference, we are confident that the reconstruction we present here is truly representative of the local climate, as seen through the lens of the local instrumental record. At high elevations proximal to cool mountain lakes, such as those sampled in this study, the general warming of the 20$^{\text{th}}$ century is captured but not nearly as pronounced as in other areas of North America. While our reconstruction is in close agreement with the Wilson et al. (2019) reconstruction from the Yukon Territory, Canada, the Southern Rocky Mountains reconstruction does not show as dramatic of a warming trend in the beginning of the 21$^{\text{st}}$ century, except for the last *ca.* 5 years of the record. Comparison of this period trend in both reconstructions begins to address the varying magnitude of warming at different latitudes within North America, but further comparisons are ultimately limited by the noncontemporary lengths of the records (the Yukon reconstruction ending in 2004). Overall multi-decadal trends between our reconstruction and the reconstruction presented by Wilson et al. (2014) for southern British Columbia, are relatively similar, but they do display some misalignment of cold decades. The dissimilarities between maximum summer temperatures between southern British Columbia and the Southern Rocky Mountains suggest implications of broader climate dynamics across North America that warrants future examination.

The reconstruction also shows indications of cool periods aligning with the last *ca.* 100 years of the Little Ice Age (LIA; *ca.* 1300−1850 CE), a period of below-average temperatures. The LIA has been the focus of many studies and recent work suggests that the onset, duration, and intensity of the LIA appears to have sub-regional spatial difference (*e.g.* Wahl and Smerdon, 2012; Neukom et al., 2019). Because our reconstruction only covers the last *ca.* 100 years of the LIA, relative comparisons with other reconstructions documenting the full duration of this period are precluded by the length of our record. Nonetheless, we demonstrate contrasting cool and warm phases within the latter part of the LIA. The trend of the reconstruction shows a cooling period from 1735 to 1835, then slightly warmer-than-average conditions from 1840 to 1885. After 1885, increasingly warming conditions persist until 1955.

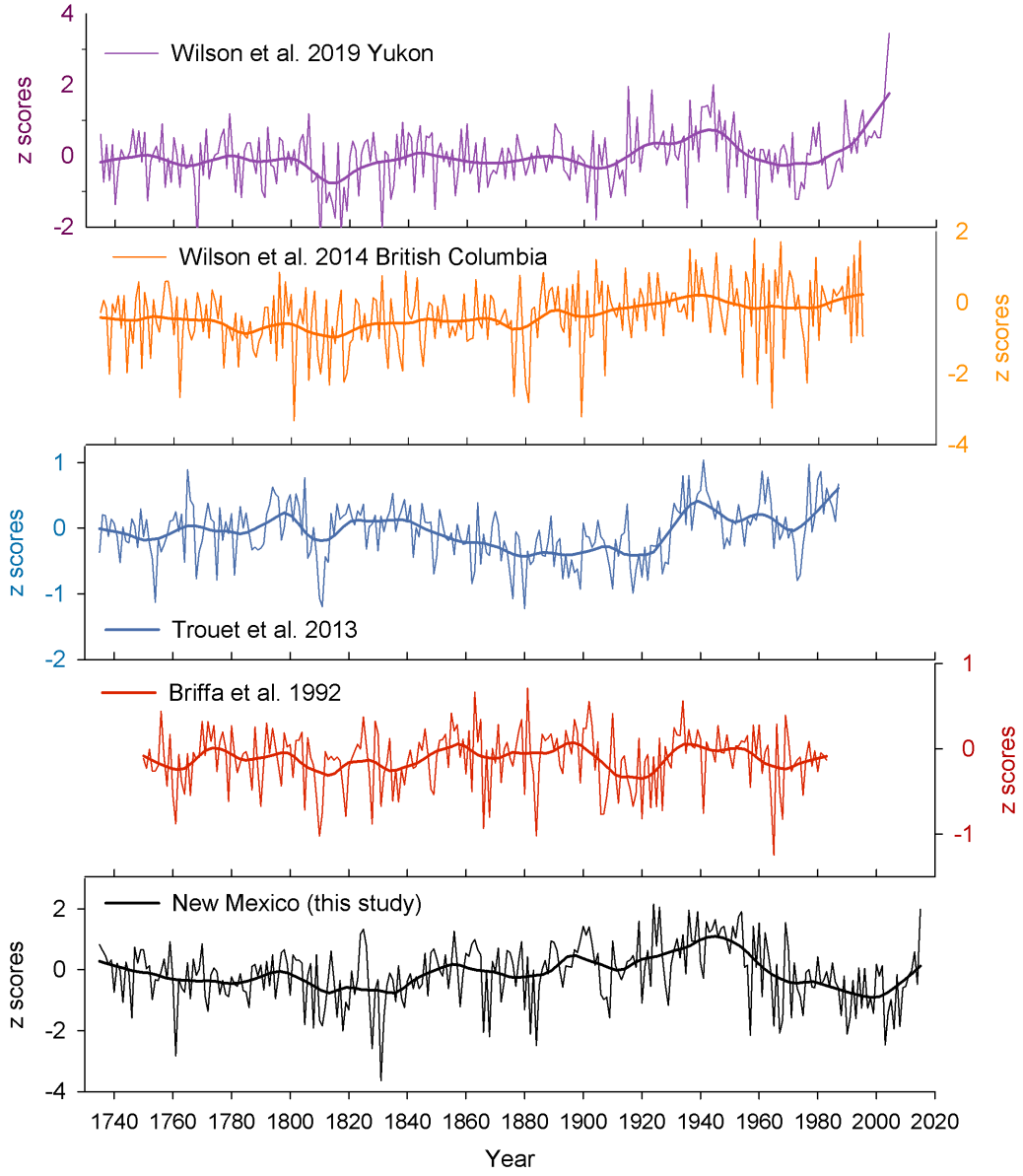

Figure 2.4: Paleo-temperature comparisons for western North America. Plotted are the records of the Southern Rocky Mountains LWB AS T_{max} reconstruction presented in this study with the Wilson et al. (2014) LWB May−Aug T_{max} record for British Columbia, Canada (orange), the Wilson et al. (2019) LWB May−Aug T_{max} record over Yukon Territory, Canada (purple), the Trouet et al. (2013) ring-width annual T_{mean} record over western North America (blue), and the Briffa et al. (1992) MXD-based reconstruction of Apr−Sep T_{mean} over the American Southwest (red; plotted is grid point #30 from 35°N, 110°W).

In the Southern Rocky Mountain region, we discovered close coupling between maximum summer temperature and hydroclimate over the past *ca.* 280 years. We note substantial association between our AS

T_{max} reconstruction and the summer drought reconstruction from El Malpais, NM (34.79°N,108.00°W; Oliver et al., 2019) with regard to intensity of anomalies, especially since the turn of the 20^{th} (Figure 2.5). We attribute this strong coupling between temperature and hydroclimate to the growing influence of modern (the start of the instrumental record to present) increasing surface air temperatures on the hydrologic cycle, as this is recently documented across the American Southwest (Weiss et al., 2009; Cayan et al., 2010; Udall and Overpeck, 2017). The decreased synchrony between either wet+cool or dry+warm events in the earlier parts of the record suggests that the relationship between temperature and hydroclimate in this region was more decoupled prior to the Industrial Revolution, and hence, this phenomenon is specific to the 20^{th}-21^{st} centuries (at least within the context of the past 280 years). The shift in synchrony between our temperature reconstruction and the Oliver et al. (2019) hydroclimate reconstruction after *ca.* 1835 alludes to the influence of anthropogenic warming on the modern hydrologic system in this region. Based on this trend, we suggest that more well-validated, long-term temperature proxy records are increasingly important in areas such as the Southwest US for placing modern hot-droughts into historical context, as has been shown for the Midwest US (Maxwell and Harley, 2017). The multi-millennial hydroclimate reconstruction by Oliver et al. (2019) extends from 2015 back to 492 BCE. Although our record currently extends to the 1730s, developing a longer-term record could be possible across the region, especially at high elevation sites in the Sangre de Cristo Mountains. In particular, we discovered an abundance of submerged, remnant Engelmann spruce logs at the SLE site (Figure S.5). Future efforts should be placed on extending the Southern Rocky Mountains temperature reconstruction back in time by incorporating remnant and subfossil spruce material. Such an effort would allow for longer-term understandings of hydroclimate-drought relationships, especially comparing the current warming trend with conditions during the Medieval Climatic Anomaly and LIA.

Within the context of developing temperature reconstruction networks over greater spatial extents, LWB offers an efficient and effective alternative tree-ring parameter to MXD for developing temperature-sensitive chronologies that account for periods of time that should be interpreted cautiously due to low sample depth. These periods include prior to 1400 CE and post 1988 CE (Anchukaitis et al., 2017). While this reconstruction is limited from 1735 to 2015, we do account for the most recent decades. Although the reconstruction we present here offers valuable insight regarding temperature variability over the Southern Rocky Mountains during the last 280 years, this study would be improved by additional sampling efforts resulting in the ability to evaluate longer-term, multi-centennial variability in the region. While we demonstrate the successful application of BI methods on living Engelmann spruce located at the southern range limit for the species, further investigation regarding the efficacy of BI on remnant samples (*e.g.* Wilson et al., 2017b) must be examined. The three sites from this study are all located up-slope from

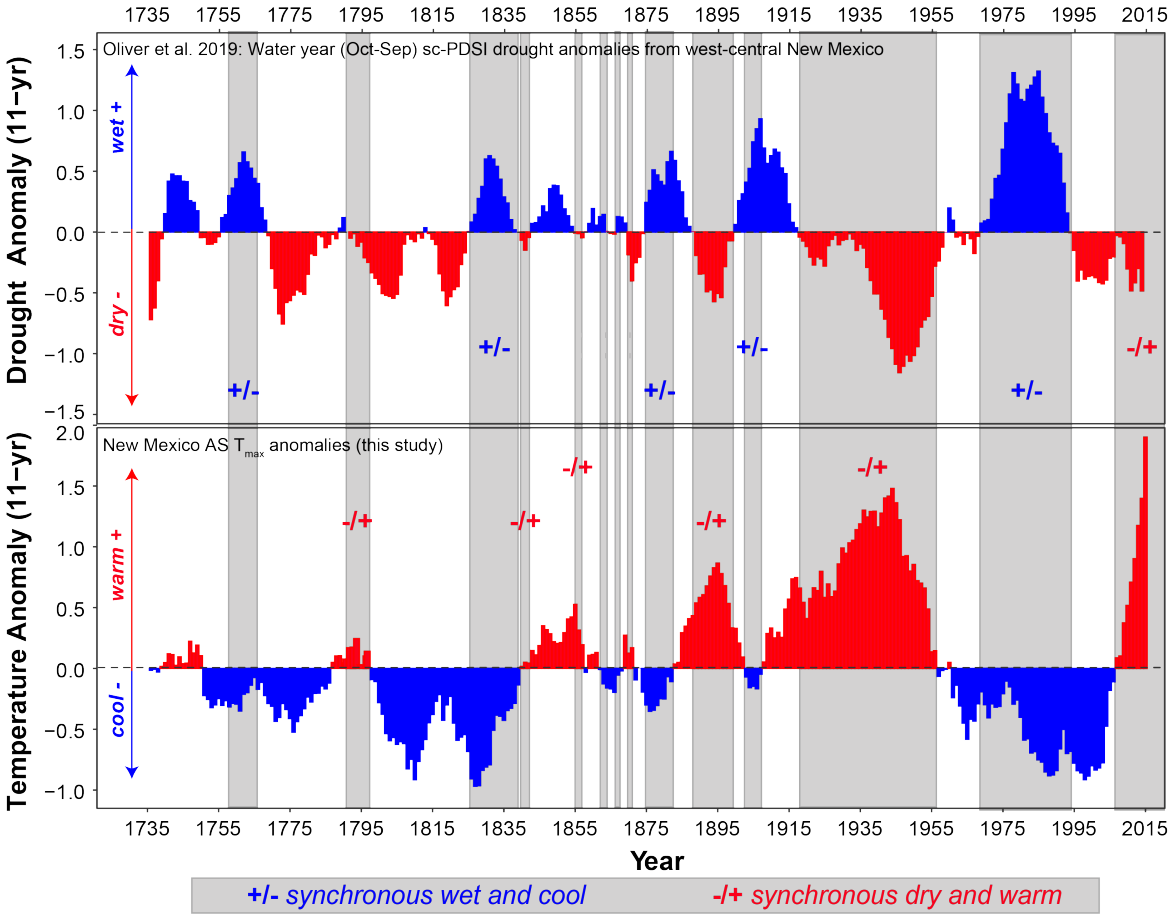

Figure 2.5: Hydroclimate-temperature comparisons for the Southern Rocky Mountains. Comparison of 11-year anomalies of (*top*) west-central New Mexico hydroclimate conditions presented by Oliver et al. (2019), and (*bottom*) reconstructed AS T_{max} presented in this study over the period of overlap 1735−2015. Identified are period of coupled wet+cool and dry+warm conditions across the region.

alpine lakes, which contain many large, likely old, logs as a result from prolonged geomorphological events (*e.g.* rock slide, avalanche) (Figure S.5). Future sampling of these logs will allow for the development of a composite chronology that extends further back in time with increased sample depth. However, one of the major issues using BI methods on non-living trees is the increased presence of discoloration due to decay and algal/fungal staining (Björklund et al., 2014; Wilson et al., 2017b). While this issue may be remedied by pre-treating discolored cores with a combination of acetone and ethanol (Rydval et al., 2014), living tree samples are often generally brighter than samples from older remnant material (Björklund et al., 2014). To reduce potential bias resultant from brightness differences between samples of live and dead trees, the ΔBI metric may be of increased importance here. As LWB and ΔBI exhibit

similar relationships to monthly T_{max}, the ΔBI metric may have additional use for investigating BI methods on subfossil wood and combining remnant BI chronologies with BI chronologies from live trees.

To our knowledge, this study is the first instance of a temperature reconstruction using BI methods at the mid-latitudes of North America. While attempts have been made to develop chronology networks in the western US (Schweingruber, 1988), these tree-line networks do not include BI-derived data. Although a considerable number of BI-derived Engelmann spruce chronologies exist in western Canada (*e.g.* Wilson et al. 2014), future efforts should also be placed towards extending the BI-data network towards the southern half of the natural species range (*e.g.* Utah, Colorado, Wyoming, Idaho, Montana, US). Such an effort would enable connections between the record presented here for the Southern Rocky Mountains, and the BI-derived temperature records from the Yukon (Wilson et al., 2019) and British Columbia (Wilson and Luckman, 2003), thus, resulting in the ability to produce broad-scale, long-term temperature information for western North America during this period of rapidly changing climate.

2.5 Conclusions

In this study, we demonstrate the successful application of BI methods on tree cores collected across three high-elevation, mid-latitude populations of Engelmann spruce located at the species southern geographical range limit. To our knowledge, this is the first published study to explore the application of this technique in the mid-latitudes of North America for the purpose of developing a temperature reconstruction. We reconstructed late summer temperatures spanning from 1735 until 2015 using the LWB metric, and demonstrate that BI metrics can provide robust climate proxy data in the mid-latitudes of the US. As this study shows both spatially and temporally resolved temperature response for the southern Rocky Mountains region of the US, this study does suggest that BI methods are useful for producing temperature-responsive parameters which are alternative to MXD. In possessing many attractive qualities such as cost and time efficiency, and do not appear to have exhibit a divergence issue as seen in other tree-ring metrics, BI methods offer an important alternative approach to spatially improving underrepresented locations within pre-existing temperature networks that rely heavily on MXD. In places such as the American Southwest, where even MXD records are spatially and temporally limited, further wide-scale examination of BI methods is necessary for more adequately capturing broader regional climate trends and placing current warming trends into greater spatial and historical contexts.

2.6 Acknowledgements

We would like to thank the University of Idaho and Indiana University for financial support of this project. JT Maxwell and students were supported during field sample collection by the Indiana University

Institute for Advanced Study. We would like thank Lamar Gillespie, George Harley, Lola Harley, Douglas Heruska, Randy Matheaus, Joshua Oliver, Karly Schmidt, Kerri Spuller, Brandon Strange, and Michael Thornton for assistance with data collection, and two anonymous reviewers for their very thorough edits and suggestions that improved earlier drafts of this manuscript.

Chapter 3: Summer temperature variability since 1730 CE across the low-to-mid latitudes of western North America from a tree ring blue intensity network

Published: Heeter KJ, Harley GL, Maxwell JT, Wilson RJ, Abatzoglou JT, Rayback SA, Rochner ML, Kitchens KA (2021) Summer temperature variability since 1730 CE across the low-to-mid latitudes of western North America from a tree ring blue intensity network. Quaternary Science Reviews 267:107064

3.1 Abstract

Regional reconstructions of air temperature over the past millennium provide critical context for ongoing climate change, but they are temporally limited in the recent period or absent for many parts of the world. We demonstrate the use of latewood blue intensity (LWB) to reconstruct current-year growing (warm) season maximum temperatures (T_{max}) in the low-to-mid latitudes (30°-50°N) of western North America. We present a new tree ring network comprised of 26 LWB chronologies developed from living, high-elevation Engelmann spruce (*Picea engelmannii* Parry ex Engelm.) sampled across the western United States. The LWB parameter shows strong, positive (r=0.65-0.73), and temporally-stable correlations with growing season T_{max}. From this network we present 4 individual T_{max} reconstructions, which characterize regional temperature histories across western North America from northern Mexico to southern British Columbia over the past 4 centuries. Our comparison of these 4 temperature reconstructions highlights the spatial patterns of regional temperature trends throughout time. These reconstructions provide important updates and increased data point density to the tree ring temperature proxy network of the Northern Hemisphere. We highlight the use of blue intensity methods at both low- and mid-latitude upper tree line locations to increase the presence of strongly temperature-sensitive records at increasingly lower latitudes of the Northern Hemisphere.

3.2 Introduction

The instrumental temperature record of the past *ca.* 120 years is too short for contextualizing recent temperature trends over longer timescales. Paleoclimate reconstructions, particularly derived from tree

ring (TR) records, provide valuable estimates of past temperature variability that extend beyond the observational period (Jones et al., 1998; Mann et al., 1999, 2009; Wahl and Ammann, 2007; Christiansen and Charpentier-Ljungqvist, 2012; Cook et al., 2013a; Linderholm et al., 2015; Esper et al., 2018). Currently, the Northern Hemisphere (NH) contains numerous regions that are underrepresented by the coverage of long (*e.g* multi-century) TR-based paleoclimate proxies (Wilson et al., 2016; Anchukaitis et al., 2017; Köse et al., 2017). This study addresses the development of a collection of TR-derived proxy records in a region underrepresented by updated paleo-temperature records—the temperate zone of western North America—and presents a substantial improvement to the spatial coverage of paleo-temperature TR proxy record coverage across the NH paleo-network.

Within the family of paleoclimate proxy records, tree rings are valuable because they provide exactly-dated, well-replicated and sub-annually-resolved data that can extend back in time for multiple millennia, allowing for the analysis of low-frequency variability and trends (Cook and Briffa, 1990; Briffa et al., 2004). As novel dendrochronological techniques are developed and refined, tree rings have become one of the most important sources of late Holocene paleoclimate information, especially in the context of providing information about past hydroclimate and temperatures over increasingly longer time periods and across broader areas of the NH (D'Arrigo et al., 2006; Cook et al., 2007; Schneider et al., 2015; Stoffel et al., 2015; Cook et al., 2015; Wilson et al., 2016; Anchukaitis et al., 2017; Esper et al., 2018; Cook et al., 2020). Most large-scale temperature reconstructions are based on either a single index, such as one hemispheric or global mean derived from many points (*e.g.* Frank et al. 2010; Masson-Delmotte et al. 2013) or a spatially-resolved climate field reconstruction, emphasizing regionality before the calculation of large-scale means (*e.g.* Tingley et al. 2012; Anchukaitis et al. 2017).

A synthesis of continental-to hemispheric-scale temperature reconstructions indicates a coherent, unprecedented increase of surface air temperatures within the last century (Mann et al., 1999; Ahmed et al., 2013; Masson-Delmotte et al., 2013). While such large-scale, single-point mean climate indices provide robust, large-scale estimates for attribution studies (Zhai et al., 2018; Stott et al., 2010), they do not perform well for examining regional-scale (100-500 km) temperature variability and relationships with internal modes of climate variability (Neukom et al., 2014; Wilson et al., 2016; Neukom et al., 2019; Christiansen and Ljungqvist, 2017; Maxwell et al., 2020). The challenges associated with the accuracy and reliability of large-scale temperature reconstructions could be due to changes in strength of the predictor-predictand relationship across geographic space (*e.g.* function of distance decay), especially in places where the data network is spatially heterogeneous or sparse. The concurrent assumptions that [1] proxies must be robust estimators of local temperature and [2] the large-scale mean is well-represented by a network of local temperature datasets (Christiansen and Ljungqvist, 2017) may not be well-maintained

as the number of records decreases back in time. Relationships between local and NH mean temperatures are largely dependent upon geography, thus, the correspondence of interannual local temperature variability to NH mean temperatures varies across space (Christiansen and Ljungqvist, 2017). To account for regional variability that is often muted in large-scale reconstructions, finer-scale models offer the benefits of more accurately characterizing local-to-regional scale climate variability and geographic expressions of atmospheric circulation patterns, radiative forcing, and ocean-atmosphere variability (Anchukaitis et al., 2017).

Across the NH, TR-derived temperature reconstructions are most highly concentrated at high latitudes (>50°N), where temperature is expected to be the most limiting factor on tree growth (*e.g.* Fritts 1976; Jacoby and D'Arrigo 1989; Briffa et al. 1992, 2001; Anchukaitis et al. 2013; Wilson et al. 2014; Björklund et al. 2014; Rydval et al. 2014; Linderholm et al. 2015; Björklund et al. 2015; Wilson et al. 2017a; Rydval et al. 2017; Fuentes et al. 2018; Wilson et al. 2019; Björklund et al. 2019). At high latitudes, spatially-resolved TR proxies have been applied successfully for the evaluation of past temperature forcing by volcanism (Anchukaitis et al., 2017; Edwards et al., 2021) and the timing and amplitude of past cool and warm events such as the Medieval Climate Anomaly (MCA), the Little Ice Agre (LIA), and the 20th-21st century warming trend (D'Arrigo et al., 2006; Schneider et al., 2015; Wilson et al., 2016). The same principle of temperature as a limiting factor for trees at high-latitudes (*e.g.* D'Arrigo et al. 2001; Gervais and MacDonald 2001; Porter et al. 2013), also applies in high-elevation zones of low-to-mid-latitude, montane environments.

Recent progress to broaden the latitudinal extent of the NH TR temperature proxy network to the lower latitudes (< 45°N, *e.g.* Briffa et al. 2001; Büntgen et al. 2008a; Dorado Liñán et al. 2012; Büntgen et al. 2017; Heeter et al. 2019; Esper et al. 2020; Reid and Wilson 2020; Heeter et al. 2020; Harley et al. 2020a; Büntgen et al. 2005; Fan et al. 2009; Buckley et al. 2018) can be attributed to [1] an increased number of investigations of high-elevation, temperature-sensitive trees, and [2] the development and application of additional TR metrics other than tree ring width (TRW) such as maximum latewood density (MXD; Schweingruber et al. 1978) and blue intensity (BI; McCarroll et al. 2002). These studies demonstrate that when TRW serves as a weak temperature predictor due to complex climate-growth relationships at lower latitudes (<40°N) (George and Ault, 2014; Fritts, 1976; Wilson et al., 2016; Büntgen et al., 2008a; Reid and Wilson, 2020), ring-density parameters (*e.g.* MXD and BI) can still be strongly representative of local to regional temperatures.

Over the last decade, BI-derived temperature proxies have become important additions to the MXD and TRW temperature proxy network across the NH. BI uses the light absorbance properties of wood compounds that comprise the cell walls (*e.g.* lignin) to obtain a measure of raw light reflectance across the

earlywood and latewood zones of an annual growth ring. Examination of minimum BI by McCarroll et al. (2002) showed the latewood reflectance exhibited a strong, negative relationship with MXD (r = -0.95, p <0.01), and thereby were the first to suggest that BI could be an important and effective surrogate for MXD to examine annual to decadal-scale changes in temperature. As raw BI measurement data are inversely correlated with MXD (*i.e.* a dense, dark latewood will express low reflectance), current protocol inverts the raw latewood BI (latewood blue intensity; LWB) to allow the same detrending procedures to be used for both LWB and MXD data (Wilson et al., 2014; Rydval et al., 2014). As such, the LWB metric response to summer maximum temperature (T_{max}) is typically very similar to that of MXD. Aside from exhibiting stronger, positive relationships with instrumental summer temperature data than TRW (*e.g.* Wilson et al. 2014), both MXD and LWB are shown to exhibit less signal contamination from biological memory of non-climatic factors and express similar auto-correlative properties to the instrumental data (Esper et al., 2014; Rydval et al., 2018; Lücke et al., 2019).

Continued efforts by the paleoclimate community to develop and archive robust temperature-proxy data are apparent by chronology network syntheses (*e.g.* Briffa et al. 1988, 1992; Schweingruber et al. 1993; Schweingruber and Briffa 1996), and most recently, the creation of NTREND-2016, a publicly available multi-TR-proxy dataset (Figure 1), as well as the PAGES 2K multi-proxy dataset (Consortium et al., 2017). While the spatial representation of paleo-temperature proxies in many parts of the low- and mid-latitudes of the NH continues to improve, many of these pre-existing proxies do not include the most recent period (*e.g.* Briffa et al., 2001); currently only a few TR based temperature reconstructions from the low-to-mid-latitudes of the NH extend past *ca.* 1990. As such, many of these records cannot be calibrated with instrumental climate data over the last *ca.* 20−30 years—a period characterized by unprecedented and extreme climatic trend. Therefore, temperature-sensitive records that extend to the most recent period are valuable, because they provide a more complete understanding of climate-tree growth relationships and past climate variability (Larson et al., 2013).

To date, few TR-based temperature reconstructions, which characterize historical regional temperature variability, exist for the western continental United States (US) (Douglas and Stockton, 1975; Graumlich and Brubaker, 1986; Briffa et al., 1992; Graumlich, 1993; Biondi et al., 1999; Salzer et al., 2014a; Heeter et al., 2020, 2021; Martin et al., 2020). However, most of these records end prior to *ca.* 2000, and thus do not contextualize recent warming trends. The western US is a region within the NH where improvements to the temperature proxy network are needed both spatially and temporally. In this paper, we present a temperature-sensitive TR proxy network comprised of LWB records from 26 sites across the western US. We use this new network to produce 4 regional reconstructions of growing-season T_{max} that represent the spatial temperature variability not only across the low-to-mid latitudes

of the western US, but also throughout southern Canada and northern Mexico. Temporally, these regional reconstructions include the most recent decade (post 2010 CE) and span several hundred years back in time. The temporal span of these reconstructions is valuable in that they track recent trends in regional temperature and their multi-century contextualization. Further, we emphasize the potential for BI parameters to fill data gaps in other low-to-mid-latitude regions globally.

3.3 Methods

3.3 Study location

Data for this study are derived from a network of 26 sample sites across various regions of the western continental US (Figure 3.1; Table 3.1). All site-level TR chronologies are derived from living Engelmann spruce (*Picea engelmanni* Parry ex Engelm.). Sites were visited between 2001 and 2020, with the majority of samples collected during the summers of 2017 and 2018. At each site, we used a hand-held increment borer to extract cores from 10 to 25 living trees, with 2 cores taken per tree at 1.3 m above the ground. We targeted *P. engelmannii* for this study, because this species is widely distributed across the most temperature-limited environments (elevations >3,000 m) of the western US. Further, *P. engelmannii* was shown previously to be favorable for BI methods due to its light-colored wood, characterized by a lack of a visual color change between heartwood and sapwood, and a lack of resin content (*e.g.* Wilson et al. 2014; Heeter et al. 2020).

3.3.1.1 Sample preparation and data collection

Each core sample was processed with the intent of collecting both TRW and LWB data. As such, we followed careful BI sample protocols to ensure high quality surface preparation, including achieving a flat sample surface plane and the removal of samples exhibiting discoloration due to resin content or fungal staining. After collection, cores were dried and mounted in the lab. Given that BI measurements can be affected by the presence of mobile wood compounds not confined to an individual annual ring, such as water and resins, chemical-based resin extraction is often required prior to BI measurement (*e.g.* 24 °C 99.5% acetone bath; Rydval et al. 2014; Buckley et al. 2018). Because the radial sections of *P. engelmannii* cores were typically free of excessive resins and were uniformly light-colored with no obvious heartwood/sapwood color change, the samples for this study were not chemically treated. However, in recent decades, widespread activity from high-density populations of spruce beetle (*Dendroctous rufipennis* Kirby [Coleoptera: Scolytinae]) has caused large-scale forest disturbances across western North America. The fungal symbiont most frequently associated with spruce beetle (95% of individuals) is

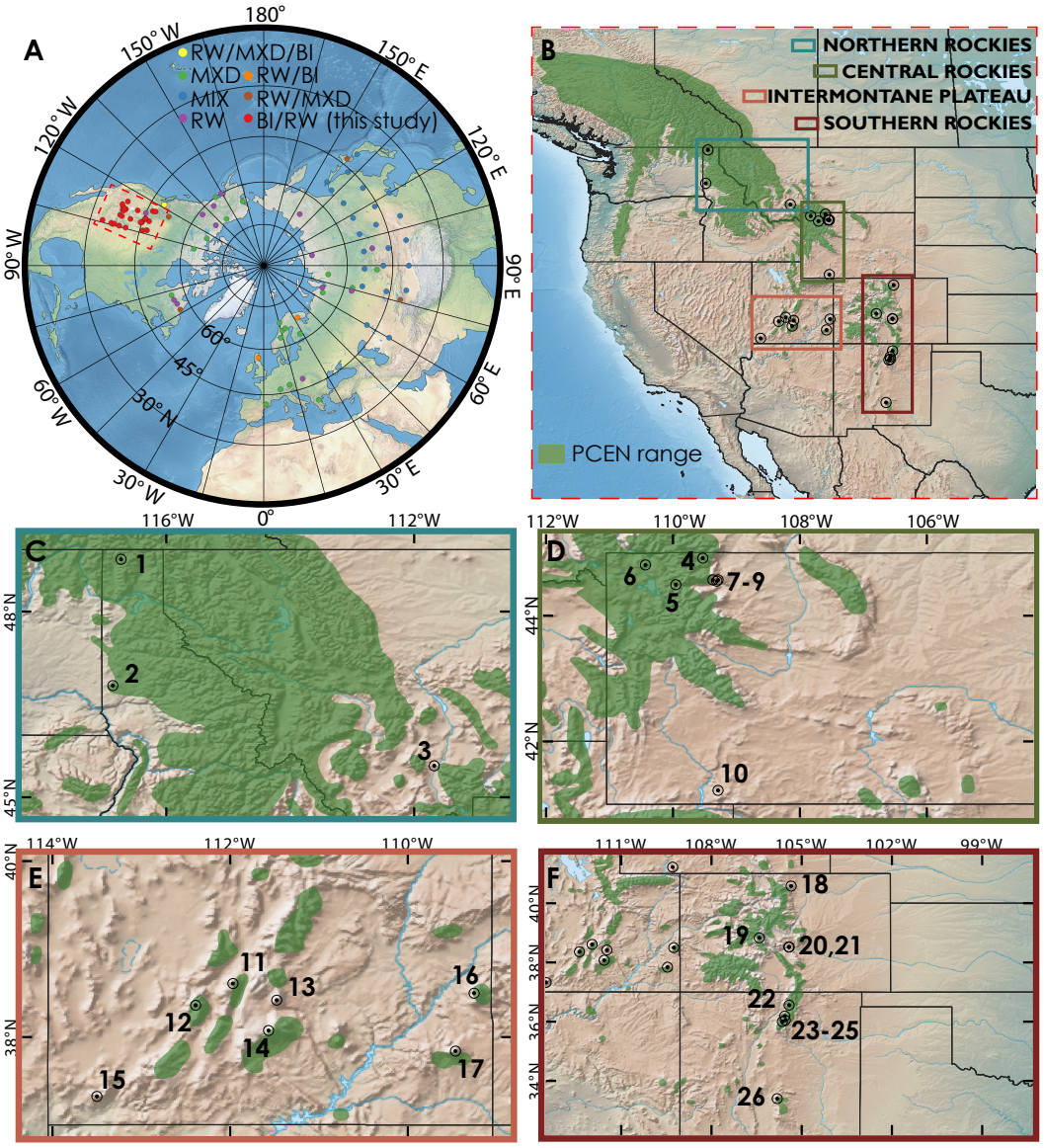

Figure 3.1: Global-spatial context of the western US blue intensity network. A) Location and data-classification of temperature-sensitive, tree-ring datasets currently included in the recent N-TREND network compiled by Wilson et al. (2016), as well as the 26 LWB chronology sites presented in this study (red circles). Map insets (B-F) displaying the locations of all 26 sites examined in this study sorted by physiographic region, as well as the species range of *Picea engelmannii* (green polygon) as indicated by Little and Viereck (1971). Chronologies are clustered by hierarchical cluster analysis into 4 regions (Figure S.7): US Northern Rocky Mountains (teal), Central Rocky Mountains (green), Intermontane Plateau (salmon), and Southern Rocky Mountains (dark red). Numbers correspond to respective chronology information and statistics displayed in Table 3.1.

Leptographium abietinum (Peck) M.J. Wingf. (Aukema et al., 2005; Cardoza et al., 2008; Six and Bentz, 2003), a blue-staining endophloedic species (Davis et al., 2018). *P. engelmannii* are particularly prone to

Table 3.1: Information for sample sites (n=26) examined for the western US latewood blue intensity network. State Codes: Idaho: ID, Montana: MT, Wyoming: WY, Utah: UT, Colorado: CO, and New Mexico: NM.*Site numbers correspond to labels in Figure 3.1. Replication (Rep) indicates number of trees for each LWB chronology required to attain EPS >0.85, Years represents the timespan of each chronology using the EPS >0.85 threshold. We also include the average RBAR of each chronology and the optimum Pearson's correlations (p<0.05) for 1920-present (1970-present) for each LWB chronology against the local 0.5°(or larger where relevant) CRU TS 4.04 (Harris et al. 2014) maximum temperature grid.

Site #	**Site code**	**US State**	**Lat. (°N)**	**Lon. (°E)**	**Elev. (m)**	**Rep**	**Years**	**RBAR**	**Correlation T_{max} (post 1970)**
1	BFL	ID	48.88	-116.81	2282	3	1721-2019	0.54	Aug: 0.61 (0.68)
2	MCO	ID	46.80	-116.86	2963	5	1920-2019	0.34	JAS: 0.43 (0.37)
3	FKY	MT	45.50	-111.67	1930	10	1901-2000	0.26	Mar-Aug: 0.56 (0.61)
4	FLS	WY	44.91	-109.53	2959	7	1766-2016	0.28	JJA: 0.64 (0.68)
5	RPS	WY	44.99	-109.92	3046	8	1781-2017	0.27	JJA: 0.67 (0.67)
6	MWS	WY	44.80	-110.43	2960	8	1760-2019	0.29	JJA: 0.52 (0.59)
7	BTP	WY	44.57	-109.29	3010	5	1756-2015	0.39	JJA: 0.65 (0.61)
8	CBS	WY	44.57	-109.37	2945	6	1730-2015	0.34	JJAS: 0.65 (0.61)
9	TOW	WY	44.54	-109.31	2960	7	1850-2015	0.28	Aug: 0.64 (0.70)
10	MBP	WY	41.21	-109.29	3225	9	1909-2015	0.26	Aug: 0.53 (0.55)
11	MON	UT	38.60	-111.96	3122	6	1886-2016	0.32	Apr-Aug: 0.60 (0.61)
12	TUS	UT	38.36	-112.38	3263	3	1667-2011	0.49	Apr-Aug: 0.53 (0.50)
13	TLM	UT	38.41	-111.47	3436	8	1848-2016	0.27	Apr-Aug: 0.51 (0.57)
14	BUP	UT	37.32	-113.50	3438	3	1654-2018	0.65	AM: 0.47 (0.52)
15	PLS	UT	38.07	-111.56	3280	13	1891-2000	0.26	AM: 0.47 (0.47)
16	HAY	UT	38.49	-109.25	3271	6	1861-2017	0.32	Apr-Aug: 0.49 (0.59)
17	ABA	UT	37.84	-109.46	3425	4	1859-2002	0.42	Apr-Aug: 0.45 (0.50)
18	MDB	CO	40.21	-105.29	3300	4	1659-2015	0.43	AS: 0.46 (0.53)
19	CPI	CO	38.82	-106.40	3580	4	1778-2015	0.43	Jun-Sep: 0.54 (0.62)
20	PPL	CO	38.52	-105.42	3460	7	1732-2015	0.30	Aug: 0.36 (0.53)
21	PPU	CO	38.52	-105.42	3550	3	1623-2015	0.53	Aug: 0.54 (0.61)
22	WHE	NM	36.55	-105.41	3708	5	1803-2015	0.39	AS: 0.57 (0.59)
23	JIS	NM	36.18	-105.56	3587	6	1776-2014	0.32	AS: 0.56 (0.62)
24	SLE	NM	36.04	-105.54	3594	7	1848-2014	0.28	Aug: 0.39 (0.43)
25	TLS	NM	35.99	-105.64	3573	5	1694-2018	0.36	Aug: 0.53 (0.58)
26	LOS	NM	33.39	-105.81	3760	4	1878-2018	0.35	AS: 0.65 (0.73)

discoloration from blue-stain fungus, which presents a potential problem for measuring BI on this species. For this reason, we avoided sampling any trees with evidence of spruce beetle infestation. Cores were also examined for any evidence of blue staining and omitted from further analysis if present.

After examining cores for discoloration, we saturated the cells of the mounted samples by brushing the surfaces with water. We incrementally shaved all saturated samples with a core-microtome until a flat planar surface was achieved (Gärtner and Nievergelt, 2010). Lastly, all shaved samples were polished with 40 micron sanding paper and treated with compressed air to remove any residual sawdust particles from the intercelluar pores or cracks in the wood.

Prepared samples were scanned as JPEG images on a calibrated Epson 12000 XL flatbed scanner at 3200 dpi. We initially calibrated our scanner using the Silverfast software in combination with an IT8 7.2 calibration card. We then measured TRW of the scanned cores to 0.001 mm precision using the software CooRecorder (Larsson, 2014). After all samples were measured, visual TRW cross-dating was statistically validated using the software COFECHA (Holmes, 1983). After absolute dating was established with TRW, we obtained LWB data for all samples in CooRecorder (Cybis, 2020).

3.3 Chronology development and regionalization

We developed TRW and LWB chronologies for each of the 26 sample sites, totalling 52 chronologies. As all chronologies showed non-climatic, growth-related age trends (Fritts, 1976), we compared multiple approaches to series detrending (*e.g.* Negative Exponential, Age-dependent, 2/3 spline) in both the ARSTAN (Cook and Holmes, 1996) and SignalFree (Melvin and Briffa, 2008) frameworks. The examination of multiple detrending options revealed minimal differences between chronology variants, however, we found that the best chronologies were consistently produced when calculated as power-transformed residuals (rather than ratios) in the SignalFree (SF) framework, detrended with the Age-dependent spline (SF-ad); we applied SF-ad detrending to all chronologies in the network. We used an expressed population signal (EPS) value of 0.85 to identify the period when chronology sample depth is not representative of the theoretical perfect chronology. Common signal fidelity of each chronology was assessed using the RBAR (average correlation between series; Fritts 1976) value.

We examined the spatio-temporal relationships between the detrended TRW and LWB chronologies and local (within 0.5°of the sample location) CRU TS 4.04 0.5°(land) T_{mean} and T_{max} data (Harris et al., 2014) using a Pearson correlation analysis in KNMI Climate Explorer (Trouet and Van Oldenborgh, 2013) over the period spanning 1920−present. This period best reflects when the representation of high-elevation areas by montane, climate-data stations is most-reliable and consistent across the western US. Because the TRW chronologies showed consistently weak correlations with CRU T_{mean} and T_{max} (Harris et al., 2014) (see section 3.4.1; Figure S.6), we focus the remaining description of methods to LWB predictors.

We sorted all LWB chronologies into sub-regional groupings using a 2 step process. First, we assessed the spatial homogeneity between all chronologies using principal component analysis (PCA; Husson et al., 2016) over the common period shared by all 26 chronologies (1920−2000). Following the Kaiser-Guttman rule (Guttman, 1954; Kaiser, 1960), we retained the first n eigenvectors with eigenvalues >1.0. The network-wide PCA on the 26 LWB chronologies resulted in 3 PCs with eigenvalues >1.0, explaining a cumulative 68.5% (PC1: 45.2%, PC2: 14.4%, PC3: 8.9%) of the overall variance amongst the LWB

chronologies. Second, regional groupings were defined using a complete linkages hierarchical cluster analysis (HCA) (Revelle, 1979) on a Euclidean distance matrix created from loading values of LWB chronologies to the final subset of PCs using the R package FactorMineR (Husson et al., 2016). Results of the complete linkage HCA on the loading values of the chronologies to PC_{1-3} suggested optimal level of division was achieved at a height of 0.70 (Figure S.7). This division level allowed us to group chronologies into 4 geographic regions: the Northern (NR), Central (CR), and Southern Rocky Mountains (SR), and the Intermontane Plateau (IP).

Once individual chronologies were sorted into regions, we examined each site chronology against regionally-averaged CRU TS 4.04 0.5°temperature (T_{max}, T_{mean}), precipitation, and self-calibrating Palmer's Severity Drought Index (scPDSI) spatial data fields (Harris et al., 2014) for each region in Climate Explorer. Since LWB predictors consistently showed the strongest relationships with regionally-averaged CRU T_{max} over the common instrumental period (Figure 3.2; Figure S.8), we proceeded with the CRU T_{max} dataset for the subsequent reconstructions. To determine the target seasonality of the subsequent reconstructions, we compared Pearson correlations across multiple months to determine which combination of months would result in the strongest positive relationship between the instrumental record and the predictors for each region.

3.3 Regional reconstruction models

Using the regional groupings identified by the HCA, we developed 4 regional T_{max} reconstructions using a nested principal components regression (PCR) approach, which accounts for the decrease in number of predictor chronologies back through time (Cook et al., 1999). Across each regional grouping, we initially pre-whitened the predictor LWB chronologies and CRU T_{max} data to provide a conservative estimate of climate-predictor relationships that are not subject to inflation via auto-correlation. Chronologies were retained for modeling if they were positively and significantly ($p<0.05$) correlated to the regionally-averaged target temperature data during the common period (shared by the CRU T_{max} data and the chronology) using the Pearson, Robust Pearson, and Spearman correlation coefficents (Table S.10). The original chronologies (non-pre-whitened) of significant predictors were then used in the PCR to develop the reconstructions. Following the Kaiser-Guttman rule, the first n eigenvectors with eigenvalues >1 were retained for the PCR. We determined the final subset of PCs by using the minimum Akaike information criterion (AIC), which includes a penalty term for increasing the number of predictors in the model (Akaike, 1974).

We use 1920 as the starting year of the common calibration period because prior to this date, there are many places across the western US where representation of high-elevation areas by montane, climate-

data stations is scarce or inconsistent. For this same reason, a similar starting year for the calibration period was used for the temperature reconstruction by Heeter et al. (2020) in north-central New Mexico, US. The end of the common calibration date depends on the common period shared by all predictors of each region. The seasonality of each regional reconstruction was determined by performing a series of regression experiments between target CRU temperature data and the LWB predictors. For each region, we split the instrumental period into 2 periods ("early" and "late") to validate and cross-validate the reconstruction model, as well as to test for stability over time (Table 3.2). We performed model validation by calculating cross-calibration statistics for the full period and verification statistics for the early period. This practice is common, as the earlier portions of the instrumental record often possess greater uncertainty than the latter part of the record (Cook et al., 2013a) We used 2 goodness-of-fit tests to validate the models: the reduction of error (RE) and coefficient of efficiency (CE) (Fritts, 1976; Cook et al., 1999). When RE values (ranges from -∞ to +1) are positive, the calibration model is a more skillful predictor of the target data than the mean of the instrumental data during the calibration period. Although CE has the same range and calculation, a positive CE value is more difficult to obtain because it relies on the verification period mean for a baseline of predictive skill. The validation statistics produced were the calibration and verification period coefficient of determination (CRSQ and VRSQ), and the validation period reduction of error and coefficient of efficiency (VRE and VCE). To quantify model uncertainty, we used the maximum entropy bootstrapping method (MEBoot) (Vinod et al., 2009) to produce 300 reconstruction replicates.

3.3 Reconstruction analyses

We first transformed reconstructed values to anomalies calculated over the full period of each reconstruction. We then calculated the top 5 single-year cool and warm anomalies for each regional reconstruction. We conducted a severity-duration analysis (González and Valdés, 2003) on reconstructed values of at least 2+ years to determine the magnitude (average cumulative departure from the long-term mean), duration (time span of each event), and intensity (duration divided by the magnitude) of warm and cool events. Duration and magnitude of each event were ranked and compiled to give each event an overall rank score. The top 5 warm and cool events are based on the overall score. We quantified and assessed the degree of between-group and within-group synchrony (the estimated proportion of common inter-annual variance; $\hat{a}_c$) of each regional reconstruction using the Dendrosync package in R (Alday et al., 2018). In order to better visualize and compare decadal trends across each region, we also transformed reconstructed values for each time series into z-scores based on the mean and standard deviation of the common reconstructed period and applied an 11-year running average smoother. We addition-

ally compared correspondence between our record and other regional and hemispheric-scale temperature reconstructions using a Pearson's correlation analysis over the common period of all reconstructions.

3.4 Results and Discussion

3.4 LWB as a temperature proxy in western North America

The preliminary response of the individual LWB chronologies and their TRW counterparts to local temperature data consistently shows that LWB chronologies exhibit a stronger relationship with current-year growing (warm) season temperatures than TRW (Figure S.6). With the exception of a few sites, the LWB chronologies in this network are not highly correlated with their respective TRW site chronologies (Table S.8). While Salzer et al. (2014a) demonstrate that TRW can be a successful parameter for developing a low-frequency temperature reconstruction for a nearby region of North America (Great Basin), our findings highlight the utility of BI methods for creating temperature-sensitive proxies from tree rings when conventional TRW series do not show as strong of correlations with instrumental temperature data. We initially experimented with using both TRW and LWB for the proposes of reconstructing temperature, but the addition of the few TRW chronologies that were significantly ($p<0.05$), but weakly correlated to temperature, to the predictor pools did not lead to any improvements in the models achieved when solely using LWB predictors. Briffa et al. (1992) reported similar findings while experimenting with the inclusion of TRW predictors in their MXD-based temperature network for the western US. Like the presentation of the MXD network presented by Briffa et al. (1992), proceeding with just the LWB predictors allows us to better emphasize the efficacy of the LWB metric for the creation of this temperature-sensitive TR network.

The replication needed to attain the 0.85 EPS threshold ranges from 3−13 trees, with an average of 6 trees. RBAR values range from 0.26−0.65, with an average of 0.36 (Table 3.1). These chronology statistics are consistent with findings from Wilson et al. (2014), who presented BI-derived temperature reconstructions using *P. engelmannii* from 7 sites across southern British Columbia, Canada.

At the local scale (within 0.5°of each site), the LWB chronologies exhibit higher correlations with T_{max} than with T_{mean}, which is consistent with other BI and MXD studies in North America (*e.g.* Wilson and Luckman 2003; Luckman and Wilson 2005; Wilson et al. 2014, 2019; Heeter et al. 2020; Harley et al. 2021). All temperature-LWB relationships are time-stable (Table 3.1). While sampling protocol aimed to avoid specimens visibly or knowingly influenced by ecological disturbance, we suspect that the chronologies at 3 sites (ABA, PLS, TUS) show the effects of heightened spruce beetle (*Dendroctonus rufipennis* Kirby) outbreaks in southern Utah during the turn of the 21st century (DeRose et al., 2011).

The original sample collections from these 3 sites contained multiple cores which were omitted due to the presence of blue staining across the outermost growth rings. For this reason, we truncated ABA to 2002, PLS to 2000, and TUS to 2011. Because linkages have been shown between increased temperatures, heightened spruce beetle outbreak severity, and *P. engelmannii* mortality (DeRose et al., 2013; Pettit et al., 2020), targeting this tree species for future temperature reconstructions across the western US may warrant additional consideration of site-level land use and examination of disturbance histories (Trotsiuk et al., 2018).

3.4.1.1 Regional-level climate response

All LWB chronologies show significant ($p<0.05$) and positive responses to CRU T_{max} during at least 2 current-year growing season months (Figure 3.2). Across most regions, statistically significant ($p<0.05$) temperature response begins in March or April, and the optimum seasonal window concludes with September. For all regions, the strongest relationship between T_{max} and the LWB chronologies over a single month occurs in August. This was expected, as the relationship between LWB and temperature has been widely shown to be strongest in late-summer months (Wilson et al., 2014; Heeter et al., 2020; Rydval et al., 2017; Wilson et al., 2019; Wiles et al., 2019; Heeter et al., 2021).

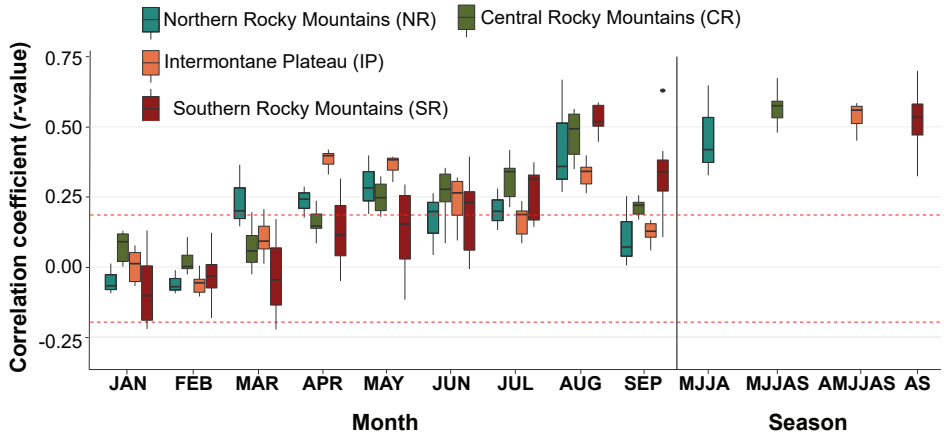

Figure 3.2: Correlations (Pearson's r) between maximum temperature and (T_{max}) latewood blue intensity (LWB) chronologies across the western US network, grouped by region. Pearson's r between all LWB chronologies across each region and current-year monthly regional target CRU 4.04 0.5°T_{max} data (Harris et al., 2014) for each region (NR: 45.0-49.0°N, 117.0-111.5°W; CR: 44.0-45.0°N, 111.0-109.0°W; IP: 37.0-41.5°N, 114.0-109.0°W; SR: 33.0-40.5°N, 106.0-105.0°W), and the optimum seasonal average of regional target CRU 4.04 0.5°T_{max} data. Correlations span the common period between the starting calibration year (1920) and the last year of each individual chronology. Dashed red lines indicate significance at the $p<0.05$ level.

Notably, the IP chronologies exhibit optimum response in the months of April, May, and August, with the June and July response being weak. Compared to the other 3 regions, the IP region simultaneously experiences the least amount of monthly precipitation and the highest mean and maximum temperatures during the mid-summer months (June and July) (Figure S.9). We suspect that the decreased temperature response of IP LWB chronologies in June and July may be resultant of mid-summer temperatures exceeding the tolerance limits of trees in this region. The IP chronologies, many of which are located in the arid regions of southern Utah, exhibit the most strongly-negative correlations with regional target CRU scPDSI than any other region during June and July (Figure S.8). Despite this characteristic, the IP chronologies do not show significantly negative correlations with precipitation during these months. Therefore, we suspect that the decreasing temperature response trend is less likely an artefact of a competing hydroclimate signal. A similar pattern of decreased mid-summer temperature response is also apparent with the NR LWB chronologies. However, unlike in the IP, where low precipitation is likely a limiting factor year-round regardless of temperature, the NR receives significantly less precipitation in June and July. The NR LWB chronologies show significant negative correlations with precipitation during these 2 months, thereby suggesting that this trend may be influenced by a competing hydroclimate signal during the mid-summer months. Similar effects of reduced TR temperature-sensitivity during mid-summer can be seen in the LWB predictors developed in southern British Columbia and Alberta by Luckman and Wilson (2005) and Wilson et al. (2014). Büntgen et al. (2017), who use MXD to reconstruct summer temperatures in the Spanish Pyrenees, suggest that a weakening of TR temperature sensitivity in mid-summer months due to increased drought stress likely occurred whenever past summers were exceptionally warm and dry.

The SR chronologies express a strong temperature response, but over the shortest season compared to the other regions. This response may be impacted by the hydroclimate and evaporative demands related to temperature on TR growth in this region, as well as is likely artefact of negative correlations between T_{max} and precipitation in this region during non-monsoonal months. Babst et al. (2016) suggest that annual growth of high-elevation conifers in the southwest US are primarily reliant on spring and monsoon precipitation, rather than winter precipitation. We suspect that the strong monsoonal influence of the SR during July−September (Figure S.9; US Climate Data 2020) is potentially influencing the onset and duration of seasonal temperature response in this region. Additionally, the *P. engelmannii* collected from some of the sites in the SR region (*e.g.* LOS) exist as disjunct populations near the southernmost extent of the species geographic range (Little and Viereck, 1971). The shortened duration of strong temperature response of southernmost chronologies within the SR supports the principle of ecological amplitude (Griggs, 1914; Fritts, 1976; Holt and Keitt, 2005). This spatial pattern suggests

that there may be differences in tree sensitivity to temperature between individuals toward the southern range periphery versus those toward the center of the species range and, further, may be evidence of the role of temperature in how climate change influences future species distribution patterns (Thuiller, 2004; Hill et al., 2011).

We found that the optimum target season for the NR is May-August (MJJA), the CR is May-September (MJJAS), the IP is April-September (AMJJAS), and the SR is August-September (AS) (Figure 3.2; Table S.9). Notably, the IP shows highest $r-$values ($p<0.05$) when April and May are included. Most of the regional chronology pools display the highest r-values when computed over a longer growing season comprised of multiple months. The SR is the exception, displaying highest r-values when computed over 2 consecutive months in the late growing season (August and September). This finding is consistent with prior results indicating reduced temperature response of LWB to earlier growing season temperatures in this southernmost region (Heeter et al., 2020).

The differences in seasonal duration of the *P. engelmannii* LWB response to T_{max} across the historical species range (Figure 3.1; Little and Viereck 1971) is likely attributable to factors such as [1] distance to upper tree-line (Lloyd and Fastie, 2002; Salzer et al., 2014b; Elliott, 2011; Kipfmueller and Salzer, 2010), [2] proximity to the interior versus the periphery of the range (Amburgey et al., 2018; McCullough et al., 2017; Herrero et al., 2013), or [3] differences in the timing of cambial reactivation (indicating start of the growing season) (Deslauriers et al., 2003; Begum et al., 2010; Gruber et al., 2009; Harley et al., 2012) based on location. Regardless of cause, differences in seasonal response can be problematic for equitably comparing temperature responses of chronologies comprising broadly-distributed temperature proxy networks. Similarly, differences in seasonality of temperature response at the local level has important implication for studies emphasizing spatial analysis of climate proxies (*e.g.* Anchukaitis et al. 2017), which use a common seasonal target over a broader area; in the case where the optimum seasonal target for reconstruction differs across space, calibration results of the spatially-resolved version of the reconstructions may appear weaker than calibration results of more localized reconstructions with variable seasonal targets, such as this study. As such, differences in seasonal response should also be taken into account when comparing TR temperature predictors across regions.

3.4 Reconstruction models

3.4.2.1 Model validation

Calibration and verification statistics are summarized in Table 3.2. The last year of the common calibration period of each model ranges from $2000-2015$. The IP common calibration period ends in 2000, because several chronologies in this group are truncated due to issues of ecological disturbance

in the most recent years of growth. The NR common calibration period is simply limited to the earlier sample date of one of the NR chronologies (FKY). Although FKY does not extend past the year 2000, the scarcity of temperature-sensitive records in this part of North America warrants its inclusion. Forward nests were then applied as needed: 1 for the NR, 3 for the CR, 4 for the IP and, and 2 for the SR (Table 3.2; Table S.11). The nested PCR models retain only the first PC for the NR, CR, and IP models, with PC1 explaining 71.2%, 79.5%, and 68.1% of the respective cumulative variance for each model. The PCR process retains the first 2 PCs for the SR, with PC1 (59.7%) and PC2 (13.4%) explaining 73.1% of the cumulative model variance. These results reflect the strong common temperature signal among intra-regional predictors identified by the HCA.

3.4.2.2 Model strength and timespan

The timespan of each model varies, with start year of each reconstruction occurring between the period 1623−1730 (Table 3.2). VRE and VCE statistics are positive for all nests across the entire reconstructed period (Table 3.2; TableS.11) for each region, indicating that all reconstructions are skillful estimates of temperature through time (Cook et al., 2013a). All reconstructions cover the most recent decades, spanning to 2018. To date, there are few published temperature reconstructions that adequately capture the first 2 decades of the 21st century in the calibration period (*e.g.* Fuentes et al. 2018; Heeter et al. 2020; Keyimu et al. 2020a,b; Heeter et al. 2021). RSQ values indicate robust model strength for each region, explaining at least 44% of the common period temperature variance (Table 3.2; Table S.11). Model strength for these 4 reconstructions are comparable to other BI- and MXD-based temperature reconstructions for North America (Briffa et al., 1992; Wilson et al., 2014, 2019; Heeter et al., 2020). Comparatively, the SR model shows the strongest overall skill, explaining 54% of the overall instrumental temperature variance of the most well-replicated nest (1878-2014). While the CR is comparatively the weakest and shortest model, it still accounts for 44% of the temperature variance of the most well-replicated nest (1850-2015).

The relationships between the LWB chronology predictors and CRU T_{max} data also show strong spatial correlations (Figure 3.3). We noted only slight increases in spatial correlations between non-transformed data and the first-differenced data, indicating that the LWB response is strong at both the inter-annual and multi-decadal timescales. While the highest correlations are centered over the immediate study areas, thereby highlighting the sub-regional differences in T_{max} patterns across the western US, these data are strongly representative of ($r > 0.60$, $p<0.05$) maximum temperature across the entire western US, northwest Mexico, and parts of southern Canada. The broad spatial implications of these results suggest the possibility to extend the NH TR based temperature proxy network southward, as

previously highlighted by Heeter et al. (2020). Similar efforts to increase coverage of under-represented areas will allow for a better understanding of the spatial patterns of historical temperature variability across broader geographical space.

Table 3.2: Summary statistics for PC regressions of each region included in the western US latewood blue intensity network. (Top) Calibration and verification periods, monthly duration of the reconstructed season, and the final reconstructed period for each regional model. (Bottom) measures of explained variance for each regional model: RSQ (calibration period coefficient of multiple determination), VRE (validation period reduction of error), VCE (validation period coefficient of efficiency) and RMSE (root mean squared error).

	Calibration period	Verification Period	Target months	Reconstructed Period	#forward nests	#backward nests
NR	1966-2000	1920-1965	MJJA	1721-2018	1	2
CR	1966-2015	1920-1965	MJJAS	1730-2018	3	4
IP	1966-2000	1920-1965	AMJJAS	1654-2018	4	7
SR	1966-2014	1920-1965	AS	1623-2018	2	7

Model	First Year	Last Year	RSQ	VRE	VCE	RMSE
NR	1920	2000	0.53	0.55	0.53	0.80
CR	1850	2015	0.44	0.44	0.44	0.84
IP	1909	2000	0.49	0.55	0.54	0.62
SR	1878	2014	0.54	0.53	0.52	0.65

3.4 Reconstruction analysis

3.4.3.1 Analysis of historical temperature variability

The 4 reconstructions show similar evidence of warm and cool periods but differ with regards to the onset, duration, and intensity of these periods (Figure 3.4; Figure S.10). We suspect that the differences among regions with regards to the magnitude and duration of warm and cool events can somewhat be attributed to the varying seasonal targets of each reconstruction. The instrumental record indicates strong spatial coherence of surface air temperatures across the western US within the last century, which is well-reflected by the 4 reconstructions. Notably, all regional reconstructions capture a substantial warming trend beginning at the end of the 20^{th} century into the present. The recent warming period of *ca.* 2000 to present, documented by the instrumental record, has somewhat limited representation by NH temperature proxy studies due to insufficient record length (*e.g.* Wilson et al. 2016; Anchukaitis et al. 2017). Specifically in western North America, the most recent decades are characterized by not only an unprecedented increase in surface air temperatures, but also anomalous drought, streamflow declines, increased wildfire activity, and reduced annual snowpack (Cook et al., 2004, 2008; Kalra et al., 2008; Pederson et al., 2011; Abatzoglou and Williams, 2016; Harley and Maxwell, 2018; Williams et al., 2020;

Harley et al., 2020b). The severity-duration analysis indicates that, despite the short duration, high magnitude rankings places 2015−2018 within the top 10 overall ranking warm events, and as the most intense event for the CR, IP, and SR regions (Table 3.3). The year 2017 is ranked among the 10 warmest single-year anomalies over each reconstructed period for all regions, and in the top 5 for the CR, IP, and SR. While the CR, IP, and SR reconstructions slightly overestimate the warming of 2017, the relative ranking of warm years spanning the period 2015−2018 is well corroborated by the instrumental record (Figure 3.3). Our ability to capture the period post *ca.* 2010 in the TR temperature proxy record for model calibration is meaningful, because it allows us to more accurately place the most recent period, characterized by severe trend, into historical context. Further, the strong correspondence between the instrumental and LWB data during the modern warming period (Figure 3.3) instills additional confidence in extending the tree ring records back in time to robustly provide estimates of other anomalously warm periods such as the MCA. Considering the serious implications of the projected continual warming (Flato et al., 2013), precise, updated proxy records are important for improved detection and attribution studies related to temperature trends and for constraining models of future temperature change.

Another pattern captured across the majority of the regions is the cooling experienced between *ca.* 1960−1980. This period has widely been related to a time of global solar dimming (Wild, 2009). This

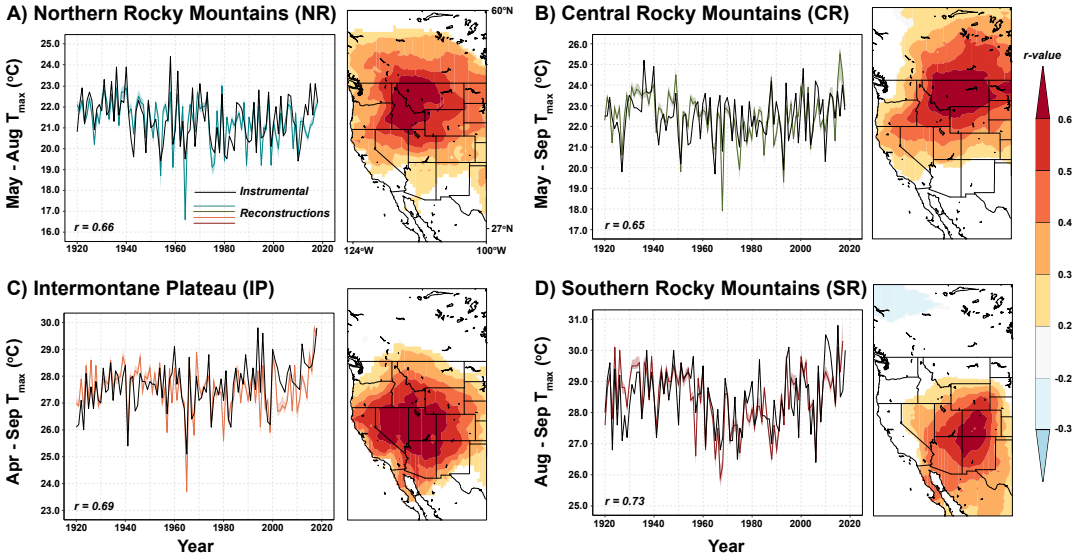

Figure 3.3: Temporal and spatial relationships between 4 western US regional maximum temperature (T_{max}) reconstructions and instrumental data. The temporal relationship (Pearson's r, p<0.05) between the regional reconstructions (colored lines, line shading represents standard error) and the CRU TS 4.04 T_{max} data (black line) (Harris et al., 2014) over the period spanning 1920-2018. We also include the extent of the spatial distribution of correlations between the predictor and predictand temperature data for each regional model over the period 1920-2018 (Pearson's r, significant at p<0.05 level).

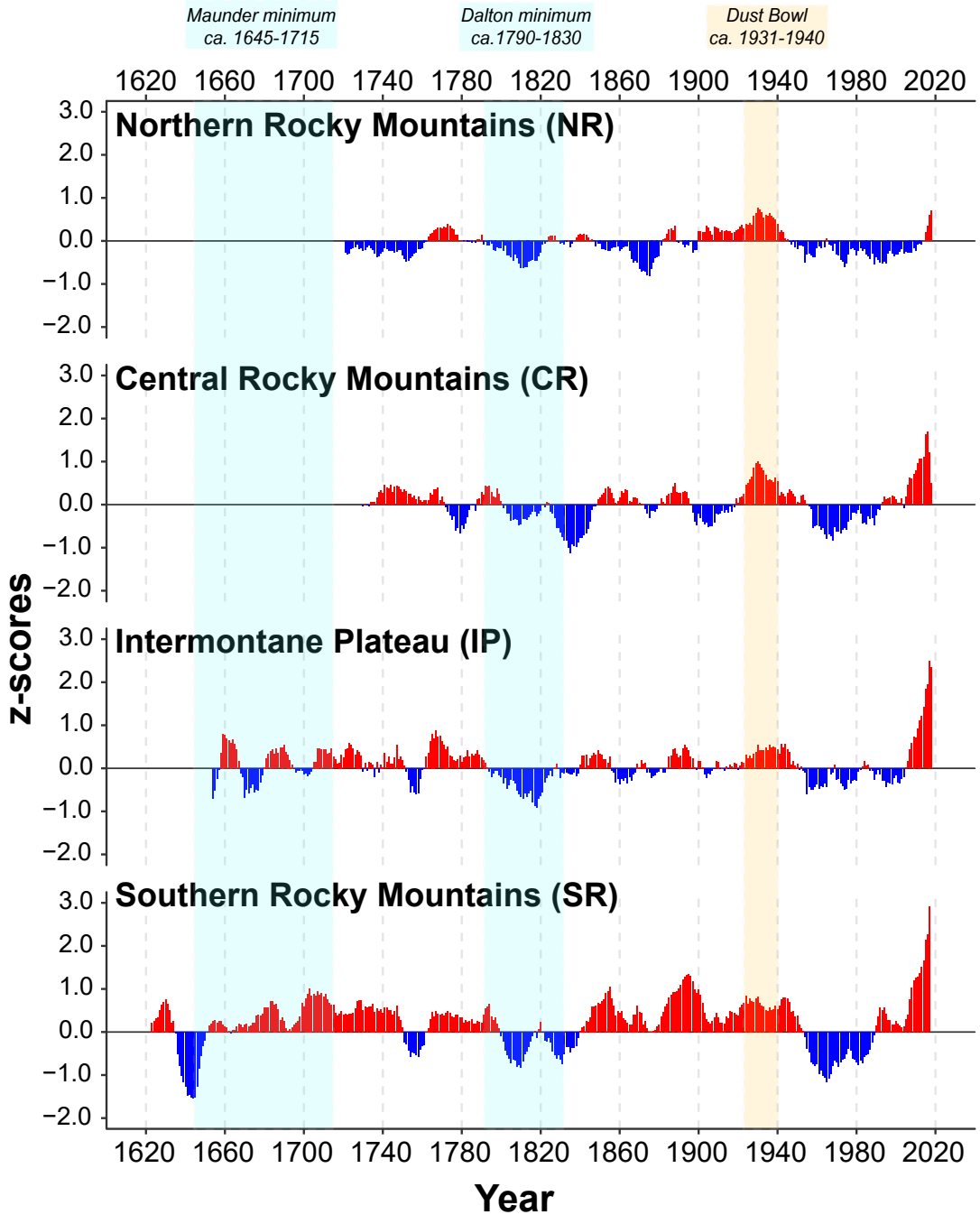

Figure 3.4: Decadal-scale variability of 4 regional temperature reconstructions derived from the western US latewood blue intensity network. Temperature anomalies calculated as z-scores from the mean and standard deviation of the common period of all reconstructions (1730−2018) for each region. Notable cool and warm periods (Maunder and Dalton Minima and the Dust Bowl) are highlighted. Z-scores are smoothed with an 11-year running average. Warm years are indicated by red and cool years are indicated by blue.

Table 3.3: Results of severity-duration analysis showing the top-five ranking warmest (+, top row) and coolest (-, bottom row) single-year anomalies (left) and event periods (right) for the each region. Single-year anomalies calculated over the full period (NR: 1730-2018, CR: 1680-2018, IP: 1646-2018, and SR: 1622-2018). Duration indicates the number of years of each event, as calculated by the severity-duration analysis from reconstructed values. Magnitude = mean cumulative departure from the longâterm reconstructed mean for each region; Intensity = duration (years) divided by the magnitude; after ranking, overall score = duration rank + intensity rank. Periods of interest are color coded: red= recent warming trend; orange= Dust Bowl; blue= Maunder Minimum; purple= Dalton Minimum.

Rank	Year	1-year Anomaly	Period	Duration (years)	Magnitude	Intensity	Duration Rank	Magnitude Rank	Overall Score
Northern Rocky Mountains									
1	1979,1910	+1.70	1773-1786	14	+6.73	+0.48	9	68	77
2	1940	+1.65	1930-1936	7	+6.80	+0.97	6	69	75
3	1936	+1.63	1888-1898	11	+5.68	+0.52	8	66	74
4	1931	+1.49	1908-1915	8	+6.20	+0.77	7	67	74
5	1958	+1.47	1938-1942	5	+5.62	+1.12	5	65	70
1	1964	-4.63	1879-1884	6	-5.45	-0.91	6	69	75
2	1899	-3.65	1818-1826	9	-4.90	-0.54	7	67	74
3	1907	-2.96	1810-1815	6	-4.32	-0.72	6	65	71
4	1954	-2.57	1974-1976	3	-5.06	-1.69	3	68	71
5	1876	-2.52	1964-1965	2	-4.82	-2.41	2	66	68
Central Rocky Mountains									
1	2016	+3.08	1928-1940	13	+13.74	+1.06	9	69	78
2	2017	+2.18	1888-1898	11	+6.38	+0.58	8	67	75
3	1949	+2.08	2015-2018	4	+7.50	+1.87	4	68	72
4	1988	+1.99	1869-1874	6	+4.31	+0.72	6	65	71
5	1748	+1.81	1946-1950	5	+5.31	+1.06	5	66	71
1	1968	-4.52	1834-1849	16	-17.71	-1.11	7	68	75
2	1993	-3.16	1972-1980	9	-8.27	-0.92	6	67	73
3	1787	-2.77	1904-1908	5	-5.44	-1.09	5	66	71
4	1838	-2.74	1915-1918	4	-4.03	-1.01	4	64	68
5	1951	-2.57	1967-1968	2	-4.54	-2.27	2	65	67
Intermontane Plateaus									
1	1669	+3.08	1767-1777	11	+7.97	+0.72	9	94	103
2	1690	+2.32	1664-1669	6	+8.08	+1.35	6	95	101
3	2017	+2.28	1931-1940	10	+5.14	+0.51	8	92	100
4	1729	+2.12	1711-1719	9	+4.65	0.52	7	91	98
5	1783	+2.06	2015-2018	4	+6.28	+1.57	4	93	97
1	1965	-3.83	1818-1824	7	-6.56	-0.94	7	94	101
2	1746	-2.41	1654-1659	6	-9.20	-1.53	6	95	101
3	1657	-2.23	1676-1678	3	-4.75	-1.58	3	93	96
4	1763	-2.17	1758-1761	4	-3.87	-0.97	4	91	95
5	1736	-2.13	1963-1965	3	-4.75	-1.58	3	92	95
Southern Rocky Mountains									
1	2018	+3.52	1894-1905	12	+12.77	+1.06	9	73	82
2	1632, 1902	+2.27	1942-1954	13	+7.33	+0.56	10	71	81
3	1900	+2.00	1859-1865	7	+6.31	+0.90	7	70	77
4	1856	+1.92	2015-2018	4	+7.48	+1.87	4	72	76
5	2017	+1.72	1715-1722	8	+5.57	+0.70	8	68	76
1	1646	-4.33	1641-1656	16	-20.50	-1.28	10	73	83
2	1761	-3.39	1970-1984	15	-12.33	-0.82	9	72	81
3	1831	-3.33	1805-1813	9	-9.07	-1.01	8	70	78
4	1647	-2.81	1963-1968	6	-9.20	-1.53	5	71	76
5	1645	-2.66	1758-1764	7	-8.87	-1.27	6	69	75

cooling event in the 20th century is most intensely and continuously experienced in the CR and SR regions and may have implications for solar forcing attribution studies in North America. During this time, the IP oscillates between moderately cool (z-score >-1.0) and slightly warm (z-score <0.50) periods, while the NR shows the predominance of slightly cool (z-score >-0.5) years. The period of *ca.* 1965−1980 is represented in both the 5 coldest single-year anomalies or the top 5 overall ranking cool events for each region. Notably, 1965 is both the single coldest year anomaly captured by both the instrumental data and reconstruction for the IP.

Another major warm period that is well documented across all regional reconstructions occurred in the 1930s. This anomalous warming is often associated with the Dust Bowl, a period of extreme drought across the western US (Cook et al., 2008; Woodhouse et al., 2010). Conditions during certain years of the Dust Bowl rival the modern warming, as the period spanning *ca.* 1928−1942 appears within the 5 top-ranking warm events for the NR, CR, and IP reconstructions. The magnitude of the Dust Bowl is comparatively strongest in the CR region, with z-scores > 1.0 for this period. The period 1928−1940 is the top-ranking warm event for the CR reconstruction. The CR differs from the other 3 regions in that the Dust Bowl warming appears to have been an abrupt change from moderately cooler years in the early 20th century to very warm years, as opposed to a continual warming trend since *ca.* 1900 that culminated in the 1930s and 1940s (Figure 3.4). The Dust Bowl is less pronounced in the SR, as *ca.* 1928−1940 is situated towards the terminus of a nearly continuous warm period since *ca.* 1830.

The 4 regions show cooling around the time of the Dalton Minimum (*ca.* 1790−1830; Wagner and Zorita 2005; Bond et al. 2001), which is widely described by numerous other temperature proxy studies of the NH (*e.g.* Briffa et al. 1998; Büntgen et al. 2005). While the cooling during the Dalton Minimum was historically attributed to solar forcing, in many areas, this period is primarily attributed to volcanic forcing (*e.g.* unknown 1809 event, Mt. Tambora eruption of 1815; Wagner and Zorita 2005; Hegerl et al. 2011; Gennaretti et al. 2014; Schurer et al. 2019). The cooling effects of volcanic eruptions during this time are widely documented in the TR record across North America (D'Arrigo and Jacoby, 1999; D'Arrigo et al., 2013; Stoffel et al., 2015; Wilson et al., 2016). Cooling begins approximately just after *ca.* 1790 for the majority of regions and lasts into the 1840s. All regions show 2 distinct pulses during this period, the former spanning *ca.* 1790−1820, and the latter spanning *ca.* 1825−1845. The second pulse is most intensely expressed in CR, with the period spanning 1834−1849 ranking as the top coldest event for the region.

The Maunder Minimum (*ca.* 1645−1715; Eddy 1976), another cooling period attributed to solar forcing and volcanic activity (Lean et al., 1992; Shindell et al., 2001; Crowley et al., 2008), is less pronounced than the Dalton Minimum in IP and SR. The length of NR and CR precludes examination of this time

period. IP characterizes the Maunder Minimum as oscillating between moderately warm and cool periods instead of a continuous cooling, whereas SR documents continuously warm temperatures interrupted by an intense cooling spanning the period *ca.* 1635−1655. IP indicated 2 of the 5 top-ranking cool events spanning the periods 1654−1659 and 1676−1678 occur during the Maunder Minimum. Similarly, the period spanning 1641−1656 is the top-ranking cool event for SR. While the Maunder Minimum can be seen in numerous longer-term reconstructions of temperatures of the extra-tropical NH, (*e.g.* Briffa et al., 2001; Esper et al., 2002; Wilson et al., 2016) the presence and magnitude of these past events are not ubiquitous across different regions and scales (Anchukaitis et al., 2017). Spatial differences can be seen at the sub-continental level as well; within North America, paleo-temperature records from the Gulf of Alaska and the Alberta Icefields show the period *ca.* 1690−1710 CE as being anomalously cold and attributed to volcanic activity (Luckman and Wilson, 2005; Wiles et al., 2014), while this period is only somewhat evident in the IP record and absent in the SR record. Like with the Dalton Minimum, non-ubiquitous observations of the Maunder Minimum are likely resultant from heterogeneous climatic effects of volcanism over space. Studies suggest that temperature forcing of many of the largest, high-latitude volcanic eruptions of the past *ca.* 1200 years (*e.g.* 1783 Laki), are varied globally (Zambri et al., 2019; Schmidt et al., 2012; Oman et al., 2006). Specific to western North America, while Crowley et al. (2008) did not find a global expression of the Laki eruption, Jacoby et al. (1999) and Edwards et al. (2021) both show cooling effects from Laki across northern Alaska. Further, Shindell et al. (2001) attribute non-ubiquitous observations of the Maunder Minimum, particularly over North America, to lowering indices of the Arctic Oscillation/North Atlantic Oscillation as solar irradiance decreases in this period.

The majority of examinations into the effects of volcanism on surface air temperatures in the NH are, to date, largely dependent on MXD chronologies. We suggest that LWB may be an additional suitable parameter for future quantification of volcanic cooling at finer timescales (*e.g.* seasonal or sub-seasonal), because like MXD, the temperature response of LWB is less likely to be influenced by biological persistence than with TRW (D'Arrigo et al., 2013; Stoffel et al., 2015; Lücke et al., 2019; Reid and Wilson, 2020). Recently, Edwards et al. (2021) use a combination of quantitative wood anatomy (QWA; von Arx et al. 2016) and climate modelling to show that the effects from the 1783 Laki (Iceland) eruption across northern Alaska were more accurately characterized as an abrupt decrease in temperature at the end of the growing season, as opposed to an entire growing season that was anomalously cool. As such, the application of novel TR parameters such as BI and QWA will likely play an important role in future examination of the effects of volcanic cooling across different spatial and temporal scales. As suggested by D'Arrigo et al. (2013), the quality, type, and spatial distribution of chronologies averaged together to derive larger-scale estimates of past temperature are important to ensure that any volcanic signal

is not muted. Attempts to decrease uncertainty in larger-scale estimates of temperature by increasing spatial coverage of temperature-sensitive TR chronologies will be welcome, particularly in the estimation of volcanic cooling.

3.4.3.2 Reconstruction synchrony and large-scale comparisons

While all 4 records show similar decadal trends, an examination of changes in the synchrony of trends are important to better understand how internal modes of variability result in changes to local climate over geographic space and time. Unlike correlation analysis, which provides a measure of similarity between the calculated means of individual timeseries over a given period (*e.g* 10 year period), the additional value of analyzing timeseries synchrony is that it allows for examining the relative timing of climatic events and the likelihood that such events will occur at the same time (*e.g.* extreme hot or cold years). Over the common period of all 4 regional models (1730−2018), trends in between-group synchrony of temperature anomalies show patterns of spatial-dependence. For example, the IP and SR show the highest between-group synchrony, and the NR and SR show the least (Figure 3.5A). Notable periods of increasing synchrony across all 4 records include the latter half of the 20^{th} century, specifically the Dust Bowl, and the period between the Dalton Minimum and the terminus of the LIA (Figure 3.5B,C). The strongest decline in overall synchrony between the 4 regions occurs around the turn of the 20^{th} century following the LIA (*ca.* 1880−1920). Although the Rocky Mountain models (NR, CR, and SR) show strong coherence during this time, the overall declining trend is driven by strong decreases in synchrony between IP and the Rocky Mountain models. This trend reflects the complexity of land surface temperature changes across geographic space during a climatic transition period characterized by substantial changes to relative external forcing by atmospheric and oceanic circulation patterns (*e.g.* AMO, PDO), as well as increased anthropogenic influence at the end of the LIA (Kreutz et al., 1997; Knudsen et al., 2014; Brönnimann et al., 2019). Future studies examining historical periods of asynchronous temperature trends across western North America are needed to more fully understand the effects of broad-scale ocean/atmospheric forcings on internal modes of temperature variability for this region.

The ability to compare our records with other regional and hemispheric-scale reconstructions provides evidence to better understand the relationship between volcanism, atmospheric circulation, and changes to surface air temperatures across space, especially at lower latitudes. Our records show strong agreement with nearby temperature records from North America (Figure 3.6A,C). The strongest agreement between the 4 records we present and the MXD-based temperature record for the western US by Briffa et al. (1992) is not surprising given the similarities between LWB and MXD, as well as the close spatial proximity of the records. Similarly, the coherence of the NR record with the British Columbia and Alberta records by

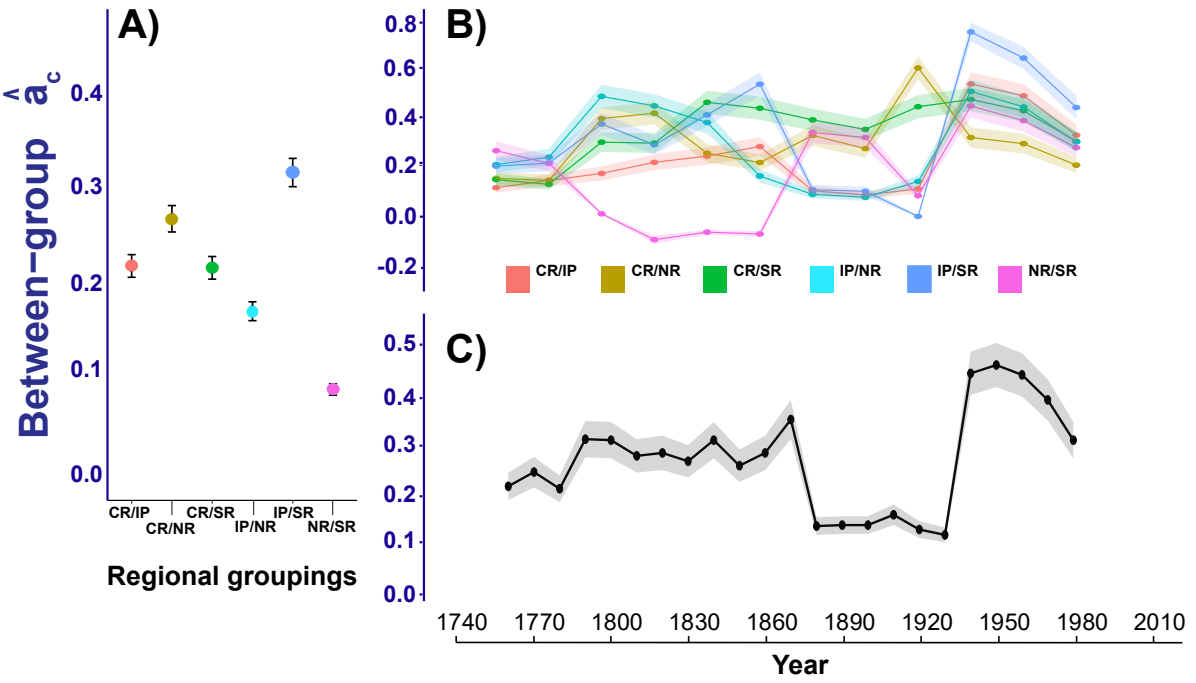

Figure 3.5: Comparison and evaluation of synchrony between 4 regional temperature reconstructions. We compare between-group synchrony (the estimated proportion of common inter-annual variance; $\hat{a}_c$) of A) individual pairings of the 4 regional reconstructions (raw reconstructed values) averaged over the entire common reconstructed period (1730-2018), B) time series of between-group synchrony trends between all 4 regional reconstructions using a 60-year window and 10-year lag (based on AIC criteria), and C) time series of between group synchrony trends of regional reconstruction pairings listed from B) using a 60-year window and 10-year lag (based on AIC criteria) over the common period (1730-2018). The error bars in A) and shadows in B) and C) depict the standard errors.

Wilson et al. (2014) and Luckman and Wilson (2005) is expected given the location and similar type and seasonality of these records. As such, we emphasize the importance of independent validation of previous studies within the region. Since many of these pre-existing temperature proxy records for North America do not extend to include the most recent decades, our corroborating records provide valuable updates to this region of the NH temperature proxy network.

To date, many ensemble reconstructions, providing estimates of historical temperature variability, exist for the NH. However, there is poor representation of temperature-sensitive predictors from the mid-latitudes of North America in these ensemble reconstructions. We compare decadal trends for each of the regional reconstructions presented in this study with 3 independent, ensemble temperature reconstructions of the extra-tropical NH (Figures 3.6B, 3.6C). The 4 western US reconstructions show significant ($p<0.05$), positive agreement with the NH reconstructions over their common period of over-

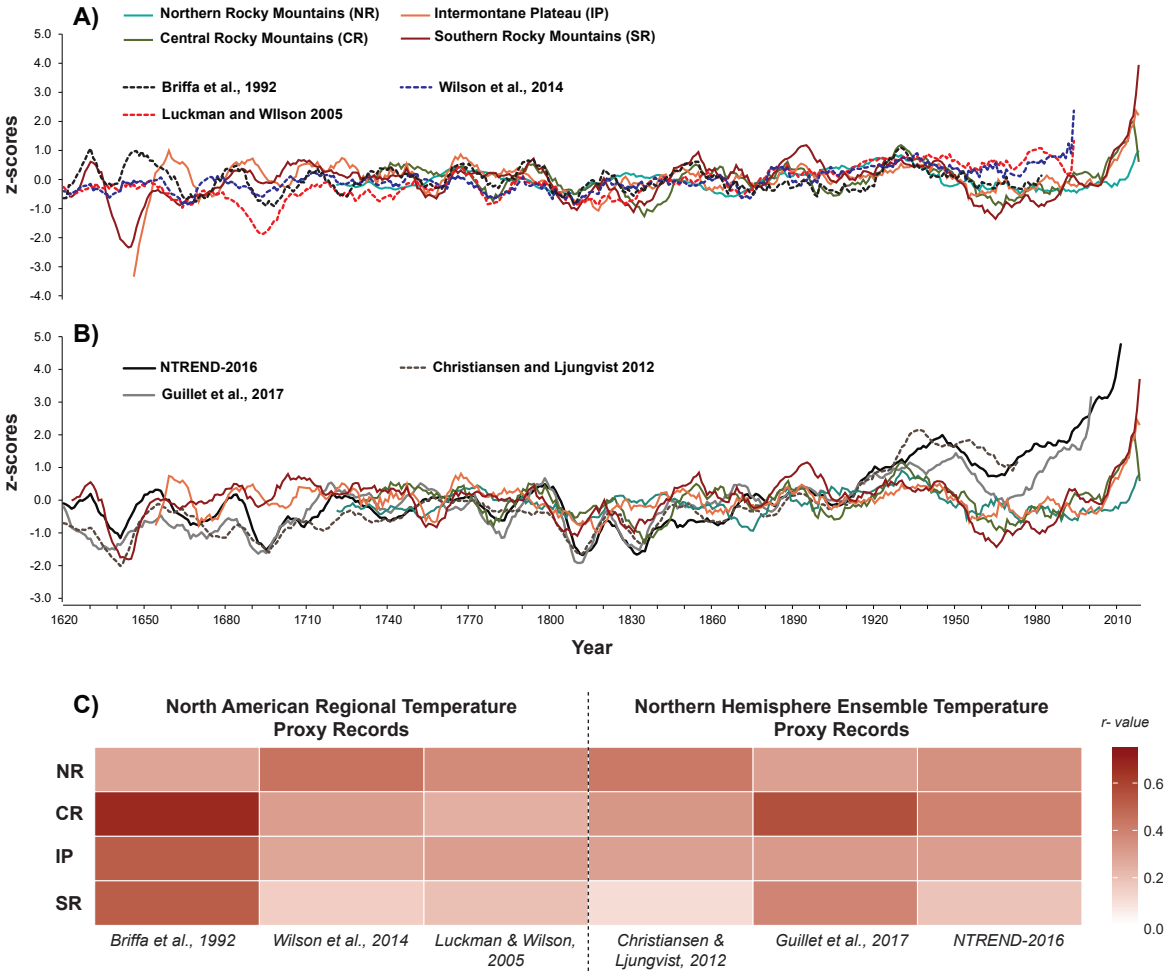

Figure 3.6: Coherence of 4 western US temperature reconstructions with independent regional- and large-scale paleo-temperature reconstructions. Comparison of plotted time series (as z-scores) between the 4 western US regional temperature reconstructions with A) 3 independent regional temperature reconstructions from North America: Western US (Briffa et al., 1992), Alberta, Canada (Luckman and Wilson 2005), and British Columbia, Canada (Wilson et al., 2014), and with B) 3 independent ensemble temperature reconstructions for the Northern Hemisphere: N-TREND 2016 (Wilson et al., 2016), Guillet et al., 2017, and Christiansen and Ljungvist 2012. All time series displayed as z-scores calculated over the common period for all records (1730-1973) and smoothed with an 11-year running average. C) Correlation matrix (Pearsons r-value) over the common period 1730-1973 between the 4 regional reconstructions from this study and the independent records listed in A) and B). All values in the matrix are significant at the $p<0.05$ level.

lap (1730−1973). The strongest agreement occurs between the CR reconstruction and the multi-proxy summer (JJA) temperature reconstruction by Guillet et al. (2017) (r=0.57). We suspect that lower correlations between SR and the hemispheric reconstructions by Christiansen and Charpentier-Ljungqvist (2012) and Wilson et al. (2016) are partially due to differences in seasonality of input records, and po-

tentially the decreased representation of low-latitude (<40°N) temperature-sensitive predictors in these NH estimates. Increasing the density of robust, local temperature records at lower latitudes of the NH may result in improved accuracy of future large-scale, ensemble NH temperature reconstructions in that they will be more representative of a greater latitudinal range for the NH. Both trends in asynchrony of regional temperature trends and differences between regional and large-scale models highlight the importance of regional temperature models for constraining the full range and variability of global temperature models.

3.5 Conclusions and future work

Using the LWB parameter, we provide 4 regional reconstructions of growing season T_{max} over much of the western North America temperate zone spanning the past *ca.* 300−400 years to present. Strong calibration/verification statistics for each reconstruction model indicates that LWB is a robust predictor of growing-season T_{max}, especially during late-summer. This LWB network provides paleo-temperature estimates which could further contribute increased understanding of the role of temperature on historical drought events, especially "hot droughts" (*e.g.* Overpeck 2013; Udall and Overpeck 2017) across the western US. As numerous temperature-sensitive MXD records exist across the western US, we suggest that future investigation of a multi-variate ensemble network of MXD, TRW, and LWB will considerably improve the current understanding of paleo-temperature across this portion of the NH network. While we have demonstrated the ability of LWB to contribute a collection of updated data points to the North American temperature proxy network, additional work is needed to extend the network back in time (*e.g.* sampling remnant or subfossil wood as in Luckman and Wilson 2005; Wiles et al. 2014; Gennaretti et al. 2014). Further, we posit that the continued exploration and application of BI methods at other mid-to-low latitude locations of the NH will contribute substantially to a more complete understanding of local to global climate histories and dynamics.

3.6 Acknowledgements

This project was supported by the National Science Foundation under BCS-2012482, BCS-1759694, and AGS-2002524, the United States Forest Service, the University of Idaho, and Indiana University Institute for Advanced Studies. We would like to thank the following: Yellowstone National Park for facilitating access to the MWS and SLS sites and the Shoshone National Forest to the FLS and RPS sites, Dr. Lauren Stachowiak, Zach Merrill, Kyle Landolt, Dr. Jessie Pearl, April Kaiser, and Dr. Bryan Black for field assistance at the FLS site; Lara van Akker, Dr. Jodi Axelson, Dr. Richard Stockton Maxwell, Dr. Christine Lucas, Jessie Mitchell, James McGee, and Dr. James Hardy Speer for field assistance at the

RPS site; and April Kaiser and Ty Reinemann for field assistance at the FLS and MWS sites, Brian Van Winkle and the staff at the Dixie and Fishlake National Forests for assistance across multiple IP sites, Peter Brown, and the North American Dendroecological Fieldweek (NADEF) 2017−2020 instructors and participants for assistance with sample acquisition across the IP and CR regions, Joshua Bregy for assistance at the LOS and TLS sites. Reconstruction data are available at the National Centers for Environmental Information (NOAA).

Chapter 4: Chapter 4: Concluding remarks on the current and future states of tree-ring blue intensity

Assessments of climate change impacts rely heavily on instrumental data, which is limited prior to the early 20th century. Temperature proxies derived from natural records (*e.g.* tree-rings) provide essential baseline data in the absence of instrumental records and allow for an improved understanding of both modern and historic climate variability. Networks of tree-ring climate proxies, which allow for longer-term, spatially-resolved reconstructions of climate variables, are especially valuable for better understanding the spatial patterns of climate impacts. At the present time, the tree-ring record provides annually-resolved, well-replicated, and multi-centennial length paleoestimates of hydroclimate varaibility for most of the Northern Hemisphere (*e.g.* Cook et al., 2007; Stahle et al., 2016; Cook et al., 2015, 2010, 2020). By comparison, while substantial improvements have been made over the last two decades, the tree-ring-based *paleotemperature* record provides substantially less spatial coverage of the Northern Hemisphere. This spatial trend is directly related to the dendroclimatology community's historical reliance on tree-ring chronologies derived from radial-growth metrics rather than from densiometric growth or quantitative anatomical metrics. Historically, the development of tree-ring based temperature proxies at decreasing latitudes in the Northern Hemisphere was problematic, because the relationship between radial tree growth and temperature is often relatively weak due to increasingly complex hydroclimate-growth relationships (i.e. moisture availability exerts a stronger limitation on growth) (Fritts, 1976; George and Ault, 2014; Wilson et al., 2016). The historical issues related to complex and competing temperature-hydroclimate signals in tree-ring chronologies are directly addressed in this dissertation. As such, this dissertation contributes to the broader understanding about the relationships between different tree-ring parameters and climatic variables across the mid-latitudes of the continental United States.

The development of novel tree-ring metrics that reflect tree-ring wood density rather than radial growth, such as maximum latewood density (MXD; Schweingruber et al. 1978) and blue intensity (BI; Sheppard et al. 1996, McCarroll et al. 2002) has greatly remedied the lack of tree-ring temperature proxies in the Northern Hemisphere. While tree-ring parameters produced using x-ray techniques, such as MXD, were the preferred tree-ring parameter for reconstructing past temperatures throughout the 1980s-early 2000s, the time and cost-intensive nature of these techniques motivated the tree-ring community to explore the development of new tree-ring parameters that could provide representative metrics of ring density,

but at a fraction of the cost. Since the pioneering work of Sheppard et al. (1996), who were the first to experiment with visible light-based techniques on tree-rings for the purposes of dendroclimatology, the exploration of new methods to create light-based alternatives to MXD has been wildly successful. Since the work of McCarroll et al. (2002) first established the use of visible-light-based BI methods for dendroclimatology, the tree-ring community has rapidly embraced this method across multiple sub-disciplines of tree-ring research.

As of January 2022, the global tree-ring blue intensity network is comprised of over 230 BI chronologies, with 221 BI chronologies representing the Northern Hemisphere, and with 185 chronologies being developed and published within the last four years (2018-2022; Figure 4.1A). Specifically, the work presented in this dissertation contributes substantial spatial improvements to the North American region of the Northern Hemisphere BI network (Figure 4.1B). Notably, this dissertation research emphasizes the utility of BI methods on conifers at decreasing latitudes in North America by targeting tree-ring collections derived from high elevation locations. Using a similar approach, many other recent studies (since 2020) have also emphasized increasing the latitudinal extent (southward) of the temperature-sensitive tree-ring network by targeting collections from mountainous environments at lower latitudes (*e.g* Tsvetanov et al. 2020; Christopoulou et al. 2021; Cao et al. 2020; Akhmetzyanov et al. 2020; Reid and Wilson 2020). Despite major spatial improvement in the last decade, obvious spatial gaps still occur in the Northern Hemisphere paleotemperature record, such as Mexico and north eastern Asia. Aside from New Zealand, the Southern Hemisphere is virtually devoid of temperature-sensitive tree-ring records. In the future, concerted efforts should be made by the tree-ring community to remedy this issue.

Since the commencement of this dissertation research in 2018, the the diversity of conifer representation in the global BI network has significantly increased. Prior to 2018, BI studies were dominated by the *Picea* and *Pinus* genera, whereas today, the global BI network is comprised of chronologies from 18 different genera of conifer (Figure 4.2. To date, BI methods have not been successfully applied to non-coniferous, diffuse-porous species. Future examination of BI methods on diffuse-porous species may be an effective approach for 1] developing tree-ring based temperature proxies in conifer-excluded environments and for 2] better understanding the relationships between tree densiometric growth and climatic variables in new locations, globally.

Although BI has rapidly evolved since the initial work by McCarroll et al. (2002), the methods are still in a relative state of infancy. As the methods continue to progress, additional research is needed to understand the biological basis of BI methods at the cellular level. Recent work using quantitative wood anatomy has begun to examine issues related to what exactly is being captured by BI methods across each annual ring. Prior to the recent work by Björklund et al. (2021), BI was thought to be a

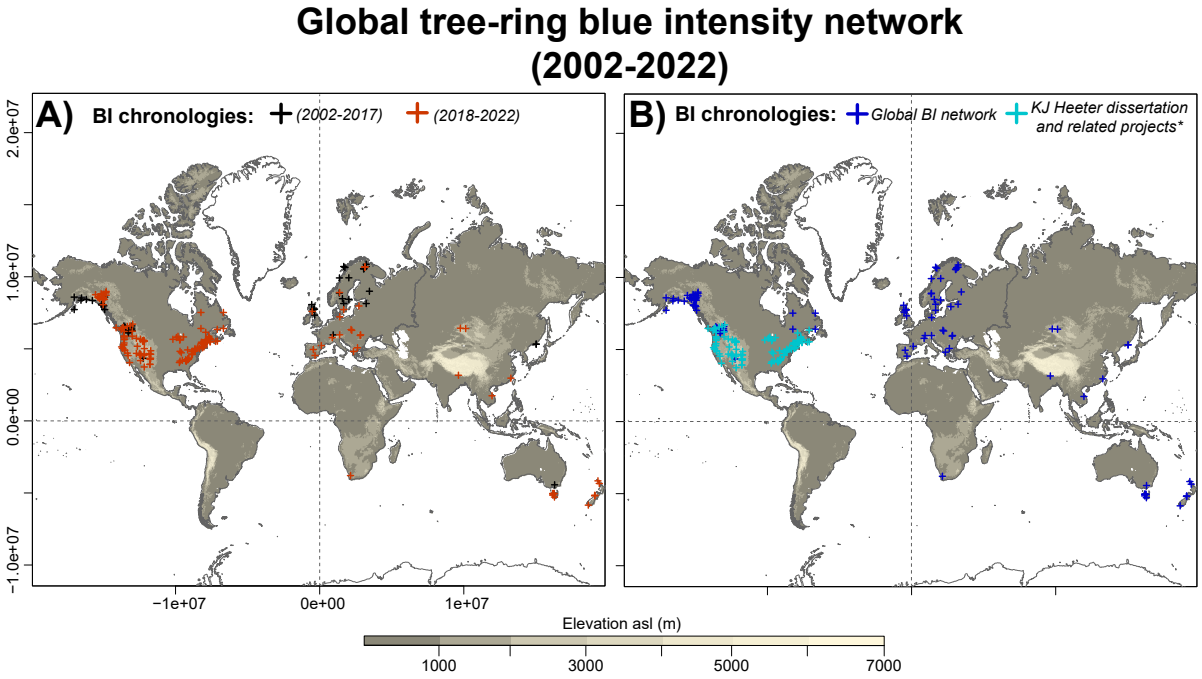

Figure 4.1: Locations of all blue intensity (BI) chronologies in the current global network of peer-reviewed, published BI studies. A) Displays the location of BI chronologies developed from 2002-2017 (black crosses) and from 2018-2022 (red crosses). B) Highlights the BI chronologies developed for Karen Heeter's dissertation or related projects* (teal crosses) in relation to the other chronologies currently comprising the global BI chronology network (dark blue crosses). *Related projects are not directly associated with Karen Heeter's dissertation but were developed by Heeter during her tenure at the University of Idaho.

representative measure of ring density that could be explained by the relationship between lignin content in the latewood cell walls and its respective reflective properties. Findings from Björklund et al. (2021) counter the general consensus that BI is related to lignin content, suggesting that BI is significantly related to the quantitative ratio of cell wall area to cell lumen area; BI is more closely related to cell wall geometry rather than chemical composition.

As BI-based chronologies increasingly populate the tree-ring record, BI methods should be considered in future conversations regarding the influence of climate proxy resolution on the subsequent paleoclimate reconstructions (c.f. the assessment of MXD records in Björklund et al. 2019). The quality and resolution of BI data are directly related to the wood surface image from which the data are collected. The capabilities of current visible light-based scanner technology has arguably plateaued, where even the most high end, commercially available flatbed scanners are incapable of producing wood surface images greater than 3200 dpi. However, recent innovations with high-resolution digital imaging systems that use microscope cameras (*e.g.* Griffin et al. 2021) are promising for their future applications in BI methods.

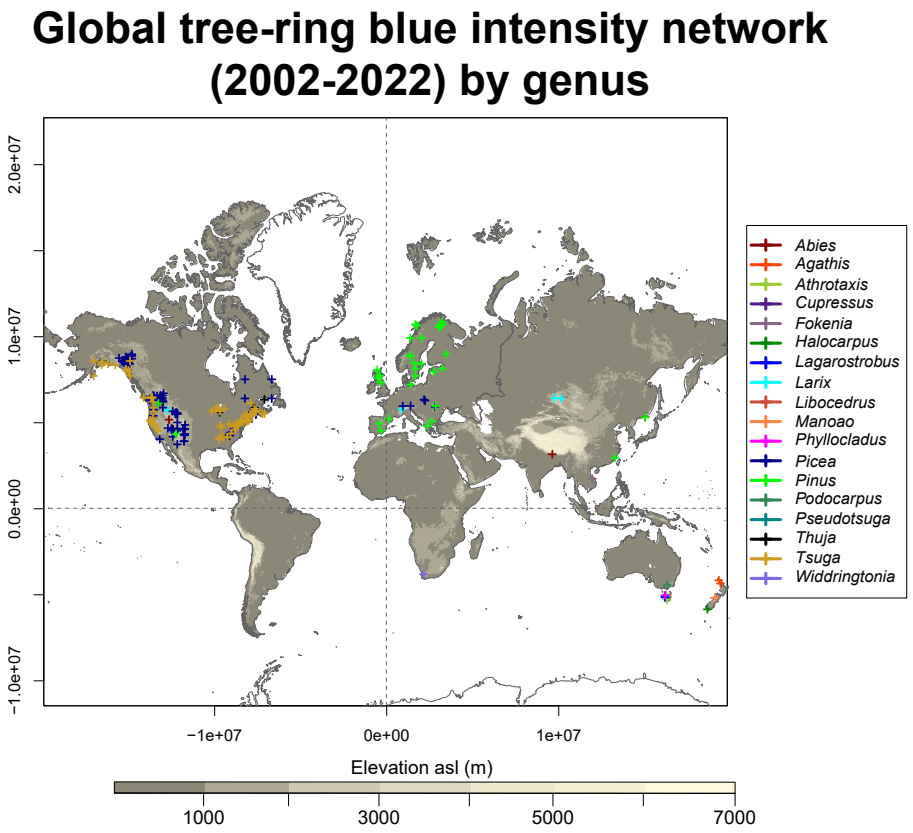

Figure 4.2: Locations of all blue intensity (BI) chronologies in the current global network of peer-reviewed, published BI studies, color-coded by genus.

The global-wide effort to continue developing, refining, and disseminating information about BI methods is apparent with the creation of the International Blue Intensity Development Working Group (I-BIND; Kaczka and Wilson 2021). The I-BIND group encourages and facilitates broad-scale collaboration related to BI methods. Through such efforts, it's likely that BI methods will continue to grow in popularity among the dendroclimatology community. Additionally, as BI has continuously been shown to be a cost-effective surrogate to MXD across many parts of the world, it is an amenable technique for tree-ring research programs that may be in early stages of development or have limited financial resources. Indeed, an increased scientific investment in widely affordable and accessible methods, which produce robust paleoclimate estimates, would contribute to an improved and more equitable global understanding of the Earth's long-term climate history.

References

Abatzoglou JT, Williams AP (2016) Impact of anthropogenic climate change on wildfire across western US forests. Proceedings of the National Academy of Sciences 113(42):11770–11775

Adams MB, Eagar C (1992) Impacts of acidic deposition on high-elevation spruce-fir forests: results from the spruce-fir research cooperative. Forest Ecology and Management 51(1-3):195–205

Ahmed M, Anchukaitis KJ, Asrat A, Borgaonkar HP, Braida M, Buckley BM, Büntgen U, Chase BM, Christie DA, Cook ER, et al. (2013) Continental-scale temperature variability during the past two millennia. Nature Geoscience 6(5):339–346

Akaike H (1974) A new look at the statistical model identification. IEEE transactions on automatic control 19(6):716–723

Akhmetzyanov L, Sánchez-Salguero R, García-González I, Buras A, Dominguez-Delmás M, Mohren F, Den Ouden J, Sass-Klaassen U (2020) Towards a new approach for dendroprovenancing pines in the Mediterranean Iberian Peninsula. Dendrochronologia 60:125688

Alday JG, Shestakova TA, de Dios VR, Voltas J (2018) Dendrosync: An R package to unravel synchrony patterns in tree-ring networks. Dendrochronologia 47:17–22

Alexander R, Sheppard W (1984) Silvicultural characteristics of Engelmann spruce. USDA Forest Service General Technical Report RM 114

Amburgey SM, Miller DA, Campbell Grant EH, Rittenhouse TA, Benard MF, Richardson JL, Urban MC, Hughson W, Brand AB, Davis CJ, et al. (2018) Range position and climate sensitivity: The structure of among-population demographic responses to climatic variation. Global Change Biology 24(1):439–454

Anchukaitis KJ, DâArrigo RD, Andreu-Hayles L, Frank D, Verstege A, Curtis A, Buckley BM, Jacoby GC, Cook ER (2013) Tree-ring-reconstructed summer temperatures from northwestern North America during the last nine centuries. Journal of Climate 26(10):3001–3012

Anchukaitis KJ, Wilson R, Briffa KR, Büntgen U, Cook ER, D'Arrigo R, Davi N, Esper J, Frank D, Gunnarson BE, et al. (2017) Last millennium Northern Hemisphere summer temperatures from tree rings: Part II, spatially resolved reconstructions. Quaternary Science Reviews 163:1–22

von Arx G, Crivellaro A, Prendin AL, Čufar K, Carrer M (2016) Quantitative wood anatomy-practical guidelines. Frontiers in Plant Science 7:781

Aukema BH, Werner RA, Haberkern KE, Illman BL, Clayton MK, Raffa KF (2005) Quantifying sources of variation in the frequency of fungi associated with spruce beetles: implications for hypothesis testing and sampling methodology in bark beetle–symbiont relationships. Forest Ecology and Management 217(2-3):187–202

Babst F, Wright WE, Szejner P, Wells L, Belmecheri S, Monson RK (2016) Blue intensity parameters derived from ponderosa pine tree rings characterize intra-annual density fluctuations and reveal seasonally divergent water limitations. Trees 30(4):1403–1415

Begum S, Nakaba S, Oribe Y, Kubo T, Funada R (2010) Cambial sensitivity to rising temperatures by natural condition and artificial heating from late winter to early spring in the evergreen conifer Cryptomeria japonica. Trees 24(1):43–52

Biondi F, Perkins D, Cayan D, Hughes M (1999) July temperature during the second millennium reconstructed from Idaho tree rings. Geophysical Research Letters 26(10):1445–1448

Björklund J, Gunnarson B, Seftigen K, Esper J, Linderholm H (2013) Is blue intensity ready to replace maximum latewood density as a strong temperature proxy? A tree-ring case study on Scots pine from northern Sweden. Climate of the Past Discussions 9(5)

Björklund J, Gunnarson BE, Seftigen K, Esper J, Linderholm H (2014) Blue intensity and density from northern Fennoscandian tree rings, exploring the potential to improve summer temperature reconstructions with earlywood information. Climate of the Past 10(2):877–885

Björklund J, Gunnarson BE, Seftigen K, Zhang P, Linderholm HW (2015) Using adjusted blue intensity data to attain high-quality summer temperature information: a case study from Central Scandinavia. The Holocene 25(3):547–556

Björklund J, Seftigen K, Schweingruber F, Fonti P, von Arx G, Bryukhanova MV, Cuny HE, Carrer M, Castagneri D, Frank DC (2017) Cell size and wall dimensions drive distinct variability of earlywood and latewood density in Northern Hemisphere conifers. New Phytologist 216(3):728–740

Björklund J, von Arx G, Nievergelt D, Wilson R, Van den Bulcke J, Günther B, Loader N, Rydval M, Fonti P, Scharnweber T, et al. (2019) Scientific merits and analytical challenges of tree-ring densitometry. Reviews of Geophysics

Björklund J, Fonti MV, Fonti P, Van den Bulcke J, von Arx G (2021) Cell wall dimensions reign supreme: cell wall composition is irrelevant for the temperature signal of latewood density/blue intensity in Scots pine. Dendrochronologia 65:125785

Blunden J, Arndt DS (2016) State of the climate in 2016. Bulletin of the American Meteorological Society 98(8):Si–S280

Bond G, Kromer B, Beer J, Muscheler R, Evans MN, Showers W, Hoffmann S, Lotti-Bond R, Hajdas I, Bonani G (2001) Persistent solar influence on North Atlantic climate during the Holocene. Science 294(5549):2130–2136

Briffa KR, Jones PD, Schweingruber FH (1988) Summer temperature patterns over Europe: a reconstruction from 1750 AD based on maximum latewood density indices of conifers. Quaternary Research 30(1):36–52

Briffa KR, Jones P, Schweingruber F (1992) Tree-ring density reconstructions of summer temperature patterns across western North America since 1600. Journal of Climate 5(7):735–754

Briffa KR, Jones PD, Schweingruber FH, Osborn TJ (1998) Influence of volcanic eruptions on Northern Hemisphere summer temperature over the past 600 years. Nature 393(6684):450–455

Briffa KR, Osborn TJ, Schweingruber FH, Harris IC, Jones PD, Shiyatov SG, Vaganov EA (2001) Low-frequency temperature variations from a northern tree ring density network. Journal of Geophysical Research: Atmospheres 106(D3):2929–2941

Briffa KR, Osborn TJ, Schweingruber FH, Jones PD, Shiyatov SG, Vaganov EA (2002) Tree-ring width and density data around the Northern Hemisphere: Part 1, local and regional climate signals. The Holocene 12(6):737–757

Briffa KR, Osborn TJ, Schweingruber F (2004) Large-scale temperature inferences from tree rings: a review. Global and planetary change 40(1-2):11–26

Brönnimann S, Franke J, Nussbaumer SU, Zumbühl HJ, Steiner D, Trachsel M, Hegerl GC, Schurer A, Worni M, Malik A, et al. (2019) Last phase of the Little Ice Age forced by volcanic eruptions. Nature Geoscience 12(8):650–656

Brookhouse M, Graham R (2016) Application of the minimum blue-intensity technique to a southern-hemisphere conifer. Tree-ring Research 72(2):103–107

Buckley BM, Hansen KG, Griffin KL, Schmiege S, Oelkers R, DâArrigo RD, Stahle DK, Davi N, Nguyen TQT, Le CN, et al. (2018) Blue intensity from a tropical coniferâs annual rings for climate reconstruction: An ecophysiological perspective. Dendrochronologia 50:10–22

Büntgen U, Esper J, Frank DC, Nicolussi K, Schmidhalter M (2005) A 1052-year tree-ring proxy for Alpine summer temperatures. Climate Dynamics 25(2-3):141–153

Büntgen U, Frank D, Grudd H, Esper J (2008a) Long-term summer temperature variations in the Pyrenees. Climate Dynamics 31(6):615–631

Büntgen U, Frank D, Wilson R, Carrer M, Urbinati C, Esper J (2008b) Testing for tree-ring divergence in the European Alps. Global Change Biology 14(10):2443–2453

Büntgen U, Krusic PJ, Verstege A, Sangüesa-Barreda G, Wagner S, Camarero JJ, Ljungqvist FC, Zorita E, Oppenheimer C, Konter O, et al. (2017) New tree-ring evidence from the Pyrenees reveals Western Mediterranean climate variability since medieval times. Journal of Climate 30(14):5295–5318

Campbell R, McCarroll D, Loader NJ, Grudd H, Robertson I, Jalkanen R (2007) Blue intensity in Pinus sylvestris tree-rings: developing a new palaeoclimate proxy. The Holocene 17(6):821–828

Cao X, Fang K, Chen P, Zhang P, Björklund J, Pumijumnong N, Guo Z (2020) Microdensitometric records from humid subtropical china show distinct climate signals in earlywood and latewood. Dendrochronologia 64:125764

Cardoza YJ, Moser JC, Klepzig KD, Raffa KF (2008) Multipartite symbioses among fungi, mites, nematodes, and the spruce beetle, Dendroctonus rufipennis. Environmental Entomology 37(4):956–963

Cayan DR, Kammerdiener SA, Dettinger MD, Caprio JM, Peterson DH (2001) Changes in the onset of spring in the western United States. Bulletin of the American Meteorological Society 82(3):399–416

Cayan DR, Das T, Pierce DW, Barnett TP, Tyree M, Gershunov A (2010) Future dryness in the southwest us and the hydrology of the early 21st century drought. Proceedings of the National Academy of Sciences 107(50):21271–21276

Christiansen B, Charpentier-Ljungqvist F (2012) The extra-tropical Northern Hemisphere temperature in the last two millennia: reconstructions of low-frequency variability. Climate of the Past 8(2):765–786

Christiansen B, Ljungqvist FC (2017) Challenges and perspectives for large-scale temperature reconstructions of the past two millennia. Reviews of Geophysics 55(1):40–96

Christopoulou A, Fyllas NM, Gmińska-Nowak B, Özarslan Y, Arianoutsou M, Brandes R, Wany T (2021) Exploring the past of Mavrovouni forest in the Pindus Mountain range (Greece) using tree rings of Bosnian pines. Trees pp 1–14

Conkey LE (1979) Response of tree-ring density to climate in Maine, USA

Conkey LE (1986) Red spruce tree-ring widths and densities in eastern North America as indicators of past climate. Quaternary Research 26(2):232–243

Consortium P, et al. (2017) A global multiproxy database for temperature reconstructions of the Common Era. Scientific data 4

Cook BI, Miller RL, Seager R (2008) Dust and sea surface temperature forcing of the 1930s âDust Bowlâ drought. Geophysical Research Letters 35(8)

Cook BI, Miller RL, Seager R (2009) Amplification of the North American âDust Bowlâ drought through human-induced land degradation. Proceedings of the National Academy of Sciences 106(13):4997–5001

Cook BI, Smerdon JE, Seager R, Cook ER (2014) Pan-continental droughts in North America over the last millennium. Journal of Climate 27(1):383–397

Cook E, Briffa K (1990) A comparison of some tree-ring standardization methods.–Cook, ER, Kairiukstis, LA (eds.). Methods of dendrochronology. Applications in the environmental sciences

Cook ER, Holmes R (1996) Guide for computer program ARSTAN. The international tree-ring data bank program library version 2(0):75–87

Cook ER, Jacoby GC (1977) Tree-ring-drought relationships in the Hudson Valley, New York. Science 198(4315):399–401

Cook ER, Johnson AH (1989) Climate change and forest decline: a review of the red spruce case. Water, Air, and Soil Pollution 48(1):127–140

Cook ER, Kairiukstis LA (2013) Methods of dendrochronology: applications in the environmental sciences. Springer Science & Business Media

Cook ER, Meko DM, Stahle DW, Cleaveland MK (1999) Drought reconstructions for the continental United States. Journal of Climate 12(4):1145–1162

Cook ER, Woodhouse CA, Eakin CM, Meko DM, Stahle DW (2004) Long-term aridity changes in the western United States. Science 306(5698):1015–1018

Cook ER, Seager R, Cane MA, Stahle DW (2007) North American drought: Reconstructions, causes, and consequences. Earth-Science Reviews 81(1-2):93–134

Cook ER, Seager R, Heim Jr RR, Vose RS, Herweijer C, Woodhouse C (2010) Megadroughts in North America: Placing IPCC projections of hydroclimatic change in a long-term palaeoclimate context. Journal of Quaternary Science 25(1):48–61

Cook ER, Krusic PJ, Anchukaitis KJ, Buckley BM, Nakatsuka T, Sano M, et al. (2013a) Tree-ring reconstructed summer temperature anomalies for temperate East Asia since 800 CE. Climate Dynamics 41(11-12):2957–2972

Cook ER, Palmer JG, Ahmed M, Woodhouse CA, Fenwick P, Zafar MU, Wahab M, Khan N (2013b) Five centuries of Upper Indus River flow from tree rings. Journal of Hydrology 486:365–375

Cook ER, Seager R, Kushnir Y, Briffa KR, Büntgen U, Frank D, Krusic PJ, Tegel W, van der Schrier G, Andreu-Hayles L, et al. (2015) Old World megadroughts and pluvials during the Common Era. Science advances 1(10):e1500561

Cook ER, Solomina O, Matskovsky V, Cook BI, Agafonov L, Berdnikova A, Dolgova E, Karpukhin A, Knysh N, Kulakova M, et al. (2020) The European Russia drought atlas (1400–2016 CE). Climate Dynamics 54(3):2317–2335

Crowley TJ, Zielinski G, Vinther B, Udisti R, Kreutz K, Cole-Dai J, Castellano E (2008) Volcanism and the Little Ice Age. PAGES news 16(2):22–23

Cybis (2020) On blue channel measurements. `https://www.cybis.se/forfun/dendro/helpcoorecorder7/bluechannel80/index.htm`, accessed: 2020-03-30

Daly C, Neilson RP, Phillips DL (1994) A statistical-topographic model for mapping climatological precipitation over mountainous terrain. Journal of Applied Meteorology 33(2):140–158

D'Arrigo R, Jacoby G, Frank D, Pederson N, Cook E, Buckley B, Nachin B, Mijiddorj R, Dugarjav C (2001) 1738 years of Mongolian temperature variability inferred from a tree-ring width chronology of Siberian pine. Geophysical Research Letters 28(3):543–546

D'Arrigo R, Wilson R, Jacoby G (2006) On the long-term context for late twentieth century warming. Journal of Geophysical Research: Atmospheres 111(D3)

D'Arrigo R, Wilson R, Liepert B, Cherubini P (2008) On the âdivergence problemâin northern forests: a review of the tree-ring evidence and possible causes. Global and Planetary Change 60(3-4):289–305

D'Arrigo R, Wilson R, Anchukaitis KJ (2013) Volcanic cooling signal in tree ring temperature records for the past millennium. Journal of Geophysical Research: Atmospheres 118(16):9000–9010

D'Arrigo RD, Jacoby GC (1999) Northern North American tree-ring evidence for regional temperature changes after major volcanic events. Climatic Change 41(1):1–15

Data UC (2019) Temperature - Precipitation - Sunshine - Snowfalls

Davi NK, Jacoby GC, Wiles GC (2003) Boreal temperature variability inferred from maximum latewood density and tree-ring width data, Wrangell Mountain region, Alaska. Quaternary Research 60(3):252–262

Davis TS, Horne FB, Yetter JC, Stewart JE (2018) Engelmann spruce chemotypes in Colorado and their effects on symbiotic fungi associated with the North American spruce beetle. Journal of Chemical Ecology 44(6):601–610

DeRose RJ, Long JN, Ramsey RD (2011) Combining dendrochronological data and the disturbance index to assess Engelmann spruce mortality caused by a spruce beetle outbreak in southern Utah, USA. Remote Sensing of Environment 115(9):2342–2349

DeRose RJ, Bentz BJ, Long JN, Shaw JD (2013) Effect of increasing temperatures on the distribution of spruce beetle in Engelmann spruce forests of the Interior West, USA. Forest Ecology and Management 308:198–206

Deslauriers A, Morin H, Begin Y (2003) Cellular phenology of annual ring formation of Abies balsamea in the Quebec boreal forest (canada). Canadian Journal of Forest Research 33(2):190–200

Dolgova E (2016) June–September temperature reconstruction in the Northern Caucasus based on blue intensity data. Dendrochronologia 39:17–23

Dorado Liñán I, Büntgen U, González-Rouco F, Zorita E, Montávez J, Gómez-Navarro J, Brunet M, Heinrich I, Helle G, Gutiérrez E (2012) Estimating 750 years of temperature variations and uncertainties in the Pyrenees by tree-ring reconstructions and climate simulations. Climate of the Past 8(3):919–933

Douglas AV, Stockton CW (1975) Long-term reconstruction of seasonal temperature and precipitation in the Yellowstone National Park region using dendroclimatic techniques

Durbin J, Watson GS (1971) Testing for serial correlation in least squares regression. III. Biometrika 58(1):1–19

Eddy JA (1976) The Maunder Minimum. Science 192(4245):1189–1202

Edwards J, Anchukaitis KJ, Zambri B, Andreu-Hayles L, Oelkers R, D'Arrigo R, von Arx G (2021) Intra-annual climate anomalies in northwestern North America following the 1783-1784 CE Laki eruption. Journal of Geophysical Research: Atmospheres p e2020JD033544

Elliott GP (2011) Influences of 20th-century warming at the upper tree line contingent on local-scale interactions: Evidence from a latitudinal gradient in the Rocky Mountains, USA. Global Ecology and Biogeography 20(1):46–57

Esper J, Cook ER, Schweingruber FH (2002) Low-frequency signals in long tree-ring chronologies for reconstructing past temperature variability. Science 295(5563):2250–2253

Esper J, Düthorn E, Krusic PJ, Timonen M, Büntgen U (2014) Northern european summer temperature variations over the Common Era from integrated tree-ring density records. Journal of Quaternary Science 29(5):487–494

Esper J, George SS, Anchukaitis K, D'Arrigo R, Ljungqvist FC, Luterbacher J, Schneider L, Stoffel M, Wilson R, Büntgen U (2018) Large-scale, millennial-length temperature reconstructions from tree-rings. Dendrochronologia 50:81–90

Esper J, Klippel L, Krusic PJ, Konter O, Raible CC, Xoplaki E, Luterbacher J, Büntgen U (2020) Eastern Mediterranean summer temperatures since 730 CE from Mt. Smolikas tree-ring densities. Climate Dynamics 54(3):1367–1382

Fan ZX, Bräuning A, Yang B, Cao KF (2009) Tree ring density-based summer temperature reconstruction for the central Hengduan Mountains in southern China. Global and Planetary Change 65(1-2):1–11

Flato G, Marotzke J, Abiodun B, Braconnot P, Chou S, Collins W, Cox P, Driouech F, Emori S, Eyring V, et al. (2013) Climate change 2013: the physical science basis. contribution of working group i to the fifth assessment report of the intergovernmental panel on climate change. Evaluation of Climate Models, eds TF Stocker, D Qin, G-K Plattner, M Tignor, SK Allen, J Boschung, et al(Cambridge: Cambridge University Press)

Frank D, Esper J, Zorita E, Wilson R (2010) A noodle, hockey stick, and spaghetti plate: a perspective on high-resolution paleoclimatology. Wiley Interdisciplinary Reviews: Climate Change 1(4):507–516

Fritts H (1976) Tree rings and climate. Elsevier

Fuentes M, Salo R, Björklund J, Seftigen K, Zhang P, Gunnarson B, Aravena JC, Linderholm HW (2018) A 970-year-long summer temperature reconstruction from Rogen, west-central Sweden, based on blue intensity from tree rings. The Holocene 28(2):254–266

Garfin G, Franco G, Blanco H, Comrie A, Gonzalez P, Piechota T, Smyth R, Waskom R (2014) Southwest: the third national climate assessment. In: Climate change impacts in the United States: the third National Climate Assessment, US Global Change Research Program, pp 462–486

Gärtner H, Nievergelt D (2010) The core-microtome: a new tool for surface preparation on cores and time series analysis of varying cell parameters. Dendrochronologia 28(2):85–92

Gennaretti F, Arseneault D, Nicault A, Perreault L, Bégin Y (2014) Volcano-induced regime shifts in millennial tree-ring chronologies from northeastern North America. Proceedings of the National Academy of Sciences 111(28):10077–10082

George SS, Ault TR (2014) The imprint of climate within Northern Hemisphere trees. Quaternary Science Reviews 89:1–4

Gervais BR, MacDonald GM (2001) Tree-ring and summer-temperature response to volcanic aerosol forcing at the northern tree-line, Kola Peninsula, Russia. The Holocene 11(4):499–505

Gindl W, Grabner M, Wimmer R (2000) The influence of temperature on latewood lignin content in treeline Norway spruce compared with maximum density and ring width. Trees 14(7):409–414

González J, Valdés JB (2003) Bivariate drought recurrence analysis using tree ring reconstructions. Journal of Hydrologic Engineering 8(5):247–258

Graumlich LJ (1993) A 1000-year record of temperature and precipitation in the Sierra Nevada. Quaternary Research 39(2):249–255

Graumlich LJ, Brubaker LB (1986) Reconstruction of annual temperature (1590–1979) for Longmire, Washington, derived from tree rings. Quaternary Research 25(2):223–234

Griffin D, Porter ST, Trumper ML, Carlson KE, Crawford DJ, Schwalen D, McFadden CH (2021) Gigapixel macro photography of tree rings. Tree-Ring Research 77(2):86–94

Griggs RF (1914) Observations on the behavior of some species at the edges of their ranges. Bulletin of the Torrey Botanical Club pp 25–49

Gruber A, Zimmermann J, Wieser G, Oberhuber W (2009) Effects of climate variables on intra-annual stem radial increment in Pinus cembra (L.) along the alpine treeline ecotone. Annals of Forest Science 66(5):1–11

Guillet S, Corona C, Stoffel M, Khodri M, Lavigne F, Ortega P, Eckert N, Sielenou PD, Daux V, Churakova Ov, et al. (2017) Climate response to the Samalas volcanic eruption in 1257 revealed by proxy records. Nature Geoscience 10(2):123–128

Guttman L (1954) Some necessary conditions for common-factor analysis. Psychometrika 19(2):149–161

Harley GL, Maxwell JT (2018) Current declines of Pecos River (New Mexico, USA) streamflow in a 700-year context. The Holocene 28(5):767–777

Harley GL, Grissino-Mayer HD, Franklin JA, Anderson C, Köse N (2012) Cambial activity of Pinus elliottii var. densa reveals influence of seasonal insolation on growth dynamics in the Florida Keys. Trees 26(5):1449–1459

Harley GL, Maxwell JT, Larson E, Grissino-Mayer HD, Henderson J, Huffman J (2017) Suwannee river flow variability 1550–2005 CE reconstructed from a multispecies tree-ring network. Journal of Hydrology 544:438–451

Harley GL, Heeter KJ, Maxwell JT, Rayback SA, Maxwell RS, Reinemann TE, H Taylor A (2020a) Towards broad-scale temperature reconstructions for Eastern North America using blue light intensity from tree rings. International Journal of Climatology

Harley GL, Maxwell RS, Black BA, Bekker MF (2020b) A multi-century, tree-ring-derived perspective of the North Cascades (USA) 2014–2016 snow drought. Climatic Change pp 1–17

Harley GL, Heeter KJ, Maxwell JT, Rayback SA, Maxwell RS, Reinemann TE, H Taylor A (2021) Towards broad-scale temperature reconstructions for Eastern North America using blue light intensity from tree rings. International Journal of Climatology 41:E3142–E3159

Harris I, Jones P, Osborn T, Lister D (2014) CRU TS3. 22: Climatic Research Unit (CRU) Time-Series (TS) version 3.22 of High Resolution Gridded Data of Month-by-month Variation in Climate (jan. 1901-dec. 2013). NCAS British Atmospheric Data Centre, 24th September 2016

Heeter KJ, Harley GL, Van De Gevel SL, White PB (2019) Blue intensity as a temperature proxy in the eastern United States: A pilot study from a southern disjunct population of Picea rubens (Sarg.). Dendrochronologia 55:105–109

Heeter KJ, Harley GL, Maxwell JT, McGee JH, Matheus TJ (2020) Late summer temperature variability for the Southern Rocky Mountains (USA) since 1735 CE: applying blue light intensity to low-latitude Picea engelmannii Parry ex Engelm. Climatic Change pp 1–24

Heeter KJ, Rochner ML, Harley GL (2021) Summer air temperature for the Greater Yellowstone Ecoregion (770–2019 CE) over 1,250 years. Geophysical Research Letters 48(7):e2020GL092269

Hegerl G, Luterbacher J, González-Rouco F, Tett SF, Crowley T, Xoplaki E (2011) Influence of human and natural forcing on European seasonal temperatures. Nature Geoscience 4(2):99–103

Herrero A, Rigling A, Zamora R (2013) Varying climate sensitivity at the dry distribution edge of Pinus sylvestris and P. nigra. Forest Ecology and Management 308:50–61

Hill JK, Griffiths HM, Thomas CD (2011) Climate change and evolutionary adaptations at species' range margins. Annual Review of Entomology 56:143–159

Holmes RL (1983) Computer-assisted quality control in tree-ring dating and measurement

Holt RD, Keitt TH (2005) Speciesâ borders: a unifying theme in ecology. Oikos 108(1):3–6

Horton R (2014) 2014: Northeast. climate change impacts in the United States: The third national climate assessment, jm melillo. TC Richmond, and GW Yohe, Eds, US Global Change Research Program pp 371–395

Husson F, Josse J, Le S, Mazet J, Husson MF (2016) Package âFactoMineRâ. An R package 96:698

Jacoby GC, D'Arrigo R (1989) Reconstructed Northern Hemisphere annual temperature since 1671 based on high-latitude tree-ring data from North America. Climatic Change 14(1):39–59

Jacoby GC, Workman KW, DâArrigo RD (1999) Laki eruption of 1783, tree rings, and disaster for northwest Alaska Inuit. Quaternary Science Reviews 18(12):1365–1371

Jardine A, Merideth R, Black M, LeRoy S (2013) Assessment of climate change in the southwest United States: A report prepared for the National Climate Assessment. Island press

Johnson A, Cook E, Siccama T (1988) Climate and red spruce growth and decline in the northern Appalachians. Proceedings of the National Academy of Sciences 85(15):5369–5373

Johnson AH, Siccama TG (1983) Acid deposition and forest decline. Environmental science & technology 17(7):294A–305A

Jones P, Briffa K, Barnett T, Tett S (1998) High-resolution palaeoclimatic records for the last millennium: interpretation, integration and comparison with General Circulation Model control-run temperatures. The Holocene 8(4):455–471

Jones PD, New M, Parker DE, Martin S, Rigor IG (1999) Surface air temperature and its changes over the past 150 years. Reviews of Geophysics 37(2):173–199

Kaczka RJ, Wilson R (2021) I-BIND: International Blue Intensity Network Development Working Group. Dendrochronologia p 125859

Kaczka RJ, Spyt B, Janecka K, Beil I, Büntgen U, Scharnweber T, Nievergelt D, Wilmking M (2018) Different maximum latewood density and blue intensity measurements techniques reveal similar results. Dendrochronologia 49:94–101

Kaiser HF (1960) The application of electronic computers to factor analysis. Educational and psychological measurement 20(1):141–151

Kalra A, Piechota TC, Davies R, Tootle GA (2008) Changes in US streamflow and western US snowpack. Journal of Hydrologic Engineering 13(3):156–163

Keyimu M, Li Z, Zhang G, Fan Z, Wang X, Fu B (2020a) Tree ring–based minimum temperature reconstruction in the central Hengduan Mountains, China. Theoretical and Applied Climatology 141(1):359–370

Keyimu M, Li Z, Zhao Y, Dong Y, Fu B, Fan Z, Wang X (2020b) Reconstruction of maximum temperature on Zhegu Mountain, western Sichuan Plateau (China). Climate Research 81:1–14

Kipfmueller KF, Salzer MW (2010) Linear trend and climate response of five-needle pines in the western United States related to treeline proximity. Canadian Journal of Forest Research 40(1):134–142

Knudsen MF, Jacobsen BH, Seidenkrantz MS, Olsen J (2014) Evidence for external forcing of the Atlantic Multidecadal Oscillation since termination of the Little Ice Age. Nature Communications 5(1):1–8

Köse N, Güner HT, Harley GL, Guiot J (2017) Spring temperature variability over Turkey since 1800 CE reconstructed from a broad network of tree-ring data. Climate of the Past 13(1):1–15

Kreutz KJ, Mayewski PA, Meeker LD, Twickler MS, Whitlow SI, Pittalwala II (1997) Bipolar changes in atmospheric circulation during the Little Ice Age. Science 277(5330):1294–1296

Kunkel KE, Stevens LE, Stevens SE, Sun L, Janssen E, Wuebbles D, Kruk MC, Thomas D, Shulski M, Umphlett NA, et al. (2013) Regional climate trends and scenarios for the US national climate assessment part 4. climate of the US Great Plains

Larson ER, Allen S, Flinner NL, Labarge SG, Wilding TC (2013) The need and means to update chronologies in a dynamic environment. Tree-ring Research 69(1):21–27

Larsson L (2014) CooRecorder and Cdendro programs of the CooRecorder/Cdendro package version 7.7. https://www.cybis.se/forfun/dendro.htm

Lean J, Skumanich A, White O (1992) Estimating the Sun's radiative output during the Maunder Minimum. Geophysical Research Letters 19(15):1591–1594

Linderholm HW, Björklund J, Seftigen K, Gunnarson BE, Fuentes M (2015) Fennoscandia revisited: a spatially improved tree-ring reconstruction of summer temperatures for the last 900 years. Climate Dynamics 45(3-4):933–947

Little EL, Viereck LA (1971) Atlas of United States trees, vol 5. US Dept. of Agriculture, Forest Service

Lloyd AH, Fastie CL (2002) Spatial and temporal variability in the growth and climate response of treeline trees in Alaska. Climatic Change 52(4):481–509

Lücke LJ, Hegerl GC, Schurer AP, Wilson R (2019) Effects of memory biases on variability of temperature reconstructions. Journal of Climate 32(24):8713–8731

Luckman B, Wilson R (2005) Summer temperatures in the Canadian Rockies during the last millennium: a revised record. Climate Dynamics 24(2-3):131–144

Mann ME, Bradley RS, Hughes MK (1999) Northern hemisphere temperatures during the past millennium: Inferences, uncertainties, and limitations. Geophysical Research Letters 26(6):759–762

Mann ME, Zhang Z, Rutherford S, Bradley RS, Hughes MK, Shindell D, Ammann C, Faluvegi G, Ni F (2009) Global signatures and dynamical origins of the Little Ice Age and Medieval Climate Anomaly. Science 326(5957):1256–1260

Martin JT, Pederson GT, Woodhouse CA, Cook ER, McCabe GJ, Anchukaitis KJ, Wise EK, Erger PJ, Dolan L, McGuire M, et al. (2020) Increased drought severity tracks warming in the United Statesâ largest river basin. Proceedings of the National Academy of Sciences 117(21):11328–11336

Masson-Delmotte V, Schulz M, Abe-Ouchi A, Beer J, Ganopolski A, González Rouco J, Jansen E, Lambeck K, Luterbacher J, Naish T, et al. (2013) Information from paleoclimate archives

Maxwell JT, Harley GL (2017) Increased tree-ring network density reveals more precise estimations of sub-regional hydroclimate variability and climate dynamics in the Midwest, USA. Climate Dynamics 49(4):1479–1493

Maxwell JT, Harley GL, Matheus TJ, Strange BM, Van Aken K, Au TF, Bregy JC (2020) Sampling density and date along with species selection influence spatial representation of tree-ring reconstructions. Climate of the Past 16(5):1901–1916

Maxwell RS, Harley GL, Maxwell JT, Rayback SA, Pederson N, Cook ER, Barclay DJ, Li W, Rayburn JA (2017) An interbasin comparison of tree-ring reconstructed streamflow in the eastern United States. Hydrological Processes 31(13):2381–2394

McCarroll D, Pettigrew E, Luckman A, Guibal F, Edouard JL (2002) Blue reflectance provides a surrogate for latewood density of high-latitude pine tree rings. Arctic, Antarctic, and Alpine Research 34(4):450–453

McCullough IM, Davis FW, Williams AP (2017) A range of possibilities: Assessing geographic variation in climate sensitivity of ponderosa pine using tree rings. Forest Ecology and Management 402:223–233

McLaughlin S, Downing D, Blasing T, Cook E, Adams H (1987) An analysis of climate and competition as contributors to decline of red spruce in high elevation Appalachian forests of the eastern United States. Oecologia 72(4):487–501

Melvin TM, Briffa KR (2008) A âsignal-freeâ approach to dendroclimatic standardisation. Dendrochronologia 26(2):71–86

Melvin TM, Briffa KR, Nicolussi K, Grabner M (2007) Time-varying-response smoothing. Dendrochronologia 25(1):65–69

Mooney H, Larigauderie A, Cesario M, Elmquist T, Hoegh-Guldberg O, Lavorel S, Mace GM, Palmer M, Scholes R, Yahara T (2009) Biodiversity, climate change, and ecosystem services. Current opinion in environmental sustainability 1(1):46–54

Neukom R, Gergis J, Karoly DJ, Wanner H, Curran M, Elbert J, González-Rouco F, Linsley BK, Moy AD, Mundo I, et al. (2014) Inter-hemispheric temperature variability over the past millennium. Nature Climate Change 4(5):362–367

Neukom R, Steiger N, Gómez-Navarro JJ, Wang J, Werner JP (2019) No evidence for globally coherent warm and cold periods over the preindustrial Common Era. Nature 571(7766):550–554

Oliver JS, Harley GL, Maxwell JT (2019) 2,500 years of hydroclimate variability in New Mexico, USA. Geophysical Research Letters 46(8):4432–4440

Oman L, Robock A, Stenchikov GL, Thordarson T, Koch D, Shindell DT, Gao C (2006) Modeling the distribution of the volcanic aerosol cloud from the 1783–1784 Laki eruption. Journal of Geophysical Research: Atmospheres 111(D12)

Overpeck JT (2013) The challenge of hot drought. Nature 503(7476):350–351

Pachauri RK, Allen MR, Barros VR, Broome J, Cramer W, Christ R, Church JA, Clarke L, Dahe Q, Dasgupta P, et al. (2014) Climate change 2014: synthesis report. Contribution of Working Groups I, II and III to the fifth assessment report of the Intergovernmental Panel on Climate Change. IPCC

Parker M, Henoch W (1971) The use of Engelmann spruce latewood density for dendrochronological purposes. Canadian Journal of Forest Research 1(2):90–98

Pearl JK, Anchukaitis KJ, Pederson N, Donnelly JP (2017) Reconstructing Northeastern United States temperatures using Atlantic white cedar tree rings. Environmental Research Letters 12(11):114012

Pederson GT, Gray ST, Woodhouse CA, Betancourt JL, Fagre DB, Littell JS, Watson E, Luckman BH, Graumlich LJ (2011) The unusual nature of recent snowpack declines in the North American Cordillera. Science 333(6040):332–335

Pederson N, Cook ER, Jacoby GC, Peteet DM, Griffin KL (2004) The influence of winter temperatures on the annual radial growth of six northern range margin tree species. Dendrochronologia 22(1):7–29

Pettit JM, Voelker SL, DeRose RJ, Burton JI (2020) Spruce beetle outbreak was not driven by drought stress: Evidence from a tree-ring iso-demographic approach indicates temperatures were more important. Global Change Biology 26(10):5829–5843

Porter TJ, Pisaric MF, Kokelj SV, deMontigny P (2013) A ring-width-based reconstruction of June–July minimum temperatures since AD 1245 from white spruce stands in the Mackenzie Delta region, northwestern Canada. Quaternary Research 80(2):167–179

Reid E, Wilson R (2020) Delta blue intensity vs. maximum density: A case study using Pinus uncinata in the Pyrenees. Dendrochronologia p 125706

Revelle W (1979) Hierarchical cluster analysis and the internal structure of tests. Multivariate Behavioral Research 14(1):57–74

Rydval M, Larsson LÅ, McGlynn L, Gunnarson BE, Loader NJ, Young GH, Wilson R (2014) Blue intensity for dendroclimatology: should we have the blues? Experiments from Scotland. Dendrochronologia 32(3):191–204

Rydval M, Loader NJ, Gunnarson BE, Druckenbrod DL, Linderholm HW, Moreton SG, Wood CV, Wilson R (2017) Reconstructing 800 years of summer temperatures in Scotland from tree rings. Climate Dynamics 49(9-10):2951–2974

Rydval M, Druckenbrod DL, Svoboda M, Trotsiuk V, Janda P, Mikoláš M, Čada V, Bače R, Teodosiu M, Wilson R (2018) Influence of sampling and disturbance history on climatic sensitivity of temperature-limited conifers. The Holocene 28(10):1574–1587

Saladyga T, Maxwell RS (2015) Temporal variability in climate response of eastern hemlock in the Central Appalachian Region. Southeastern Geographer 55(2):143–163

Salzer MW, Kipfmueller KF (2005) Reconstructed temperature and precipitation on a millennial timescale from tree-rings in the southern Colorado Plateau, USA. Climatic Change 70(3):465–487

Salzer MW, Bunn AG, Graham NE, Hughes MK (2014a) Five millennia of paleotemperature from tree-rings in the Great Basin, USA. Climate Dynamics 42(5-6):1517–1526

Salzer MW, Larson ER, Bunn AG, Hughes MK (2014b) Changing climate response in near-treeline bristlecone pine with elevation and aspect. Environmental Research Letters 9(11):114007

Schmidt A, Thordarson T, Oman LD, Robock A, Self S (2012) Climatic impact of the long-lasting 1783 Laki eruption: Inapplicability of mass-independent sulfur isotopic composition measurements. Journal of Geophysical Research: Atmospheres 117(D23)

Schneider L, Smerdon JE, Büntgen U, Wilson RJ, Myglan VS, Kirdyanov AV, Esper J (2015) Revising midlatitude summer temperatures back to AD 600 based on a wood density network. Geophysical Research Letters 42(11):4556–4562

Schurer AP, Hegerl GC, Luterbacher J, Brönnimann S, Cowan T, Tett SF, Zanchettin D, Timmreck C (2019) Disentangling the causes of the 1816 European year without a summer. Environmental Research Letters 14(9):094019

Schweingruber F (1988) A new dendroclimatic network for western North America. Dendrochronologia 6:171–180

Schweingruber F, Fritts H, Bräker O, Drew L, Schär E (1978) The x-ray technique as applied to dendroclimatology

Schweingruber F, Briffa K, Nogler P (1993) A tree-ring densitometric transect from Alaska to Labrador. International Journal of Biometeorology 37(3):151–169

Schweingruber FH, Briffa KR (1996) Tree-ring density networks for climate reconstruction. In: Climatic variations and forcing mechanisms of the last 2000 years, Springer, pp 43–66

Seager R, Kushnir Y, Ting M, Cane M, Naik N, Miller J (2008) Would advance knowledge of 1930s SSTs have allowed prediction of the Dust Bowl drought? Journal of Climate 21(13):3261–3281

Sheppard PR, Graumlich LJ, Conkey LE (1996) Reflected-light image analysis of conifer tree rings for reconstructing climate. The Holocene 6(1):62–68

Shindell DT, Schmidt GA, Mann ME, Rind D, Waple A (2001) Solar forcing of regional climate change during the Maunder Minimum. Science 294(5549):2149–2152

Six DL, Bentz BJ (2003) Fungi associated with the North American spruce beetle, Dendroctonus rufipennis. Canadian Journal of Forest Research 33(9):1815–1820

Soulé PT (2011) Changing climate, atmospheric composition, and radial tree growth in a spruce-fir ecosystem on Grandfather Mountain, North Carolina. Natural Areas Journal 31(1):65–74

Speer JH (2010) Fundamentals of tree-ring research. University of Arizona Press

Stahle DW, Cook ER, Burnette DJ, Villanueva J, Cerano J, Burns JN, Griffin D, Cook BI, Acuna R, Torbenson MC, et al. (2016) The Mexican Drought Atlas: Tree-ring reconstructions of the soil moisture balance during the late pre-Hispanic, colonial, and modern eras. Quaternary Science Reviews 149:34–60

Stoffel M, Khodri M, Corona C, Guillet S, Poulain V, Bekki S, Guiot J, Luckman BH, Oppenheimer C, Lebas N, et al. (2015) Estimates of volcanic-induced cooling in the Northern Hemisphere over the past 1,500 years. Nature Geoscience 8(10):784

Stokes M, Smiley T (1968) An Introduction to Tree-ring Dating. University of Chicago. Chicago Press, IL

Stott PA, Gillett NP, Hegerl GC, Karoly DJ, Stone DA, Zhang X, Zwiers F (2010) Detection and attribution of climate change: a regional perspective. Wiley Interdisciplinary Reviews: Climate Change 1(2):192–211

Team RC, et al. (2013) R: A language and environment for statistical computing

Thornton PK, Ericksen PJ, Herrero M, Challinor AJ (2014) Climate variability and vulnerability to climate change: a review. Global Change Biology 20(11):3313–3328

Thuiller W (2004) Patterns and uncertainties of species' range shifts under climate change. Global Change Biology 10(12):2020–2027

Tingley MP, Craigmile PF, Haran M, Li B, Mannshardt E, Rajaratnam B (2012) Piecing together the past: Statistical insights into paleoclimatic reconstructions. Quaternary Science Reviews 35:1–22

Trotsiuk V, Pederson N, Druckenbrod DL, Orwig DA, Bishop DA, Barker-Plotkin A, Fraver S, Martin-Benito D (2018) Testing the efficacy of tree-ring methods for detecting past disturbances. Forest Ecology and Management 425:59–67

Trouet V, Van Oldenborgh GJ (2013) KNMI Climate Explorer: a web-based research tool for high-resolution paleoclimatology. Tree-Ring Research 69(1):3–14

Trouet V, Diaz H, Wahl E, Viau A, Graham R, Graham N, Cook E (2013) A 1500-year reconstruction of annual mean temperature for temperate North America on decadal-to-multidecadal time scales. Environmental Research Letters 8(2):024008

Tsvetanov N, Dolgova E, Panayotov M (2020) First measurements of blue intensity from Pinus peuce and Pinus heldreichii tree rings and potential for climate reconstructions. Dendrochronologia 60:125681

Udall B, Overpeck J (2017) The twenty-first century Colorado River hot drought and implications for the future. Water Resources Research 53(3):2404–2418

US Climate Data (2020) Climate Ruidoso- New Mexico. Data retrieved from `https://www.usclimatedata.com/climate/ruidoso/new-mexico/united-states/usnm0270`

Vinod HD, López-de Lacalle J, et al. (2009) Maximum entropy bootstrap for time series: the MEboot R package. Journal of Statistical Software 29(5):1–19

Wagner S, Zorita E (2005) The influence of volcanic, solar and CO 2 forcing on the temperatures in the Dalton Minimum (1790–1830): a model study. Climate Dynamics 25(2-3):205–218

Wahl ER, Ammann CM (2007) Robustness of the Mann, Bradley, Hughes reconstruction of northern hemisphere surface temperatures: Examination of criticisms based on the nature and processing of proxy climate evidence. Climatic Change 85(1-2):33–69

Wahl ER, Smerdon JE (2012) Comparative performance of paleoclimate field and index reconstructions derived from climate proxies and noise-only predictors. Geophysical Research Letters 39(6)

Webster K, Creed I, Nicholas N, Van Miegroet H (2004) Exploring interactions between pollutant emissions and climatic variability in growth of red spruce in the Great Smoky Mountains National Park. Water, Air, and Soil Pollution 159(1):225–248

Weiss JL, Castro CL, Overpeck JT (2009) Distinguishing pronounced droughts in the southwestern United States: Seasonality and effects of warmer temperatures. Journal of Climate 22(22):5918–5932

Westerling AL, Hidalgo HG, Cayan DR, Swetnam TW (2006) Warming and earlier spring increase western US forest wildfire activity. science 313(5789):940–943

White PB, Van de Gevel SL, Soulé PT (2012) Succession and disturbance in an endangered red spruce-Fraser fir forest in the southern Appalachian Mountains, North Carolina, USA. Endangered Species Research 18(1):17–25

White PB, Soulé P, van de Gevel S (2014) Impacts of human disturbance on the temporal stability of climate–growth relationships in a red spruce forest, southern Appalachian Mountains, USA. Dendrochronologia 32(1):71–77

White PS, Cogbill CV (1992) Spruce-fir forests of eastern North America. In: Ecology and decline of red spruce in the eastern United States, Springer, pp 3–39

Wigley TM, Briffa KR, Jones PD (1984) On the average value of correlated time series, with applications in dendroclimatology and hydrometeorology. Journal of Applied Meteorology and Climatology 23(2):201–213

Wild M (2009) Global dimming and brightening: A review. Journal of Geophysical Research: Atmospheres 114(D10)

Wiles G, Charlton J, Wilson RJ, DArrigo R, Buma B, Krapek J, Gaglioti BV, Wiesenberg N, Oelkers R (2019) Yellow-cedar blue intensity tree ring chronologies as records of climate, Juneau, Alaska, USA. Canadian Journal of Forest Research (ja)

Wiles GC, DâArrigo RD, Barclay D, Wilson RS, Jarvis SK, Vargo L, Frank D (2014) Surface air temperature variability reconstructed with tree rings for the Gulf of Alaska over the past 1200 years. The Holocene 24(2):198–208

Williams AP, Cook ER, Smerdon JE, Cook BI, Abatzoglou JT, Bolles K, Baek SH, Badger AM, Livneh B (2020) Large contribution from anthropogenic warming to an emerging North American megadrought. Science 368(6488):314–318

Wilson R, D'arrigo R, Buckley B, Büntgen U, Esper J, Frank D, Luckman B, Payette S, Vose R, Youngblut D (2007a) A matter of divergence: tracking recent warming at hemispheric scales using tree ring data. Journal of Geophysical Research: Atmospheres 112(D17)

Wilson R, Wiles G, DâArrigo R, Zweck C (2007b) Cycles and shifts: 1,300 years of multi-decadal temperature variability in the Gulf of Alaska. Climate Dynamics 28(4):425–440

Wilson R, Rao R, Rydval M, Wood C, Larsson LÅ, Luckman BH (2014) Blue intensity for dendroclimatology: The BC blues: A case study from British Columbia, Canada. The Holocene 24(11):1428–1438

Wilson R, Anchukaitis K, Briffa KR, Büntgen U, Cook E, D'arrigo R, Davi N, Esper J, Frank D, Gunnarson B, et al. (2016) Last millennium northern hemisphere summer temperatures from tree rings: Part I: The long term context. Quaternary Science Reviews 134:1–18

Wilson R, D'Arrigo R, Andreu-Hayles L, Oelkers R, Wiles G, Anchukaitis K, Davi N (2017a) Experiments based on blue intensity for reconstructing North Pacific temperatures along the Gulf of Alaska. Climate of the Past

Wilson R, Wilson D, Rydval M, Crone A, Büntgen U, Clark S, Ehmer J, Forbes E, Fuentes M, Gunnarson BE, et al. (2017b) Facilitating tree-ring dating of historic conifer timbers using blue intensity. Journal of Archaeological Science 78:99–111

Wilson R, Anchukaitis K, Andreu-Hayles L, Cook E, DâArrigo R, Davi N, Haberbauer L, Krusic P, Luckman B, Morimoto D, et al. (2019) Improved dendroclimatic calibration using blue intensity in the southern Yukon. The Holocene p 0959683619862037

Wilson RJ, Luckman BH (2003) Dendroclimatic reconstruction of maximum summer temperatures from upper treeline sites in Interior British Columbia, Canada. The Holocene 13(6):851–861

Woodhouse CA, Meko DM, MacDonald GM, Stahle DW, Cook ER (2010) A 1,200-year perspective of 21st century drought in southwestern North America. Proceedings of the National Academy of Sciences 107(50):21283–21288

Zambri B, Robock A, Mills MJ, Schmidt A (2019) Modeling the 1783–1784 Laki eruption in Iceland: 1. aerosol evolution and global stratospheric circulation impacts. Journal of Geophysical Research: Atmospheres 124(13):6750–6769

Zang C, Biondi F (2015) treeclim: an R package for the numerical calibration of proxy-climate relationships. Ecography 38(4):431–436

Zhai P, Zhou B, Chen Y (2018) A review of climate change attribution studies. Journal of Meteorological Research 32(5):671–692

Appendix A: Supplemental Tables

Table S.1: Contributing weather stations (n=6) to the PRISM 4K (T_{mean} and T_{max}) gridded data field proximal to the three study sites. All stations are located between 37.0−35.9 °N and 105.8−104.4 °W.

	Latitude (°N)	**Longitude (°W)**	**Elevation (m)**	**Years**	**Terrain**
Cimarron 4 SW	36.47	104.95	2071	1904−2019	Hilly, Warm grass/shrub
Red River	36.71	105.40	2981	1906−2015	Mountain valley, Cool conifer
Springer	36.36	104.58	1784	1891−2014	Hilly, Warm grass/shrub
Raton/Crews Field	36.75	104.75	1966	1948−1968	Mountain valley, Warm grass/shrub
Manassa	37.17	105.94	2354	1893−2014	Mountain valley, Warm grass/shrub
Trinidad	37.18	104.49	2016	1899−2019	Mountain valley, Cool irrigated

Table S.2: Correlation matrix for all ring-width (RW), latewood blue intensity (LWB), Delta BI (ΔBI), and maximum latewood density (MXD) records developed from Engelmann spruce at the Wheeler Peak (WHE), Serpent Lake (JIS), and San Leonardo Lakes (SLE) sites in the Sangre de Cristo Mountains, northern NM. Bold coefficients denote $p<0.001$. See Table 2.1 for lengths of records.

	WHE.RW	WHE.EWB	WHE.LWB	WHE.ΔBI	WHE.MXD	JIS.RW	JIS.EWB	JIS.LWB	JIS.ΔBI	SLE.RW	SLE.EWB	SLE.LWB	SLE.ΔBI
WHE.RW	-	-0.02	**0.20**	**0.32**	0.11	**0.45**	-0.15	0.12	**0.27**	**0.41**	-0.07	0.10	0.18
WHE.EWB	-.02	-	**0.76**	**0.51**	**0.37**	-0.02	**0.43**	**0.53**	**0.39**	0.05	**0.58**	**0.62**	**0.42**
WHE.LWB	0.20	**0.76**	-	**0.92**	**0.48**	0.11	0.29	**0.65**	**0.64**	0.10	**0.40**	**0.64**	**0.60**
WHE.ΔBI	**0.32**	**0.51**	**0.92**	-	**0.48**	0.18	0.16	**0.62**	**0.71**	0.17	0.24	**0.54**	**0.61**
WHE.MXD	0.11	**0.37**	**0.48**	**0.48**	-	**0.34**	0.17	**0.41**	**0.57**	**0.30**	0.20	**0.40**	**0.47**
JIS.RW	**0.45**	-0.02	0.11	0.18	**0.34**	-	0.12	**0.42**	**0.59**	**0.71**	-0.24	**0.40**	**0.40**
JIS.EWB	-0.15	**0.43**	0.29	0.16	0.17	0.12	-	**0.73**	0.31	0.14	0.28	0.28	**0.33**
JIS.LWB	0.12	**0.53**	**0.65**	**0.65**	**0.41**	**0.42**	**0.73**	-	**0.84**	**0.36**	0.20	**0.52**	**0.67**
JIS.ΔBI	**0.27**	**0.39**	**0.64**	**0.71**	**0.57**	**0.59**	0.31	**0.84**	-	**0.49**	0.05	**0.44**	**0.70**
SLE.RW	**0.41**	0.05	0.10	0.17	0.30	**0.71**	0.14	**0.36**	**0.49**	-	-0.02	**0.31**	**0.59**
SLE.EWB	-0.07	**0.58**	**0.40**	0.24	0.20	-0.24	0.17	0.20	0.05	-0.02	-	**0.80**	**0.35**
SLE.LWB	0.10	**0.62**	**0.64**	**0.64**	**0.40**	**0.40**	0.28	**0.52**	**0.44**	**0.31**	**0.80**	-	**0.77**
SLE.ΔBI	**0.27**	**0.46**	**0.60**	**0.61**	**0.47**	**0.40**	**0.33**	**0.67**	**0.70**	**0.59**	**0.33**	**0.77**	-

Table S.3: Summary statistics (r values) for individual PCAs (RW, LWB, and ΔBI) of all series from WHE, JIS, and SLE and loadings of each site into the first three PCs.

	% of variance	WHE	JIS	SLE
RW PC1	40.9%	0.72	0.37	0.37
EWB PC1	30.7%	0.54	0.45	0.40
LWB PC1	35.5%	0.62	0.44	0.48
ΔBI PC1	30.8%	0.61	0.44	0.35
RW PC2	9.6%	0.05	0.16	0.27
EWB PC2	10.5%	0.01	0.14	-0.01
LWB PC2	11.4%	0.10	0.18	0.0
ΔBI PC2	10.5%	0.05	0.25	0.03
RW PC3	7.5%	-0.12	0.16	0.08
EWB PC3	7.0%	0.03	0.02	0.03
LWB PC3	6.6%	0.0	-0.04	0.06
ΔBI PC3	6.4%	0.06	0.05	0.00

Table S.4: RBAR and EPS statistics. Included metrics are the RBAR, number of series needed to attain an EPS of 0.80, and the year at which EPS is >0.80 threshold for all detrended (AD-sf) composite chronologies.

	RW	**EWB**	**LWB**	**ΔBI**
RBAR	0.33	0.24	0.29	0.28
No. series EPS>0.80	6	12	13	9
Year EPS>0.80	1713	1721	1738	1724

Table S.5: Correlation coefficients of composite chronologies with PRISM 4k August−September mean (AS T_{mean}) and maximum (AS T_{max}) temperature, as well as precipitation data proximate to the three sample locations in the Southern Rocky Mountains region of northern NM (37.0−35.9°N, 105.8−104.4°W). **Bold** coefficients = p<0.001

	RW	EWB	LWB	Δ BI	MXD
T_{mean} (1907−2015)	0.03	0.21	**0.54**	**0.43**	-
T_{max} (1907−2015)	0.07	**0.37**	**0.64**	**0.56**	-
T_{mean}(1907−1983)	0.01	0.15	**0.56**	**0.55**	0.13
T_{max}(1907−1983)	-0.03	**0.41**	**0.65**	**0.64**	0.18
Previous Year May Precip (1907−2015)	0.08	0.04	-0.01	0.03	-
Previous Year May Precip (1980−2015)	**0.54**	-0.23	0.23	**0.44**	-
Current April−May Precip (1907−2015)	-0.04	0.20	-0.01	-0.10	-
Current April−May Precip (1980−2015)	0.06	-0.16	-0.09	0.02	-
Current August Precip (1907−2015)	0.01	**-0.30**	**-0.40**	**-0.31**	-
Current August Precip (1980−2015)	0.15	**-0.54**	**-0.46**	-0.14	-

Table S.6: Cross-validation statistics for the Southern Rocky Mountains composite LWB AS T_{max} reconstruction spanning 1735−2015 CE. To ensure model stability over time, validation statistics are calculated for calibrating on the early period (1907-1961) and verifying on the late period (1962-2015), and vice-versa. CR^2 (VR^2) = calibration (verification) period coefficient of determination; VRE (VCE) = validation period reduction of error (coefficient of efficiency); RMSE = root-mean-square error.

Validation/Cross-validation	CR^2	VR^2	VRE	VCE	RMSE
Early Period Calibration / Late Period Verification					
Calibration (1907-1961)	0.30	–	–	–	0.93
Verification (1962-2015)	–	0.31	0.57	0.16	–
Late Period Calibration / Early Period Verification					
Calibration (1962-2015)	0.31	–	–	–	0.96
Verification (1907-1961)	–	0.30	0.61	0.22	–
Full Period (1907−2015)	0.42	0.28	0.41	0.28	0.94

Table S.7: Top five warmest and coolest single-year and decade anomalies based on the composite LWB AS T_{max} reconstruction for the Southern Rocky Mountains spanning 1735-2015.

Coldest	Years	Anomaly	Decade	Anomaly
1	1831	-3.64	1990−1999	-1.04
2	1761	-2.28	1810−1819	-0.98
3	1828	-2.58	1830−1839	-0.96
4	1884	-2.49	2000−2009	-0.93
5	2003	-2.47	1760−1769	-0.28
Warmest	Years	Anomaly	Decade	Anomaly
1	1924	+2.15	1940−1949	+1.05
2	1926	+2.05	1930−1939	+0.88
3	2015	+1.99	1950−1959	+0.62
4	1936	+1.95	1890−1899	+0.34
5	1939	+2.47	1910−1919	+0.33

Table S.8: Pearson's correlations between individual latewood blue (LWB) chronologies and their tree ring width (TRW) site counterparts over the common period of each chronology pairing. * indicates significance at p <0.01 level.

Site Code	r-value
TLM	0.22*
HAY	0.05
ABA	0.10
PLS	0.29*
BUP	0.55*
TUS	0.43*
MON	0.08
MBP	0.30*
TLS	0.11
PPU	0.52*
PPL	0.61*
SLE	0.18
JIS	0.18
WHE	0.41*
CPI	0.15
MDB	0.26*
LOS	0.35
BTP	0.53*
CBS	0.42*
TOW	0.28*
MWS	0.37*
RPS	0.17
FLS	0.14
MCO	0.12
BFL	0.29*
FKY	0.20

Table S.9: Results of Pearson's correlation tests to determine the optimum CRU T_{max} seasonal target for reconstruction of each regional model. We compare r-values (p<0.05) across seasonal periods of varying duration and are comprised of at least 2 consecutive months, ranging from July-August (JA) to March-September (MAMJJAS). Correlations calculated over the common calibration period for each region (NR: 1920-2000, CR: 1920-2015, IP:1920-2000, and SR:1920-2014). The optimum season for each regional reconstruction is highlighted with a green box.

Months	**NR**	**CR**	**IP**	**SR**
JA	0.68	0.61	0.52	0.62
JJA	0.67	0.64	0.54	0.61
MJJA	0.72	0.66	0.64	0.57
AMJJA	0.69	0.61	0.67	0.52
MAMJJA	0.70	0.51	0.56	0.40
AS	0.50	0.50	0.49	0.73
JAS	0.55	0.57	0.53	0.68
JJAS	0.60	0.64	0.58	0.66
MJJAS	0.66	0.66	0.68	0.63
AMJJAS	0.65	0.64	0.70	0.58
MAMJJAS	0.68	0.56	0.60	0.47

Table S.10: Pearson (P), Spearman (S), and Robust Pearson (RP) correlation coefficients (significant at $p<0.05$ level) for each chronology against the regional target CRU T_{max}, and the standardized regression coefficient (beta value; β) for each chronology in the regression model.

Site Name	P	S	RP	β
Northern Rocky Mountains (NR)				
MCO	0.42	0.40	0.43	0.28
BFL	0.71	0.77	0.72	0.85
FKY	0.38	0.38	0.42	0.23
Central Rocky Mountains (CR)				
MWS	0.50	0.50	0.46	0.17
RPS	0.67	0.63	0.64	0.28
FLS	0.64	0.63	0.58	0.26
BTP	0.59	0.51	0.54	0.23
CBS	0.48	0.44	0.44	0.18
TOW	0.56	0.52	0.52	0.21
Intermontane Plateau (IP)				
BUP	0.34	0.39	0.47	0.10
HAY	0.59	0.54	0.55	0.23
TLM	0.41	0.35	0.35	0.14
TUS	0.65	0.66	0.66	0.26
MON	0.66	0.60	0.62	0.25
MBP	0.52	0.48	0.49	0.15
ABA	0.65	0.60	0.56	0.24
PLS	0.45	0.47	0.53	0.16
Southern Rocky Mountains (SR)				
LOS	0.69	0.69	0.73	0.56
TLS	0.46	0.48	0.49	0.18
CPI	0.51	0.53	0.52	0.03
MDB	0.40	0.39	0.42	0.04
PPL	0.29	0.24	0.27	0.07
PPU	0.53	0.55	0.54	0.23
SLE	0.31	0.32	0.32	0.04
WHE	0.60	0.63	0.65	0.21
JIS	0.56	0.56	0.58	0.21

Table S.11: Calibration/verification statistics for all regional reconstructions, including all forward and backward nests. **CP** indicates common period.

Nest	Years	CRSQ	VRE	VCE	RMSE
NR					
-2	1721-1909	0.51	0.50	0.48	0.82
-1	1910-1919	0.52	0.52	0.51	0.81
CP	1920-2000	0.53	0.55	0.53	0.80
+1	2001-2018	0.43	0.52	0.50	0.86
CR					
-4	1730-1759	0.23	0.17	0.17	0.98
-3	1760-1769	0.31	0.20	0.20	0.93
-2	1770-1789	0.41	0.40	0.40	0.86
-1	1790-1849	0.44	0.44	0.44	0.84
CP	1850-2015	0.44	0.44	0.44	0.84
+1	2016	0.42	0.40	0.44	0.84
+2	2017	0.43	0.40	0.41	0.84
+3	2018	0.25	0.14	0.14	0.96
IP					
-7	1646-1659	0.06	0.04	0.03	0.78
-6	1660-1679	0.22	0.12	0.12	0.71
-5	1680-1849	0.42	0.44	0.44	0.61
-4	1850-1859	0.43	0.49	0.49	0.60
-3	1860-1869	0.45	0.52	0.52	0.59
-2	1870-1889	0.45	0.52	0.52	0.59
-1	1890-1908	0.45	0.51	0.51	0.59
CP	1909-2000	0.49	0.55	0.54	0.62
+1	2001-2002	0.48	0.53	0.53	0.63
+2	2003-2015	0.41	0.47	0.45	0.65
+3	2016	0.41	0.50	0.43	0.66
+5	2017-2018	0.10	0.02	0.04	0.83
SR					
-7	1623-1659	0.28	0.19	0.16	0.81
-6	1660-1699	0.32	0.19	0.16	0.79
-5	1700-1739	0.33	0.20	0.17	0.78
-4	1740-1779	0.32	0.16	0.14	0.79
-3	1780-1809	0.37	0.27	0.24	0.76
-2	1810-1849	0.42	0.36	0.33	0.73
-1	1850-1877	0.41	0.35	0.33	0.73
CP	1878-2014	0.54	0.53	0.52	0.65
+1	2015	0.56	0.52	0.50	0.65
+2	2016-2018	0.47	0.50	0.49	0.71

Appendix B: Supplemental Figures

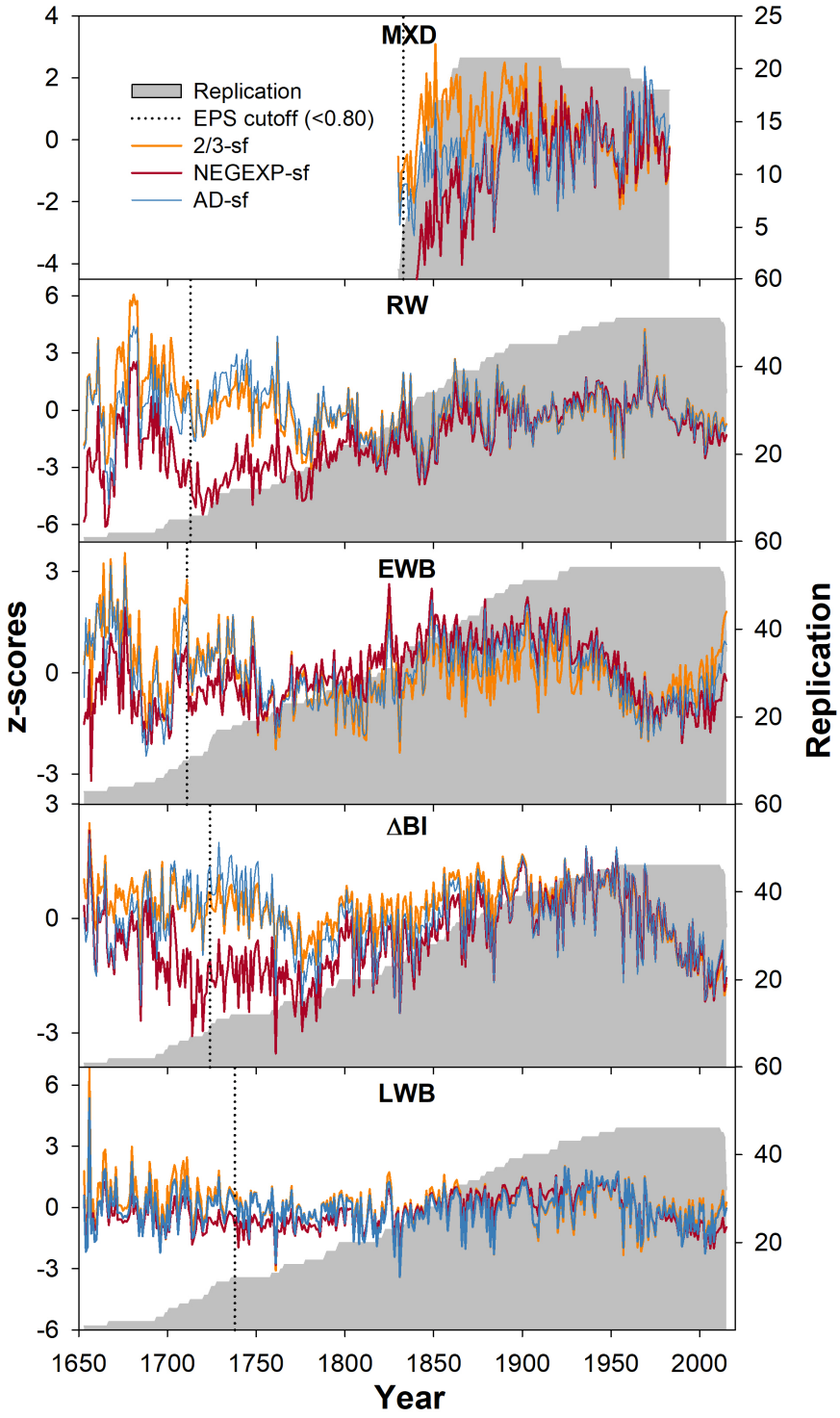

Figure S.1: WHE maximum latewood density (MXD), composite ring-width (RW), earlywood blue intensity (EWB), delta blue intensity (ΔBI), and latewood blue intensity (LWB) chronology variants, EPS, and replication. Composite chronologies derived from PCA of pooled series from WHE, JIS, and SLE. Differential chronology variants for each tree ring parameter result from detrending with the $\frac{2}{3}$ spline in SignalFree ($\frac{2}{3}$sf, red line), the Age-dependent spline in SignalFree (AD-sf, blue line), and the Negative Exponential spline in SignalFree (NegExp-sf, orange line). EPS determination based on tree ring chronology developed with AD-sf detrending.

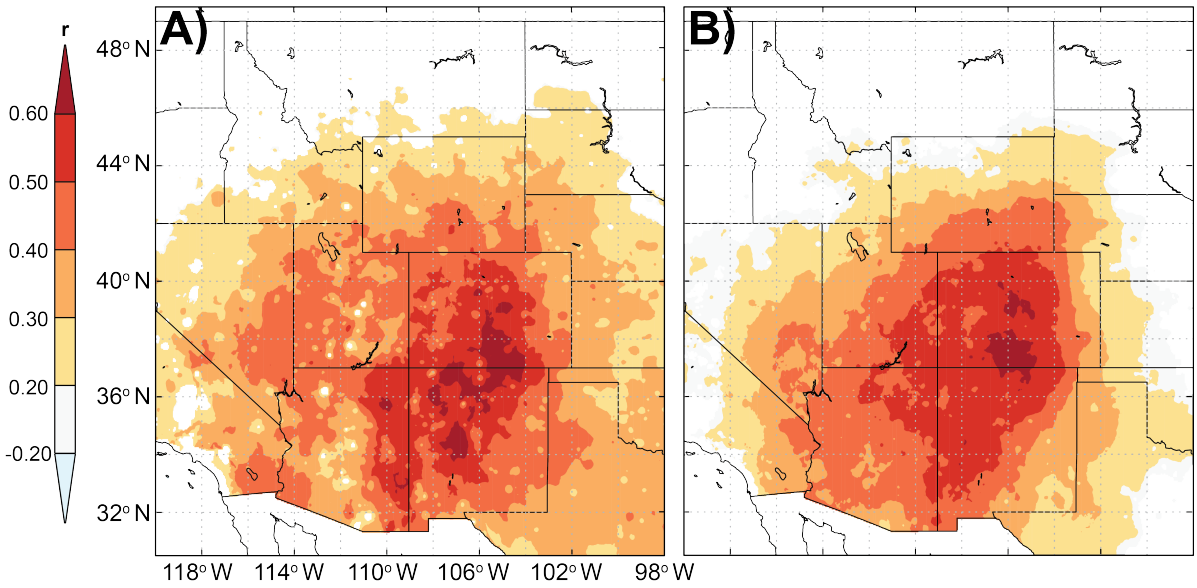

Figure S.2: Spatial correlations (α=0.10) across the Southern Rocky Mountains/American Southwest regions between the (A) non-transformed and (B) first year difference composite AD-sf LWB chronology and regional PRISM 4k AS T_{max} over the period 1907−2015.

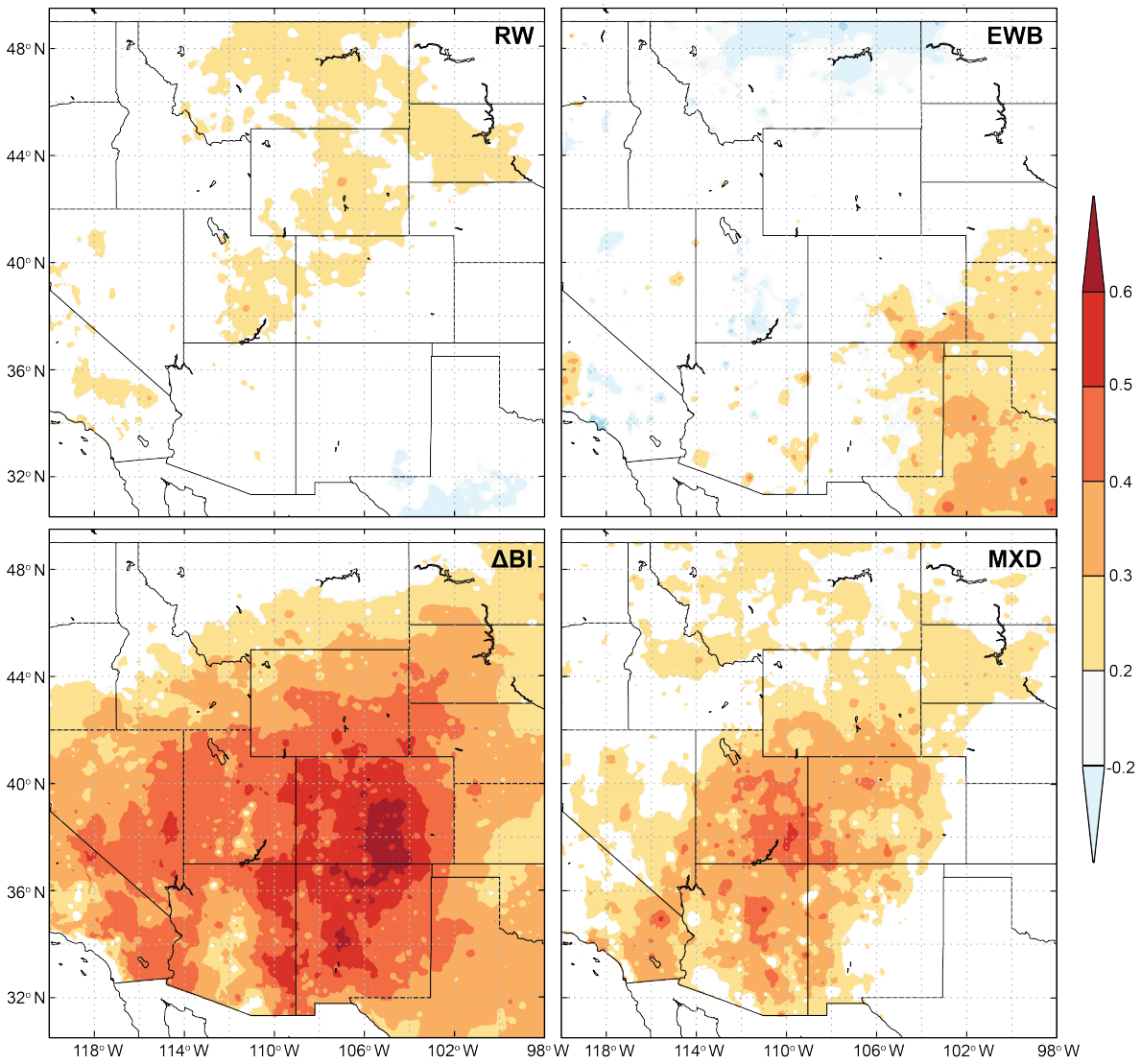

Figure S.3: Spatial correlations (α=0.10) across the Southern Rocky Mountains between composite RW, EWB, and ΔBI chronologies and regional PRISM 4k AS T_{max} over the period 1907−2015, and between WHE MXD chronology regional PRISM 4k AS T_{max} over the period 1907−1983.

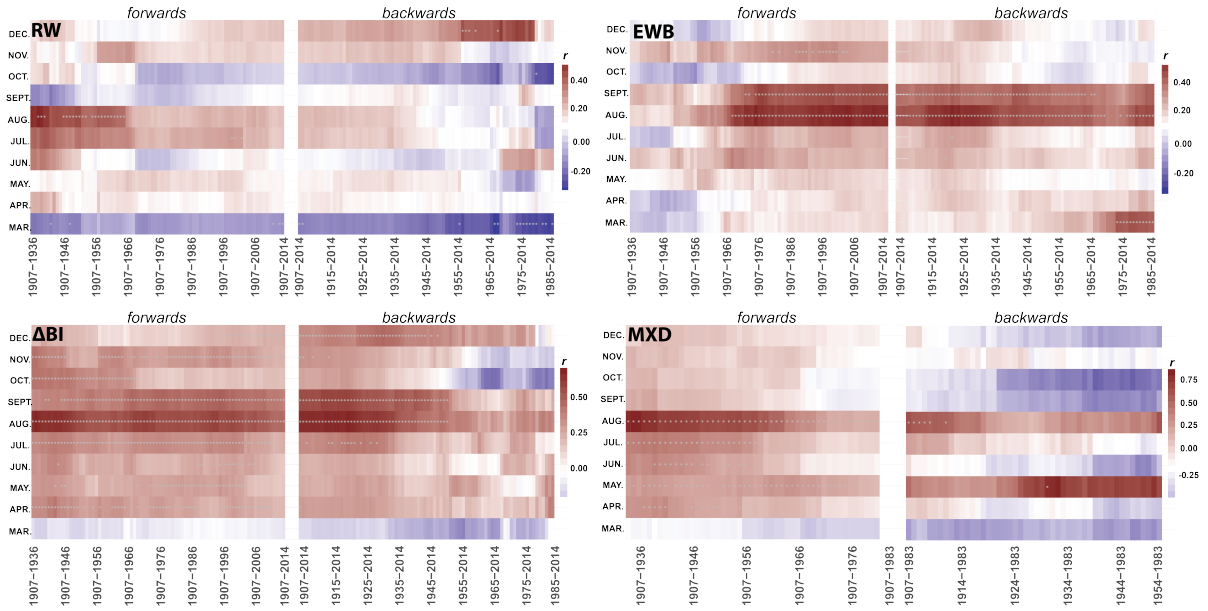

Figure S.4: Forward and backward (evolutionary) moving correlation (α=0.05) of composite RW, LWB, and ΔBI chronologies and regional PRISM 4k AS T_{max} over the period 1907−2014, and between WHE MXD chronology regional PRISM 4k AS T_{max} over the period 1907−1983. Note differential color scales for correlation coefficient (r) between parameters.

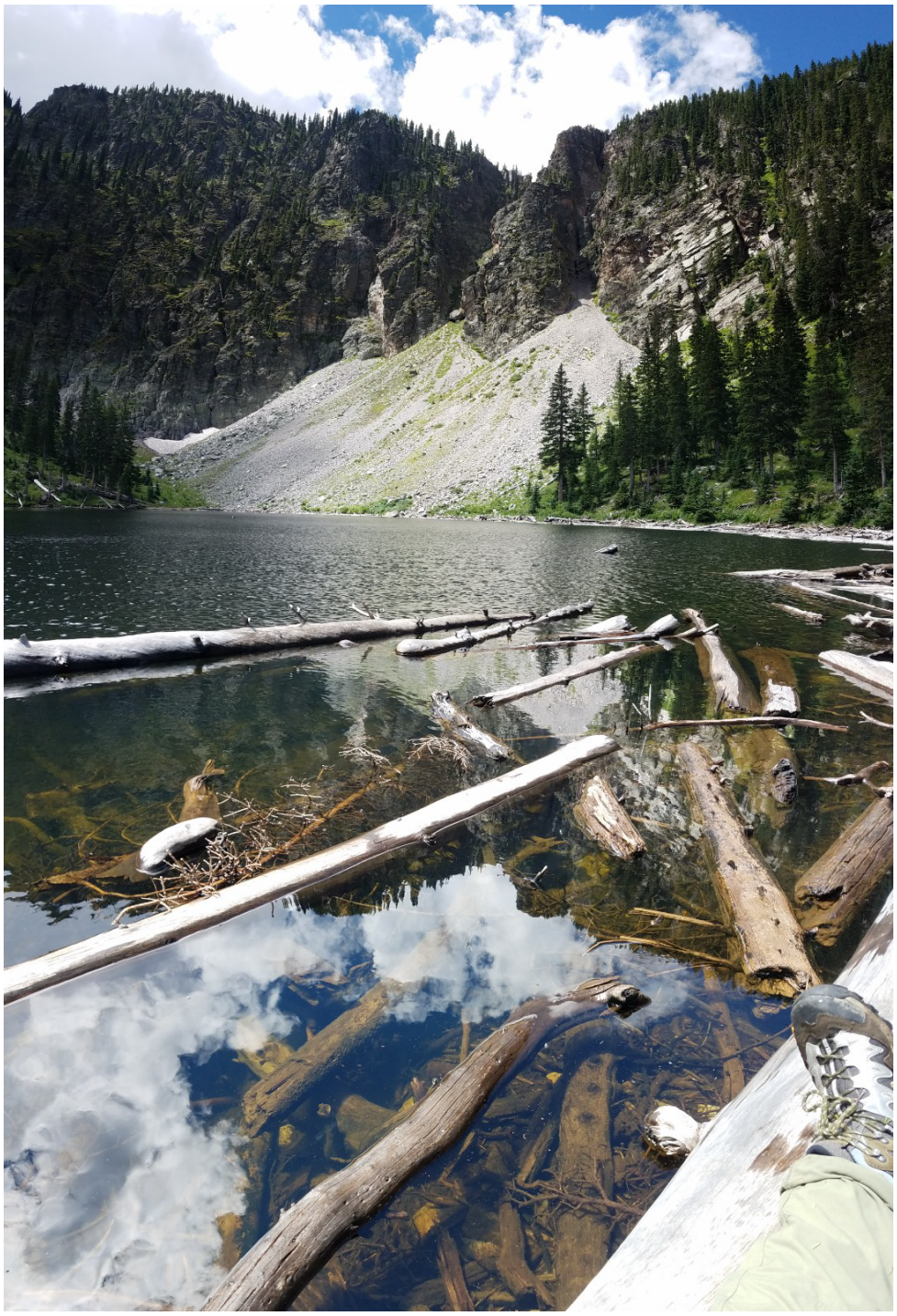

Figure S.5: Photograph of Upper San Leonardo Lake, Sangre de Cristo Mountains, northern NM showing abundance of floating and submerged Engelmann spruce logs.

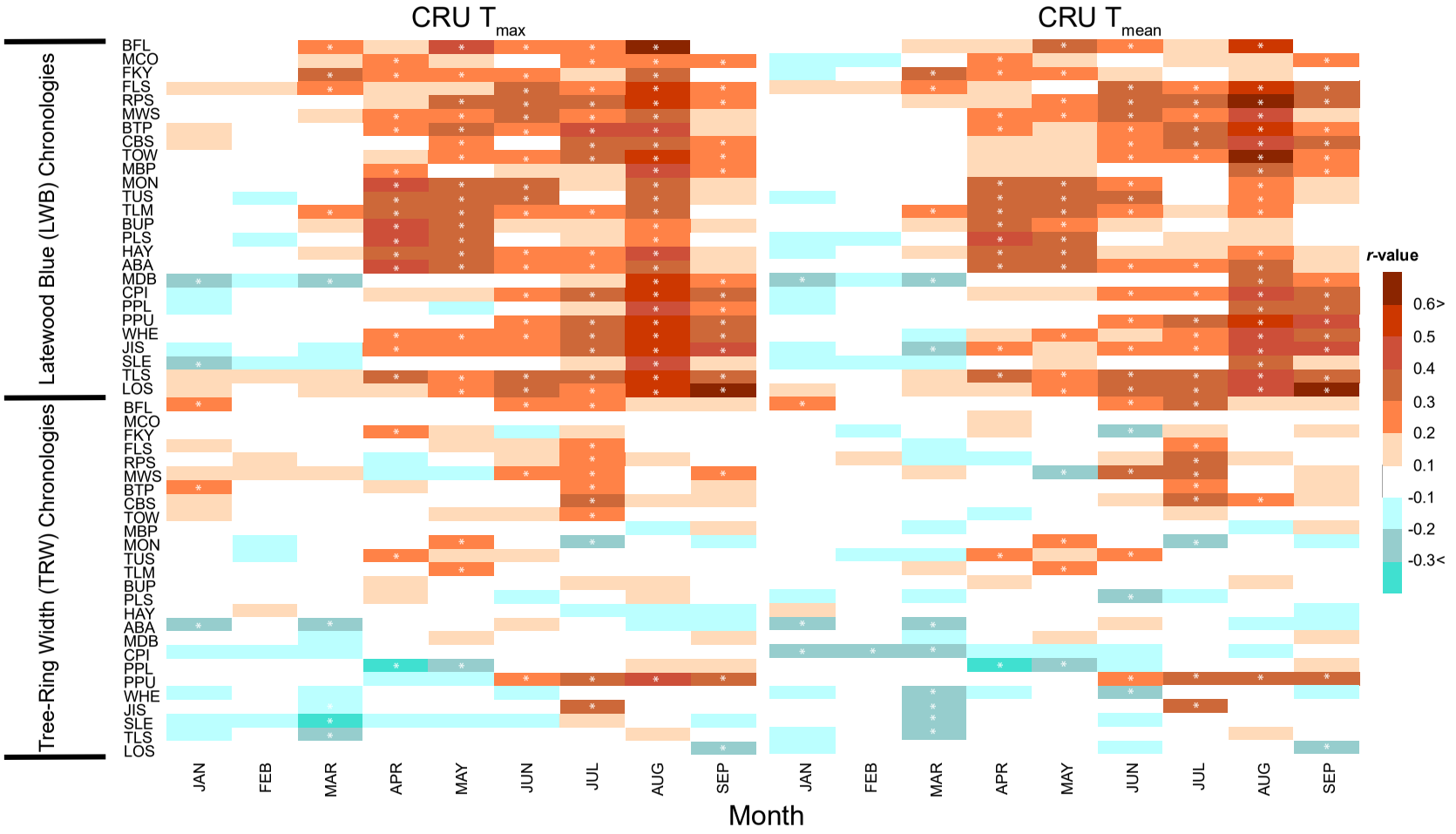

Figure S.6: Comparison of Pearson's r (p<0.05) between each site-specific LWB and TRW chronology and current-year monthly local CRU 4.04 0.5°T_{max} and T_{mean} data for each site. Correlations span the common period between the starting calibration year for each region (1920) and the last year of each individual chronology.

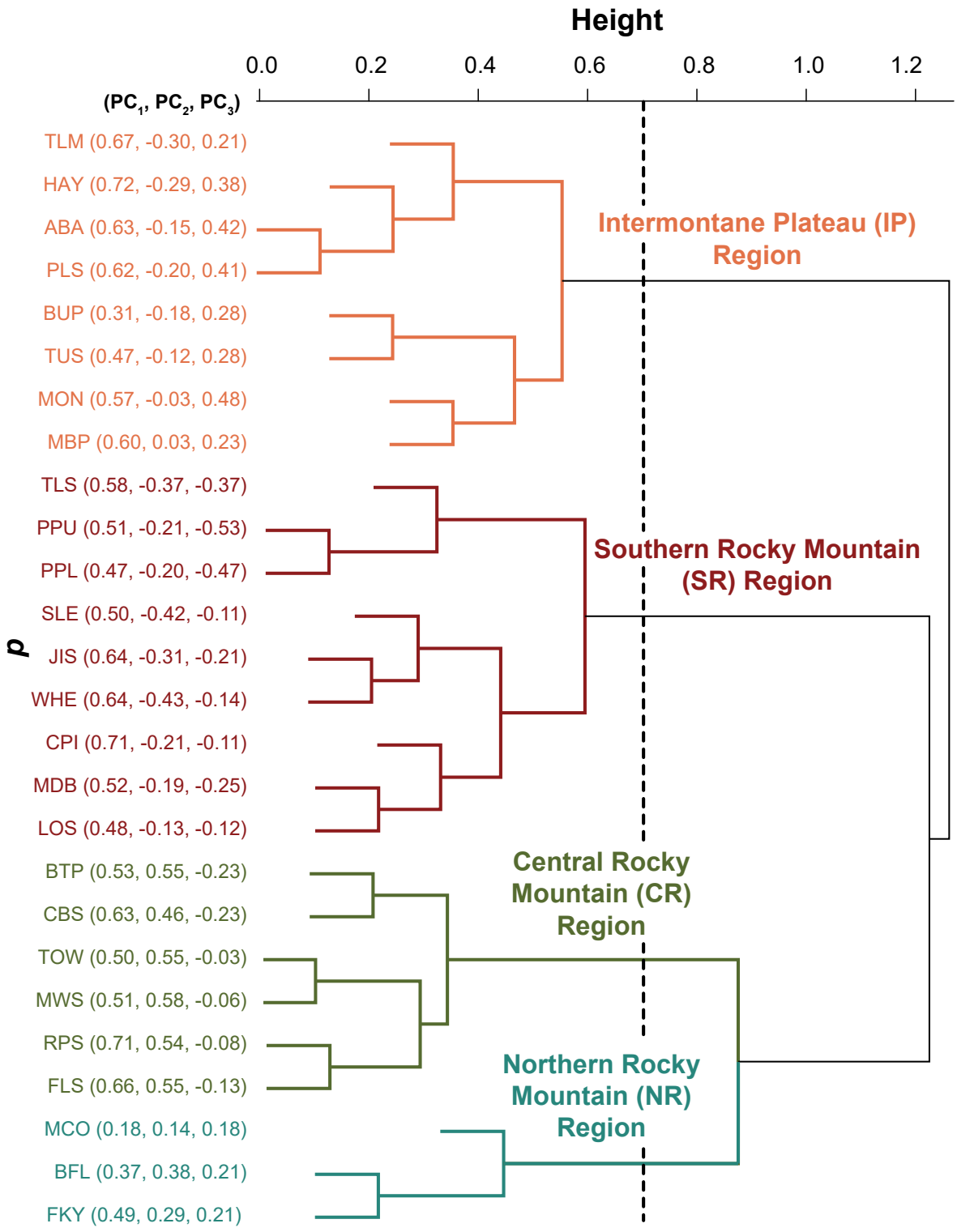

Figure S.7: Dendrogram displaying results of a complete linkage hierarchical cluster analysis (HCA) performed on the 26 LWB chronologies. Cluster analysis based on euclidean distance matrix of chronology loading values on PCs1-3. Final regional groups were determined with a cutoff height value of 0.7.

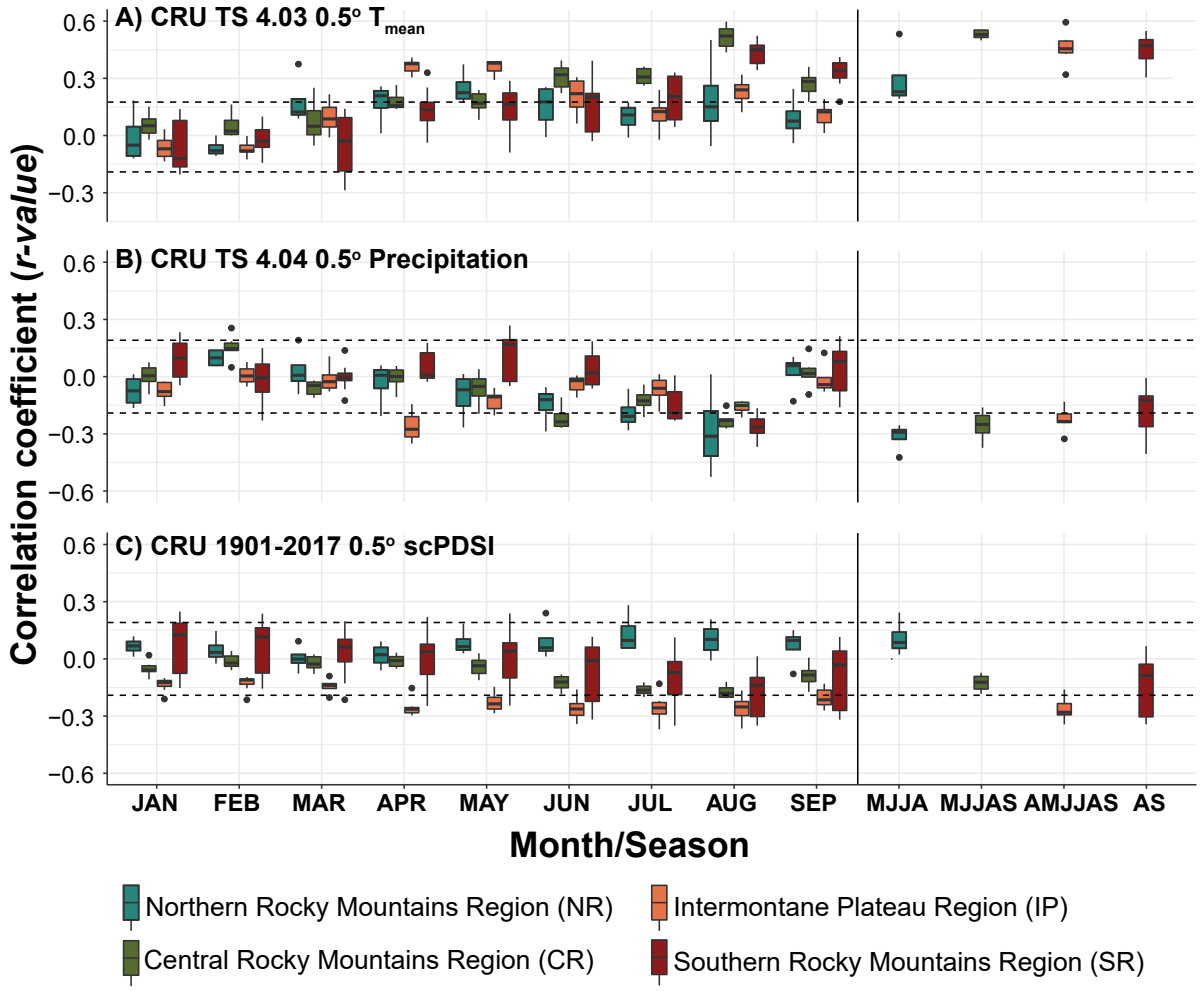

Figure S.8: Pearson's r (p<0.05) between all 26 LWB chronologies across each region and current year monthly and optimum season A) CRU 4.04 0.5°T_{mean}, B) CRU 4.04 0.5°precipitation, and C) CRU 1901-2017 0.5°self-calibrating Palmer's Severity Drought Index (scPDSI) data (Harris et al., 2014) for each region. Correlations span the common period between the starting calibration year (1920) and the last year of each individual chronology.

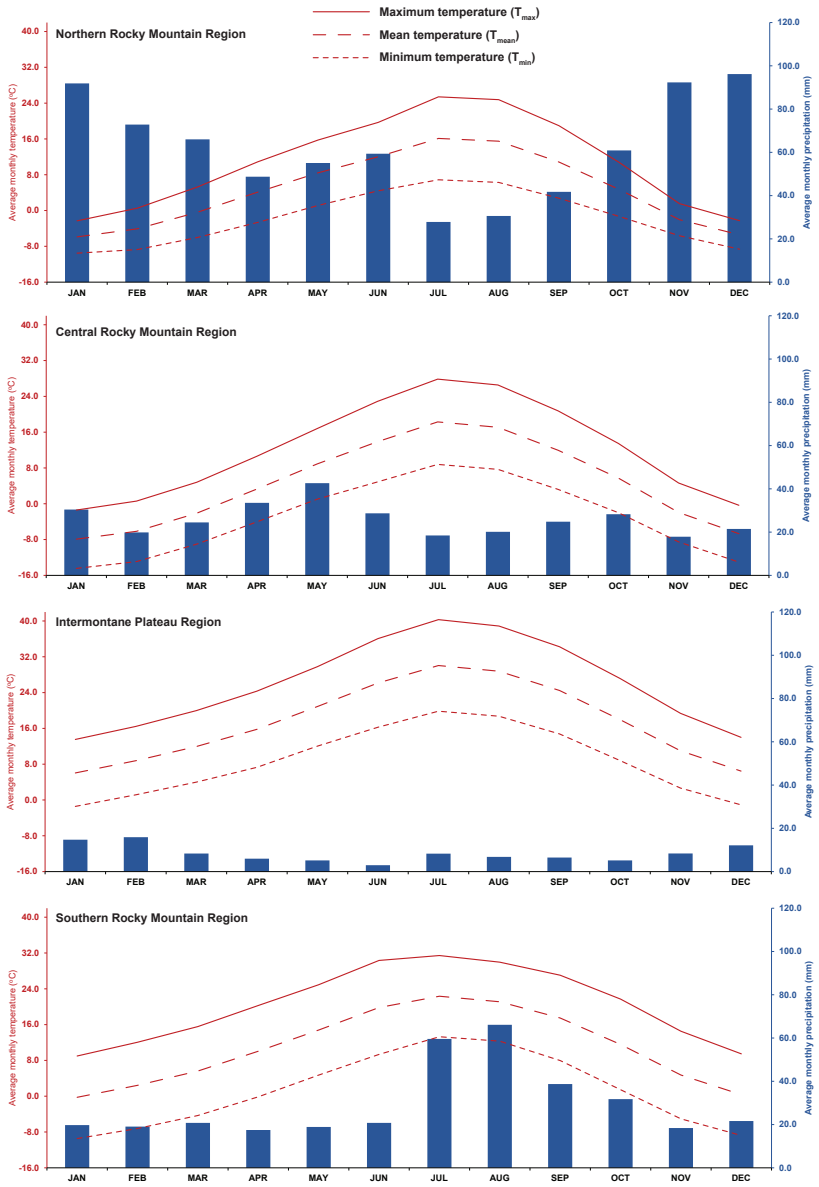

Figure S.9: Regional climographs of mean monthly maximum, mean, and minimum temperature, and precipitation, derived from the CRU TS 4.04 0.5°land dataset (Harris et al., 2014) over the period 1920−2019 for the Northern, Central, Southern Rocky Mountain, and Intermontane Plateau regions. Temperature is represented by the red lines and precipitation by the blue boxes.

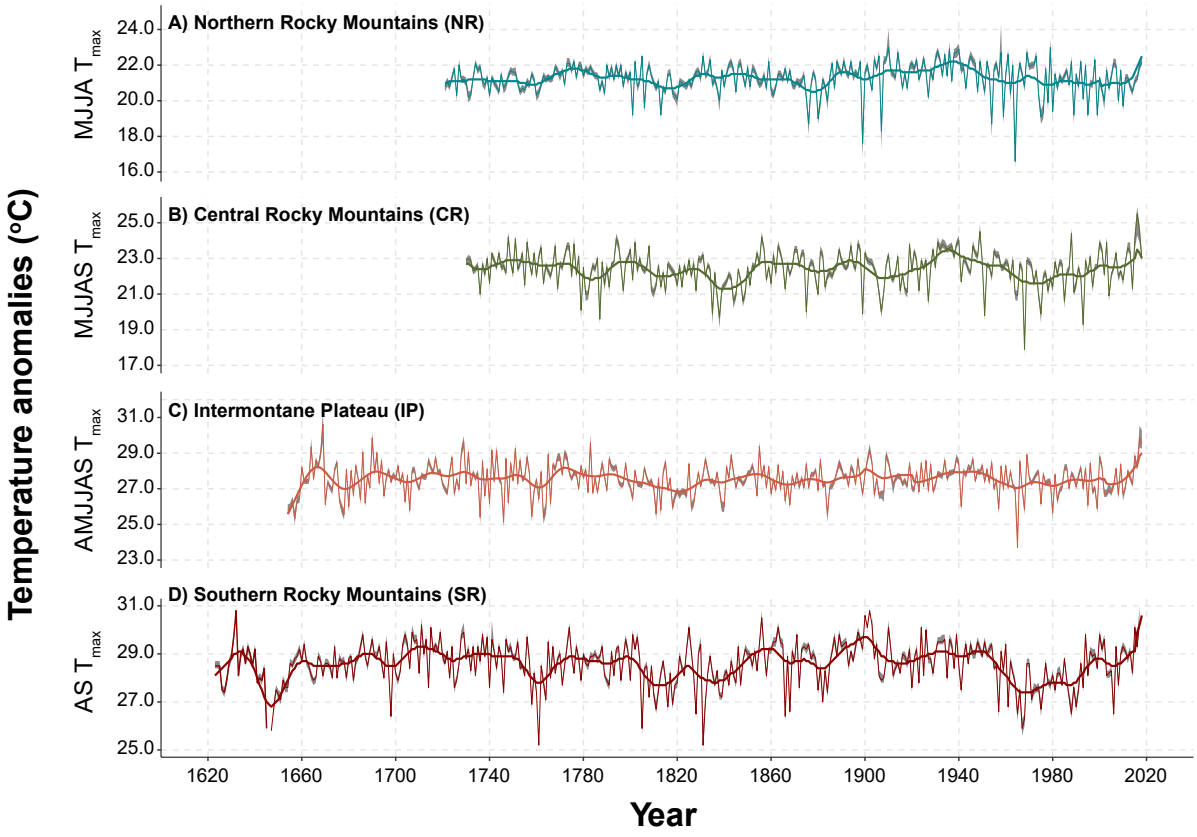

Figure S.10: Plotted 4 regional T_{max} reconstructions. Time series of yearly reconstructed values indicated by thin lines, and overlaid with 20-year low pass filter smoothed time series. Associated standard zerror with the yearly values shaded in dark grey.